ARL 63-81

PRESSURE AND HEAT TRANSFER MEASUREMENTS OVER A CIRCULAR CYLINDER AT ANGLES OF ATTACK UP TO 15° AT M = 11

C. C. HORSTMAN

PRINCETON UNIVERSITY
PRINCETON, NEW JERSEY

MAY 1963

AERONAUTICAL RESEARCH LABORATORIES
OFFICE OF AEROSPACE RESEARCH
UNITED STATES AIR FORCE

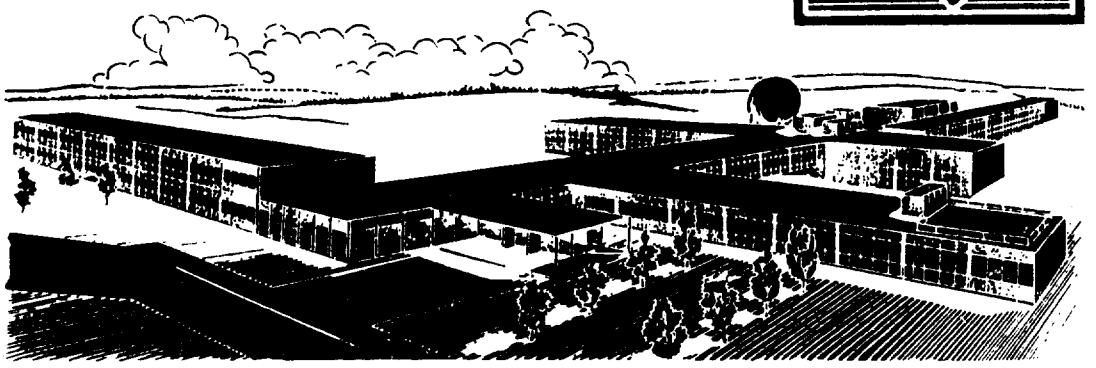

NOTICES

When Government drawings, specifications, or other data are used for any purpose other than in connection with a definitely related Government procurement operation, the United States Government thereby incurs no responsibility nor any obligation whatsoever; and the fact that the Government may have formulated, furnished, or in any way supplied the said drawings, specifications, or other data, is not to be regarded by implication or otherwise as in any manner licensing the holder or any other person or corporation, or conveying any rights or permission to manufacture, use, or sell any patented invention that may in any way be related thereto.

- - - - - - - - -

Qualified requesters may obtain copies of this report from the Armed Services Technical Information Agency, (ASTIA), Arlington Hall Station, Arlington 12, Virginia.

- - - - - - - - -

This report has been released to the Office of Technical Services, U. S. Department of Commerce, Washington 25, D. C. for sale to the general public.

- - - - - - - - -

Copies of ARL Technical Documentary Reports should not be returned to Aeronautical Research Laboratory unless return is required by security considerations, contractual obligations, or notices on a specific document.

UNCLASSIFIED

Aeronautical Research Laboratories, Wright-Patterson AFB, O. PRESSURE AND HEAT TRANSFER MEASUREMENTS OVER A CIRCULAR CYLINDER AT ANGLES OF ATTACK UP TO 15° at M = 11 by C. C. Horstman, Princeton U., Princeton, N.J. May 1963. 75 p. incl. illus. (Project 7064;Task 7064-01)(Contract AF 33(616) 7629) (ARL 63-81) Unclassified Report

A continuation of a fundamental study of hypersonic wings and control surfaces, some detailed pressure distribution and heat transfer results have been obtained about a circular cylinder with various nose shapes at angles of

(over)

UNCLASSIFIED

attack up to 15° and at azimuth angles from zero to 180°. The tests were carried out in the Princeton University 3 inch helium hypersonic wind tunnel at a Mach number of 11. The experimental results were compared with theory along the windward side and in the crossflow plane for both the pressure and heat transfer distributions. Some effects of the nose shapes on the flow over the circular cylinder under study were determined up to 13 cylinder diameters back from the nose.

UNCLASSIFIED

UNCLASSIFIED

Aeronautical Research Laboratories, Wright-Patterson AFB, O. PRESSURE AND HEAT TRANSFER MEASUREMENTS OVER A CIRCULAR CYLINDER AT ANGLES OF ATTACK UP TO 15° at M = 11 by C. C. Horstman, Princeton U., Princeton, N.J. May 1963. 75 p. incl. illus. (Project 7064;Task 7064-01)(Contract AF 33(616) 7629) (ARL 63-81) Unclassified Report

A continuation of a fundamental study of hypersonic wings and control surfaces, some detailed pressure distribution and heat transfer results have been obtained about a circular cylinder with various nose shapes at angles of

(over)

UNCLASSIFIED

attack up to 15° and at azimuth angles from zero to 180°. The tests were carried out in the Princeton University 3 inch helium hypersonic wind tunnel at a Mach number of 11. The experimental results were compared with theory along the windward side and in the crossflow plane for both the pressure and heat transfer distributions. Some effects of the nose shapes on the flow over the circular cylinder under study were determined up to 13 cylinder diameters back from the nose.

UNCLASSIFIED

ARL 63-81

PRESSURE AND HEAT TRANSFER MEASUREMENTS OVER A CIRCULAR CYLINDER AT ANGLES OF ATTACK UP TO 15° AT M = 11

C. C. HORSTMAN

PRINCETON UNIVERSITY
PRINCETON, NEW JERSEY

MAY 1963

CONTRACT AF 33(616)-7629
PROJECT 7064
TASK 7064-01

AERONAUTICAL RESEARCH LABORATORIES
OFFICE OF AEROSPACE RESEARCH
UNITED STATES AIR FORCE
WRIGHT-PATTERSON AIR FORCE BASE, OHIO

FOREWORD

The present study is part of a program of theoretical and experimental research on hypersonic flow being conducted by the Gas Dynamics Laboratory, the James Forrestal Research Center, Princeton University, Princeton, New Jersey, on Contract AF 33(616)-7629 for the Aeronautical Research Laboratories, Office of Aerospace Research, United States Air Force. The work reported in this interim report was on Task 7064-01, "Research on Hypersonic Flow Phenomena" of Project 7064, "Aerothermodynamic Investigations in High Speed Flow" under the technical cognizance of Col. A. Boreske.

The author would also like to gratefully the advice received from Prof. S. M. Bogdonoff and Mr. I. E. Vas.

ABSTRACT

As a continuation of a fundamental study of hypersonic wings and control surfaces, some detailed pressure distribution and heat transfer results have been obtained about a circular cylinder with various nose shapes at angles of attack up to 15° and at azimuth angles from zero to 180°. The tests were carried out in the Princeton University 3 inch helium hypersonic wind tunnel at a Mach number of 11. The experimental results were compared with theory along the windward side and in the crossflow plane for both the pressure and heat transfer distributions. Some effects of the nose shape on the flow over the circular cylinder under study were determined up to 13 cylinder diameters back from the nose.

TABLE OF CONTENTS

LIST OF FIGURES

SYMBOLS

c	Specific heat of stainless steel - BTU/lb ^{o}R.
C_p	Specific heat at constant pressure - BTU/lb ^{o}R.
D	Cylinder diameter - ft.
D_N	Nose drag - lbs.
h	Heat transfer coefficient - BTU/ft^2 sec ^{o}R.
H	Total enthalpy - BTU/lb
k	Thermal conductivity - BTU/ft sec ^{o}R.
M	Mach number
p	Pressure - lb/ft^2
p_l'	Free stream static pressure at an orifice location if no model were present
Pr	Prandtl number
R	Cylinder radius - ft
Re_D	Free stream Reynolds number based on body diameter
$\mathcal{R}$	Universal gas constant - ft^2/sec^2 ^{o}R.
t	Time - sec
T	Temperature - ^{o}R.
u	Velocity in axial direction - ft/sec
w	Velocity in crossflow direction - ft/sec
x	Axial distance along cylinder from shoulder of nose - ft
y	Normal distance from body - ft
z	Distance from stagnation line in crossflow direction - ft
α	Angle of attack
β	$\frac{D}{w_l}\frac{dw_e}{dz}$
μ	Viscosity coefficient - slug/ft sec
ρ	Density - lb/ft^2
Λ	Yaw angle
ϕ	Azimuth on cylinder starting from stagnation line
γ	Ratio of specific heats
ϵ	$\gamma-1/\gamma+1$

Subscripts:

c	Cone
b	Edge of effective body
e	Edge of boundary layer
en	Edge of entropy layer
IN	Inside surface of thin skin model
N	Conditions normal to axis of cylinder
OUT	Outside surface of thin skin model
r	Recovery
s	Conditions at shock
se	External flow at stagnation line of cylinder
SL	Stagnation line
W	Conditions at wall
∞	Free stream
Λ	Conditions pertaining to yawed cylinder
Λ=0	Conditions pertaining to unyawed cylinder

INTRODUCTION

As part of a basic study of hypersonic wings, an experimental program has been initiated to determine the heat transfer and pressure distribution over the leading edge of a swept wing at sweepback angles from zero to 90°. Some preliminary results of this study at sweep angles up to 75° are contained in Ref. 1. To simulate a wing leading edge at even higher sweepback angles (greater than 75°), a circular cylinder at angle of attack was used. The advantages of model simplicity and opportunity to examine axisymmetric body at angle of attack at the same time led to this particular configuration. Results of this study at zero angle of attack are contained in Ref. 2.

For an axisymmetric body at zero angle of attack, it is known that the inviscid flow over the after body is completely determined by the entropy layer which is solely a function of the nose shape. Ladyzhenskii (Ref. 3) has shown that (for fixed nose shape) as long as the after body is immersed in the entropy layer, the pressure distribution will remain similar regardless of changes in the after body shape or angle of attack. When the body breaks through the edge of the entropy layer (which has been calculated in Ref. 2), by increasing its angle of attack, a qualitative change in the pressure distribution must be expected. Following this reasoning, a change must also be expected in the shock wave shapes and in the heat transfer distributions.

The configuration studied consisted of an instrumented circular cylinder with various noses attached. To examine the effect of a wide variation of nose drag coefficient, a 20° semi-angle cone, a hemisphere, and a flat face were used. The model was tested at a Mach number of 11 and a free stream Reynolds number based on the cylinder's diameter of 130,000.

Manuscript released by the author (February 1963) for publication as an ARL Technical Documentary Report.

EXPERIMENTAL FACILITIES AND MODELS

The test program was conducted in the three inch diameter Princeton University helium hypersonic wind tunnel (Ref. 8). The nozzle was contoured giving a uniform test section Mach number equal to 11. The free stream Reynolds number was about 0.5×10^6 per inch. Helium at room temperature was used as a test fluid.

The pressure model was $\frac{1}{4}$ inch in diameter, about 6 inches long, and constructed of brass (Fig. 1). The location of the pressure taps is shown in Fig. 2. To the basic model (the 6 inch long cylinder) various tips were attached. The tips used included a 20° half angle cone, a hemisphere, and a flat faced end. The tips were constructed of lucite to limit heat conduction on the heat transfer and recovery models. The model was mounted from the side of the tunnel.

The heat transfer model was of the thin skin type with the same physical dimensions as the pressure model. The thermocouples were located at the same stations as the pressure orifices. The thermocouples were copper-constantan wires of 0.010 inches diameter. Holes 0.006 inches in diameter were drilled in the skin 0.016 inches apart. The wires were etched to approximately 0.005 inches in diameter and inserted in the holes. They were then spot welded in place from the outside.

To obtain recovery temperatures a lucite model was constructed to have the same physical dimensions as the heat transfer model. A slotted groove 0.002 inches deep was made on the surface through which the thermocouple wires, etched to 0.003 inches in diameter, were brought. The groove was filled with silver circuit paint and the wires cut

level with the surface. Ten of these junctions were spaced evenly along the cylinder.

The pressures over the model were recorded on manometers using silicone oil with a 20 micron reference pressure. Copper tubing was used throughout to prevent outgasing.

The heat transfer was measured using the transient technique. The temperature time history of the model was recorded on Leeds and Northrup Speedomax recording potentiometers having a full scale response of less than $\frac{1}{4}$ second. The tunnel was equipped with a quick start mechanism that established the flow in about one millisecond. During the run the model was cooled from an initial room temperature to recovery temperature during which period the stagnation temperature varied less than one degree.

To obtain recovery temperatures, the lucite model was used. The tunnel was run until no temperature variation could be detected (until equilibrium was established), then the temperature was recorded.

A dummy model was built for the express purpose of determining the shock wave shape along the windward side by means of schlieren photographs.

To examine the general character of the flow on the leeward side of the model, several exploratory oil trace studies were made. These studies were carried out by injecting a very low viscosity oil through three of the pressure orifices on the model during the test and photographically and visually recording the resulting flow streaks.

THEORETICAL CONSIDERATIONS

The theories available for predicting the pressure distribution over a circular cylinder at angle of attack are limited. Considering the

crossflow pressure distribution, a combination of "modified Newtonian" and Prandtl-Meyer expansion has some theoretical justification and seems to fit experimental results over circular cylinders normal to the flow at lower Mach numbers.

For high angles of attack, the pressure on the windward side or "stagnation line" can be calculated using the normal Mach number approximation which applies to a supersonic leading edge. This body is considered two-dimensional using the normal Mach number and neglecting the parallel flow component. This, of course, assumes a stagnation point. In reality, the neglected parallel flow component (along the body axis) is hypersonic and there is no "stagnation line" for the cylinder at angle of attack. The term, stagnation line, will be used herein to identify this region on the windward side to the model.

To obtain the heat transfer in the crossflow direction, Reshotko (Ref. 4) further simplified the analysis of Cohen and Reshotko (Ref. 5) for prediction of the heat transfer over a two-dimensional body providing the pressure distribution is known. The approximations include a linear viscosity temperature law, perfect gas, constant specific heats, isothermal body and Prandtl number equals a constant. Their analysis is based on Thwaites' concept of unique interdependence between the wall shear, heat transfer, and free stream velocity. To obtain the heat transfer an integral must be evaluated using the experimentally obtained pressure distribution. This was accomplished with the aid of an electronic computer.

Beckwith (Ref. 6) assumed a perfect gas, constant specific heats, similar velocity and temperature profiles through the boundary layer, constant Prandtl number and a constant wall temperature to solve for the

heat transfer along the stagnation line of a yawed cylinder. Beckwith then compared the solutions for the heat transfer coefficient for all yaw angles and obtained the following correlation:

$$h = C_{p_w} \sqrt{\rho_w \mu_w \frac{dw_e}{dz}} \; \frac{0.5}{Pr} \left(\frac{\rho_{se} \mu_{se}}{\rho_w \mu_w} \right)^{0.44}$$

Following the same procedure as Liu (Ref. 7) and assuming that the viscosity is proportional to the 0.647 power of the temperature, the following is obtained:

$$\frac{h_\Lambda}{h_{\Lambda=0}} = \left[\frac{1 + \frac{\gamma-1}{2} M_1^2}{1 + \frac{\gamma-1}{2} M_{N_1}^2} \right]^{0.155} \left[\frac{p_{w_\Lambda}}{p_{w_{\Lambda=0}}} \right]^{0.5} \left[\cos \Lambda \frac{\beta_{M_{N_1}}}{\beta_{M_1}} \right]^{0.5}$$

and by approximating the pressure term by the isentropic pressure relation through a normal shock using the normal Mach number and letting $M_1 \to \infty$, the above equation reduces to:

$$\frac{h_\Lambda}{h_{\Lambda=0}} = \cos^{1.19} \Lambda$$

Liu (Ref. 7) has included some spanwise effects by treating the case of a highly yawed finite cylinder as opposed to the infinite cylinder in the above theory. The solution gives the heat transfer coefficient along the stagnation line as a function of the distance from the origin of the cylinder.

The assumptions include:

1. The shock wave is parallel to the cylinder
2. A Falkner-Skan velocity distribution in the crossflow direction
3. $\rho\mu$ = constant
4. Pr = constant
5. Tw = constant

The three-dimensional boundary layer equations are first transformed by the Dorodnitsyn transformation and then the velocity and enthalpy functions are perturbed from the 90° yaw or zero angle of attack conditions.

The zero order equations were found to reduce to the Blasius equation for which a solution is known. For the first order equations the further assumption that $u_e^2/2He = 1$ is needed to solve the case for Prandtl number not equal to one. It was shown that the solution for different Prandtl numbers varied less than a few percent in the case of a cold wall so that for the present case of a hot wall, the Prandtl number was taken to be equal to one. A similarity transformation was then applied and the equations which resulted were easily solved. It should be noted that the perturbation technique required that

$$\frac{x}{R}\frac{\beta}{2}\cot\Lambda \ll 1$$

for the method to be correct. The solution can be expressed in the form:

$$h_\Lambda = k_w\left(\frac{u_e P_w}{\mu_w T_w R D}\right)^{0.5}\left[\,0.332\sqrt{\frac{D}{x}} + 0.166\,\beta\cot\Lambda\sqrt{\frac{x}{D}}\,\right].$$

DATA REDUCTION

To determine the heat transfer coefficient the following equation was used

$$h = \frac{\rho c}{T_w - T_r} \frac{R_{out}^2 - R_{in}^2}{2 R_{out}} \frac{dT}{dt}$$

This equation represents the solution of the heat equation in polar coordinates and neglects radiation and conduction. This reduces the effective skin thickness by 5½% because of the small scale of the model. From the temperature-time history, the slope at time equal to zero (when the model is isothermal) can be found and from this the heat transfer coefficient can be calculated.

The initial slope was calculated by fitting the curve to an exponential curve and extrapolating back to zero time. A maximum of 2 seconds of data was used to minimize the conduction errors. Considering all possible errors such as data reduction errors, physical properties of the stainless steel, recovery temperatures, and conduction along the model and down the thermocouple wires, the maximum error involved in the results was plus 5% or minus 10% . To reduce the errors in the actual data reduction (determining the initial temperature-time slope) several tests at each point were conducted and each test calculated twice independently. An average of these data, whose scatter was $\pm$ 4%, is presented in the results. For a more complete coverage of the data reduction technique, refer to Ref. 1.

DISCUSSION AND RESULTS

A summary of the shock wave shapes on the windward side of the model for the higher angles of attack is presented in Fig. 3. At $\alpha = 9^\circ$ (Fig. 3a), the shock waves approach a constant standoff distance downstream

of the nose. Similar results were obtained for the lower angles of attack. For $\alpha = 12^{\circ}$ and 15° (Fig. 3b and 3c), the standoff distance first increases reaching a maximum then decreases to a minimum and in some cases gradually increasing as x/R increases. This behavior seems to be a function of the nose drag and angle of attach which was also noticed in Ref. 1. An explanation for this behavior will be offered later.

The pressure distributions over the body are presented on Figure 4. Measurements were obtained at x/R from zero to 24, angles of attack from zero to 15°, and azimuth angles of zero, 45°, 90°, 135° and 180°. On the windward size ($\phi = 0^{\circ}$), the pressure distributions are similar to the zero angle of attack case up to $\alpha = 12^{\circ}$. Then the data show the same minimum observed by the shock wave shapes. At $\phi = 45^{\circ}$ no major changes are observed from the windward side results. For the higher azimuth angles, the changes in pressure from the zero angle of attack case are small compared to windward side except for the flat face at $\phi = 135^{\circ}$ and 180°. The pressure distributions for these two exceptions seem to indicate separated flow or the formation of vortices on the leeward side. At these higher azimuth angles, data at $\alpha = 12^{\circ}$ and 15° again show a minimum pressure located in approximately the same place as for the lower azimuth angles.

The pressure distributions for three nose shapes are compared with each other at $\phi = 0^{\circ}$ and all angles of attack on Fig. 5. At angles of attack greater than 6°, the distinction between the various nose shapes has practically disappeared. This was also noticed at azimuth angles of 45° and 90° but to a lesser extent. At the higher azimuth angles, the values of the pressure obtained were noticed to be distinct functions of

nose shape. On Figs. 5d, 5e and 5f, the theoretical inviscid cone pressure (p_c/p_l) is indicated. The pressure calculated by passing through a normal shock (assumed to be parallel to the body axis) based on the normal Mach number, based on wind tunnel surveys, is indicated by a solid line. The dotted lines represent the pressure based on the local Mach number, normal to the experimentally determined shock wave as opposed to the body axis, passing through a normal shock. It is seen that using the shock wave shape to calculate the normal Mach number gives a better indication of the general trend of the data but its absolute value is incorrect. An explanation for this will be offered later. On Fig. 5f the two-dimensional data from Ref. 1 is plotted, and is in general agreement with the present results.

The pressure distribution in the crossflow direction is plotted at $x/R = 25$ for angles of attack of 6^o, 9^o, 12^o and 15^o on Fig. 6. The solid line on each figure represents the combination of modified Newtonian theory ($p/p_{SL} = \cos^2 \phi$) and a Prandtl-Meyer expansion. The two theories are joined where their slopes are equal. The data are in poor agreement with this "theory" for low normal Mach numbers but, as the normal Mach number becomes greater, the agreement improves. This shows that the Mach number component parallel to the body axis is important at these low angles of attack. On Fig. 6b and 6d , the data of Beckwith and Gallagher (Ref. 9) and Penland (Ref. 10) are plotted matching the normal Mach numbers as closely as possible. Beckwith and Gallagher's data were obtained in air at $Re_D = 1.6$ to 3.5×10^6 on an infinite cylinder at sweepback angles of zero and 90^o for Fig. 6b and 40^o and 45^o for Fig. 6d. Penland's data were obtained in air at $Re_D = 129{,}000$ at a sweepback angle of 75^o and

x/R = 26 for Fig. 6b and at a sweepback angle of 60°and x/R = 22 for Fig. 6d. These results are also in poor agreement with the present data due to the huge difference in parallel Mach number components. Data from Ref. 1 are presented on Fig. 6d and are in good agreement with the present data. The present results for x/R = 5 and 15 were found to be similar to the data presented.

A summary of the heat transfer distribution over the body is presented on Fig. 7. The data follow the same general trend as the pressure distribution with the exception of additional slight decrease in the heat transfer observed far away from the nose at $\alpha = 15^{\circ}$ and $\phi = 0^{\circ}$. Nevertheless, on the windward side the data show the same maximums and minimums as were observed on the shock wave shapes and pressure distributions. The data presented are the average of two or more independent tests whose scatter were less than $\pm$ 4%.

The three nose shapes are compared with each other at $\phi = 0^{\circ}$ over the angle of attack range on Fig. 8. At angles of attack greater than 6°, the various nose shapes have no major effects on the data over the body as was also noticed for the pressure distribution. This was also noticed but to a lesser extent for the other azimuth angles. For angles of attack of 3°, 6°, 9°, 12° and 15°, the data are compared with the theories of Liu and Beckwith. Beckwith's theory is for $M_1 \rightarrow \infty$ and if the actual pressure distribution were used or the pressure calculated by the normal Mach number hypothesis the theoretical results would even be higher. The value used for $h_{\Lambda=0}$ was 0.137 BTU/ft^2 sec °R, calculated from Ref. 11.

The modified version of Liu's theory was obtained by evaluating the properties at the edge of the boundary layer. This was done by using the measured pressure distribution and assuming isentropic flow over the body from the stagnation point. Since the differences for the three nose shapes were less than 2%, only one curve is presented. Within the limits of the theory (small x/R) the modified version of Liu's theory is in fair agreement with the present data. For the quantity $\frac{x}{R}\frac{\beta}{2}\cot\Lambda$ to be less than 0.5 the theory should be cut off at an x/R of 20, 10, 7, 5, and 4 for $\alpha = 3^{\circ}$, 6°, 9°, 12° and 15°, respectively. On Fig. 8f, the two-dimensional data corrected for Reynolds number at the stagnation line of the body are presented and are in good agreement with the present data.

The heat transfer distribution is plotted at x/R = 25 and compared with theory in the crossflow direction for angles of attack from 6° to 15° on Fig. 9. The solid line represents the theory of Ref. 4 calculated using the measured pressure distributions and is in good agreement with the data. The variation of the theory between the different nose shapes or by evaluating the quantities at the edge of the boundary layer was less than 2%. Data from Ref. 1 are presented on Fig. 9d and are in fair agreement with the present data. The present results for x/R = 5 and 15 were found to be similar to the data presented.

The cause of the unique shapes of the shock wave shape, pressure distribution and heat transfer distribution at high angles of attack on the windward side of the body can be answered by considering the entropy layer. As was mentioned in the introduction, the entropy layer which forms over a body is only a function of the nose shape and, in hypersonic

flow, completely determines the flow properties over the after body. As the angle of attack increases, the after body will eventually break through this layer and the flow properties on the body will now be determined by the local external flow. The edge of the entropy layer (defined by the edge of the low density region where the relation $cD_N = \pi p_b(y_{en}^2 - y_b^2)$ holds) has been solved (Ref. 2) and is presented on Fig. 10 for the cone, hemisphere and flat face. The dashed lines on these curves represent the edge of the body as it is rotated about the nose through the angles of attack. The break through points are clearly defined for the hemisphere and flat face while for the cone at $\alpha = 12^\circ$ and 15° they are not. It must be remembered here that the theory which defined this entropy layer is not expected to hold for low nose drag coefficients such as the cone since a primary assumption is that a strong bow shock exists.

The various shapes of the shock wave, pressure distribution and heat transfer distribution are compared at $\alpha = 12^\circ$ and 15° on Fig. 11. The first decrease in the pressure and heat transfer curves is similar to the zero angle of attack case which is definitely in the entropy layer. The minimum point and increase of these curves can be considered the break through point and finally the curves level off or reach a maximum where two-dimensional effects become important. The shock wave shape undergoes the transition further downstream since the body is first affected by the break through which must in turn propagate downstream to the shock wave. It can be observed that as the nose bluntness increases or the angle of attack decreases, the minimum points of the curves definitely move downstream which is exactly what the entropy layer considerations predict. Finally, if one considers the inflection point of the heat transfer and pressure curves between the minimum and maximum points as the break through points, the present explanation predicts these points with excellent accuracy for the hemisphere and flat face nose shapes.

To further examine the leeward side of the model with respect to the possibility of boundary layer separation, some oil trace studies were undertaken. A small amount of very thin oil was injected through a pressure orifice and the resulting streak was observed. This technique gives the flow direction at the surface of the model but, of course, does not define the stream direction. For both $\phi = 90^{\circ}$ and 135°, the flow direction was observed to be slightly in the direction of $\phi = 180^{\circ}$ and substantially in the downstream direction with the exception of a very small region behind the shoulder of the flat face nose. Since no characteristic "dividing streamline" or back flow in the parallel direction was observed, it is assumed that the boundary layer remained attached over most of the model. This can also be established by the fact that no drastic reduction in heat transfer occurred over the body (see Figs. 9a-9d) which is characteristic of laminar boundary layer separation. At $\phi = 180^{\circ}$, the flow was observed to be slightly in the radial direction. This presents the possibility of a slight separation in the radial direction as is observed on a delta wing at angle of attack but the effect of this separation is too small to be examined on the present scale; note the heat transfer and pressure distribution results.

CONCLUSIONS

1. On the windward side, the normal Mach number hypothesis agrees with the pressure distribution for high angles of attack and large x/R.
2. Theories for predicting the crossflow pressure distribution are poor due to the large parallel Mach number.
3. The various nose shapes have little effect on the pressure and heat transfer distributions on the windward side at angles of attack greater than 3°.

4. Liu's theory for predicting the heat transfer on the windward side is in good agreement with the experimental results when the quantities are evaluated at the edge of the boundary layer.

5. If the crossflow pressure distribution is known, Cohen and Reshotko's theory is an excellent means for calculating the heat transfer coefficient.

6. The variation of the shock wave shapes, pressure and heat transfer distributions can be predicted by entropy layer considerations.

7. Both the pressure distribution and heat transfer data from Ref. 1 are in good agreement with the present results.

BIBLIOGRAPHY

1. Horstman, C. C. and Vas, I. E.: The Flow About the Leading Edge of a Swept Blunt Plate at Hypersonic Speeds. PUAED 616, August 1962; also ARL 62-405, August 1962.

2. Horstman, C. C.: The Flow Over a Cylinder With Various Nose Shapes at Zero Angle of Attack at Hypersonic Speeds. PUAED 627, September 1962; to be published as ARL report.

3. Ladzhenskii, M. D.: Hypersonic Rule of Areas. Eng. Journal No. 1, 1961 (in Russian).

4. Reshotko, Eli: Simplified Method for Estimating Compressible Laminar Heat Transfer with Pressure Gradient. NACA TN 3888, December 1956.

5. Cohen, Clarence B. and Reshotko, Eli: The Compressible Laminar Boundary Layer with Heat Transfer and Arbitrary Pressure Gradient. NACA Report 1294, 1956.

6. Beckwith, I. E.: Similar Solutions for the Compressible Boundary Layer on a Yawed Cylinder with Transition Cooling. NACA TN 4345, 1958.

7. Liu, J. T. C.: Heat Transfer to the Stagnation Line Region of a Swept Wing with Cylindrical Leading Edge. Convair Report ZA-321, September 1959.

8. Hammitt, A. G. and Bogdonoff, S. M.: The Princeton University Helium Hypersonic Tunnel and Preliminary Results Above M = 11. PUAED 260, June 1954; also WADC TR 54-124, July 1954.

9. Beckwith, I. E. and Gallagher, J. J.: Local Heat Transfer and Recovery Temperatures on a Yawed Cylinder at a Mach Number of 4.15 and High Reynolds Numbers. NASA TR R-104, 1961.

10. Penland, J. A.: Aerodynamic Characteristics of a Circular Cylinder at a Mach Number 6.86 and Angles of Attack up to 90°. NACA RM L54A14, March 1954.

11. Reshotko, Eli and Cohen, C. B.: Heat Transfer at the Forward Stagnation Point of Blunt Bodies. NACA TN 3513, July 1955.

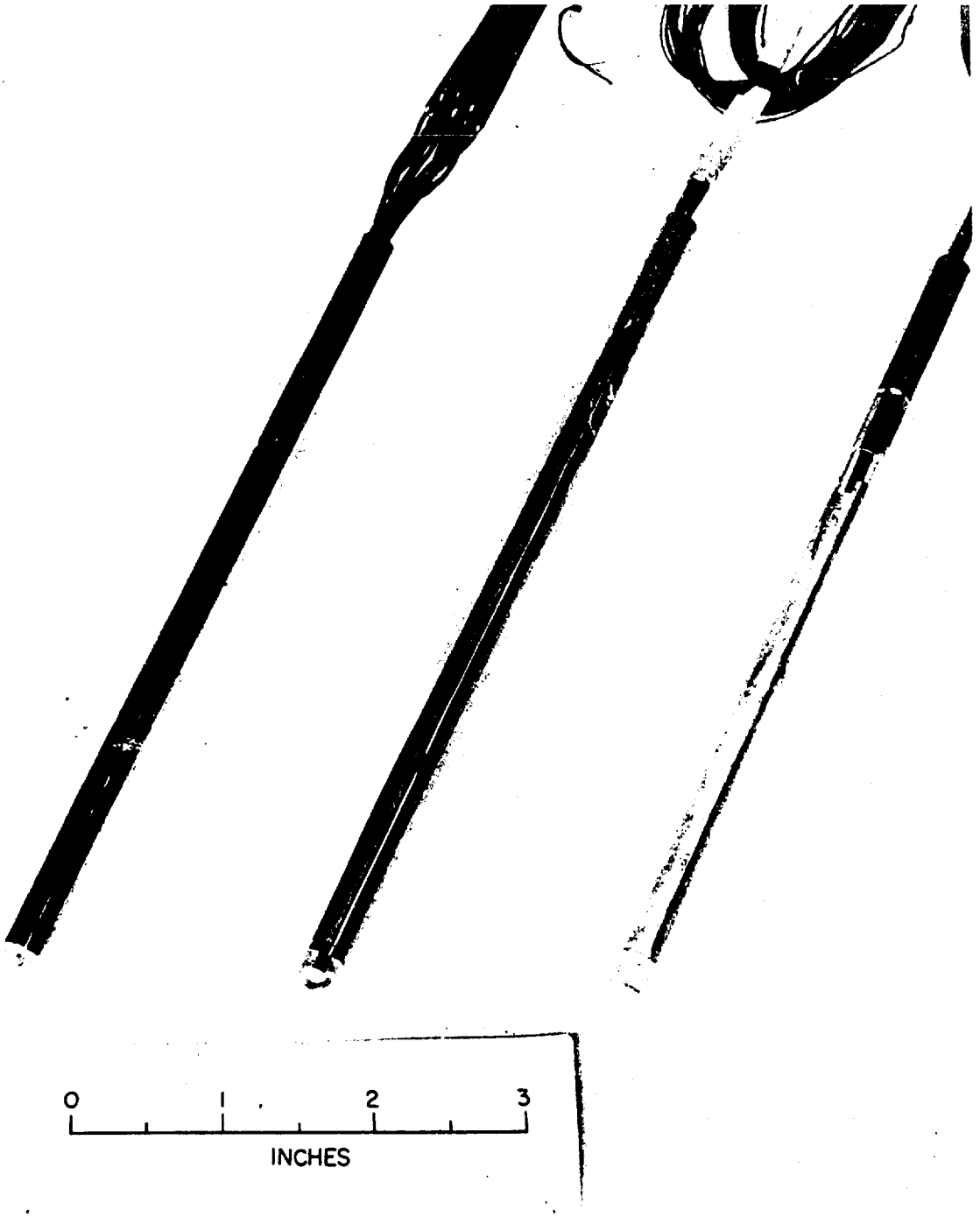

Figure 1. The pressure (left), heat transfer (center), and recovery (right) models with the various nose shapes.

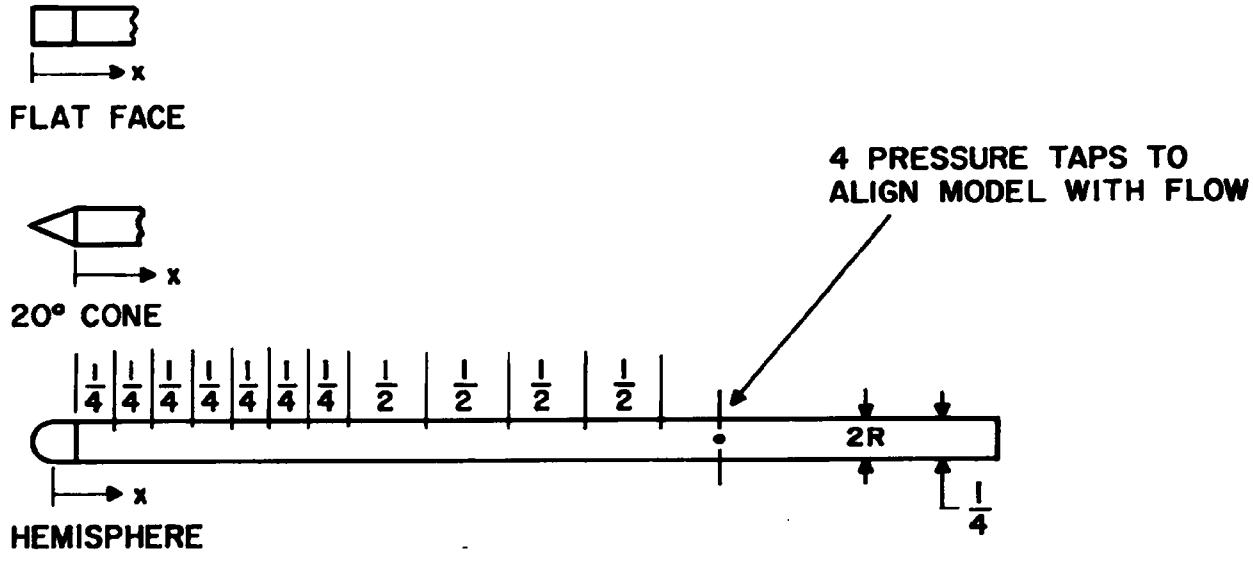

Figure 2. Location of pressure orifices and thermocouples.

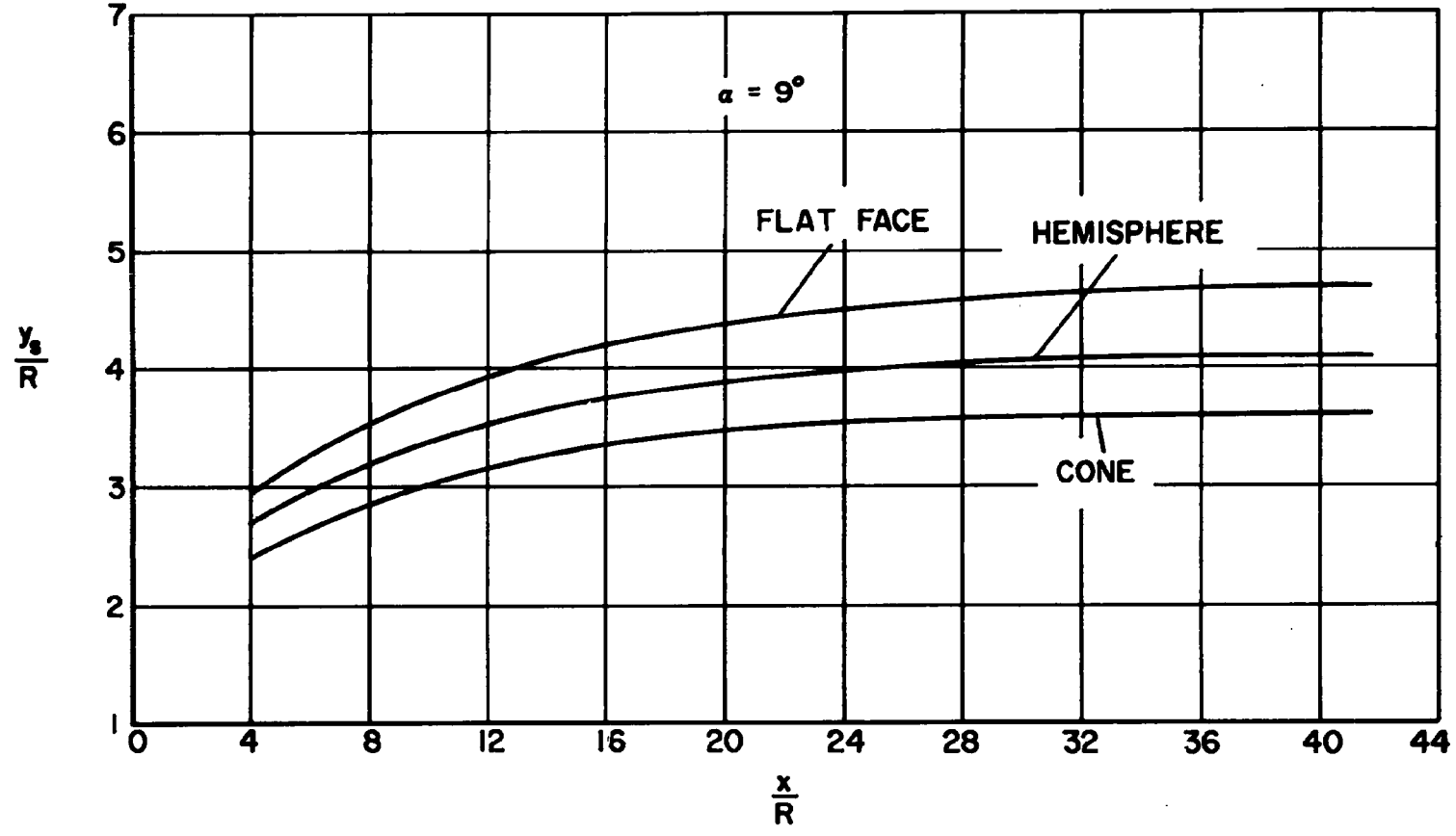

Figure 3a. Shock wave shapes at $\alpha = 9^{\circ}$, $\phi = 0^{\circ}$.

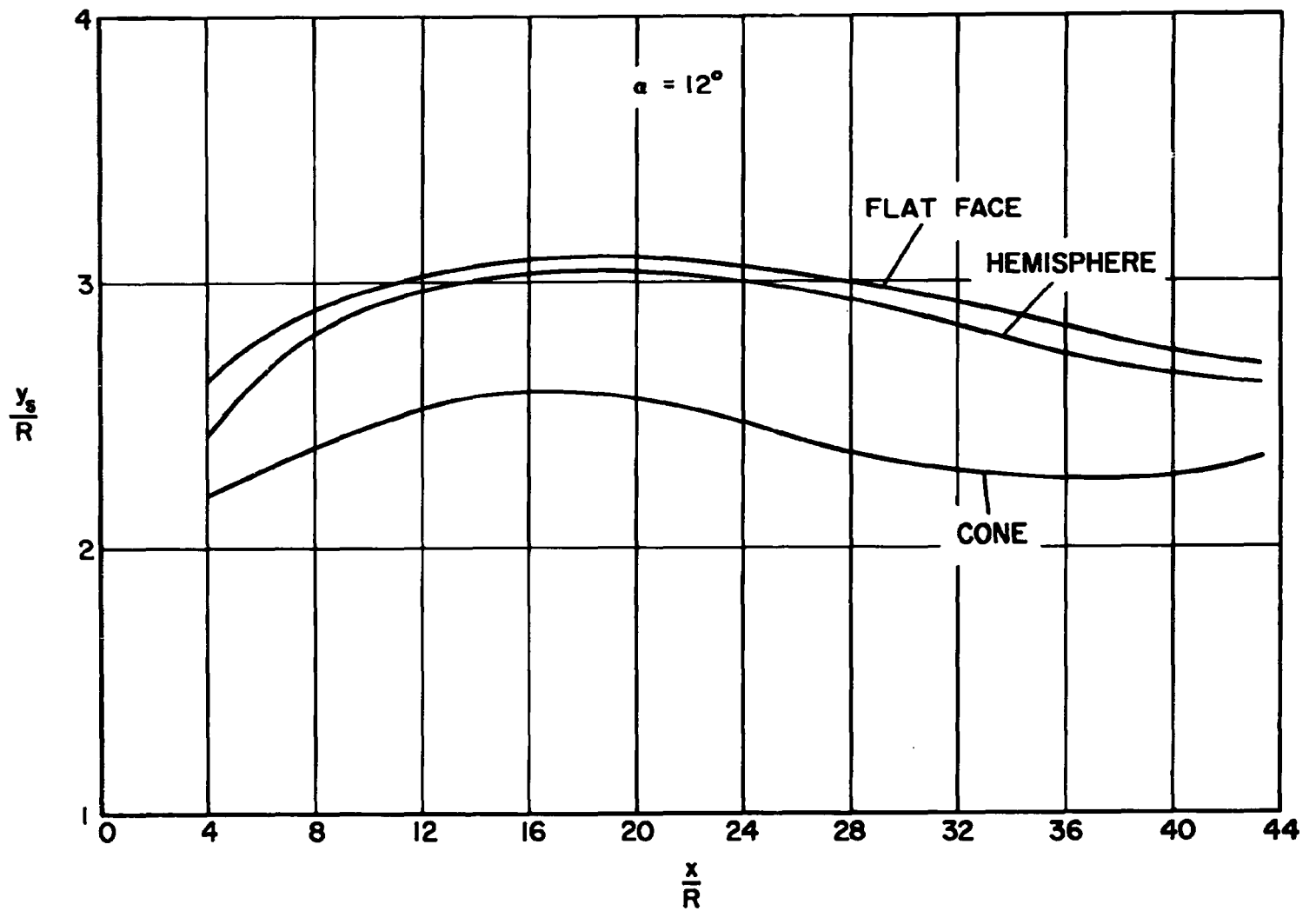

Figure 3b. Shock wave shapes at $\alpha = 12^{\circ}$, $\phi = 0^{\circ}$.

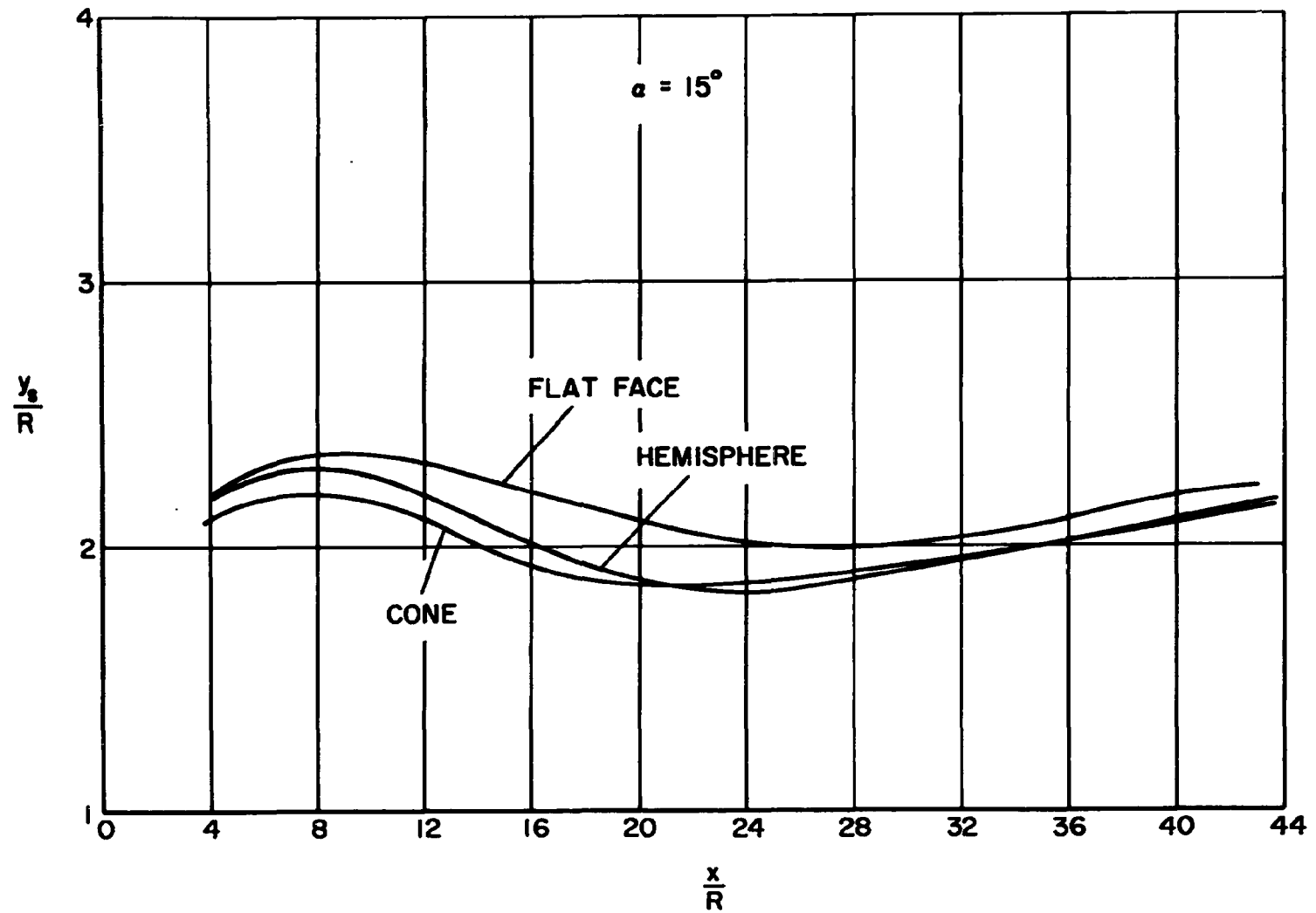

Figure 3c. Shock wave shapes at $\alpha = 15^{\circ}$, $\phi = 0^{\circ}$.

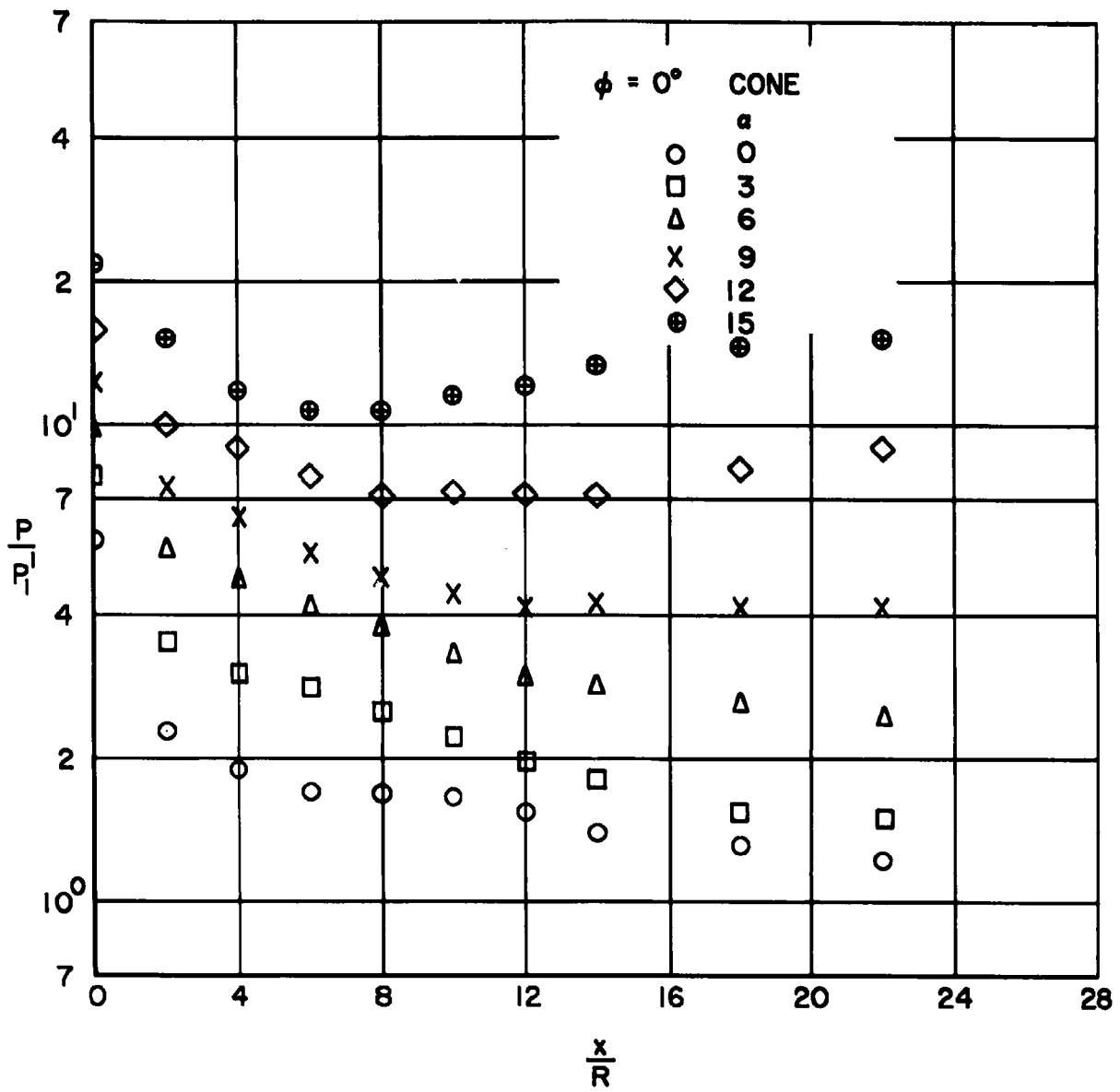

Figure 4a. Pressure distributions for conical nose at $\phi = 0^{o}$.

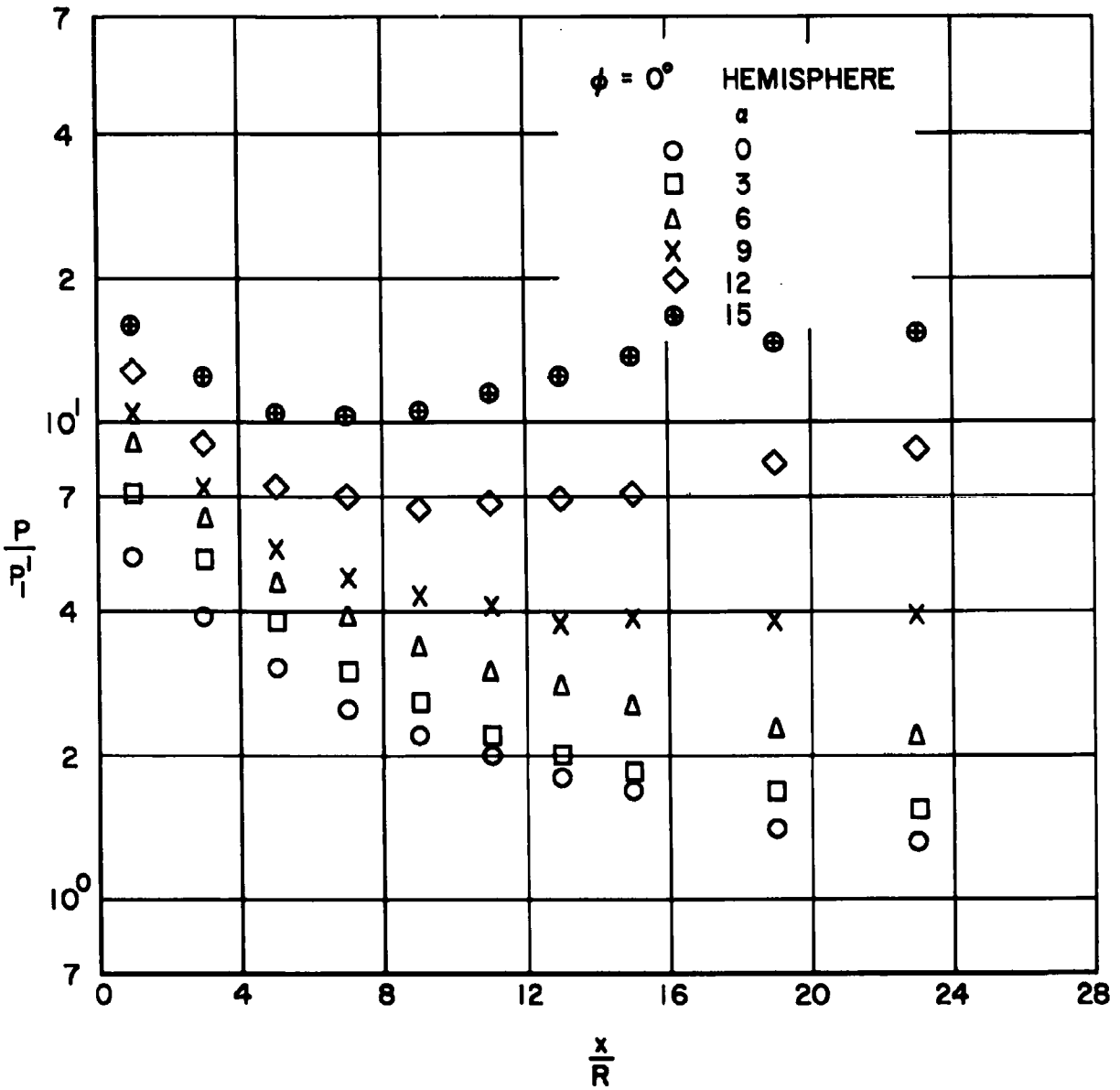

Figure 4b. Pressure distributions for hemispherical nose at $\phi = 0^\circ$.

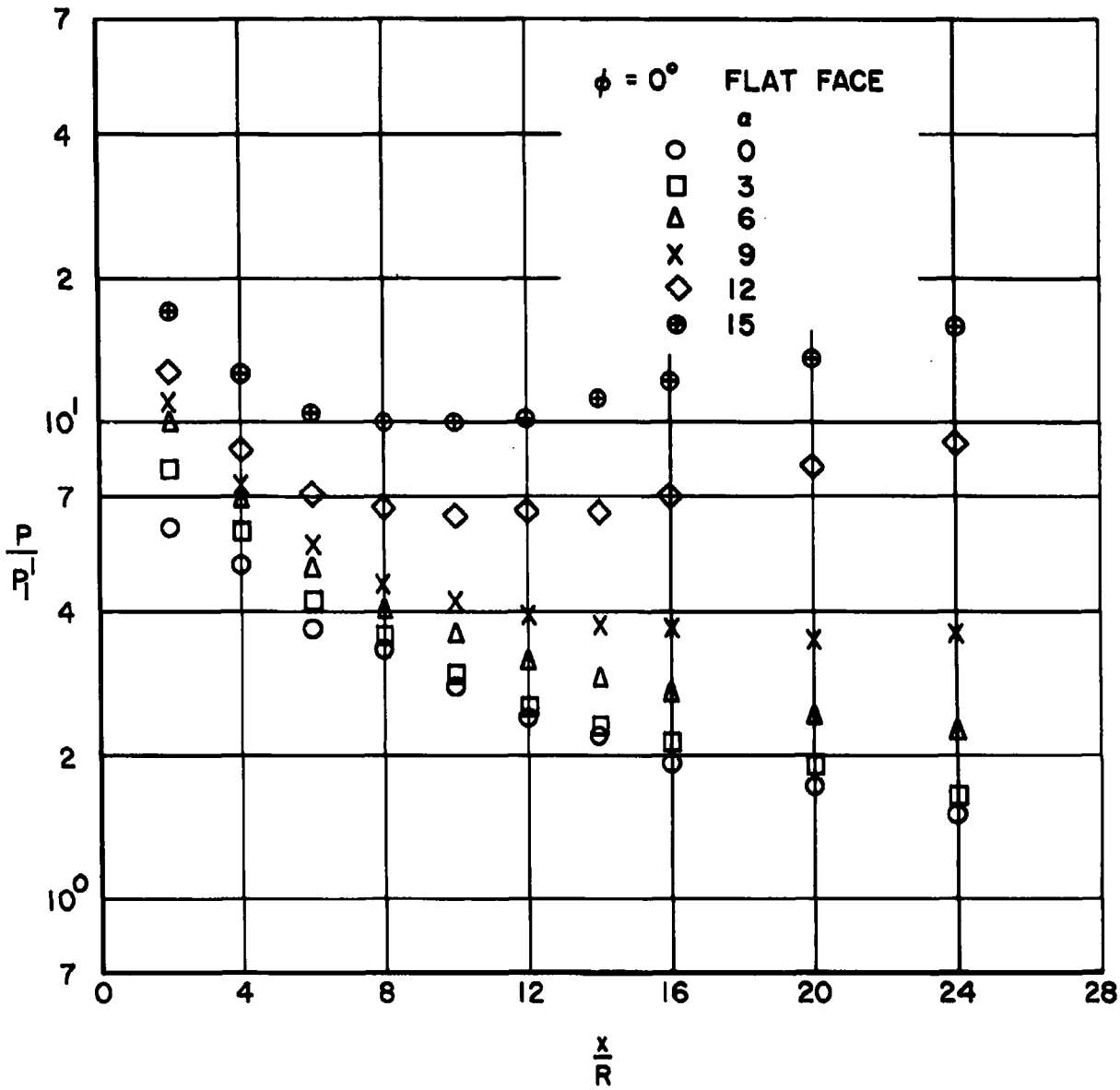

Figure 4c. Pressure distributions for flat faced nose at $\phi = 0^{\circ}$

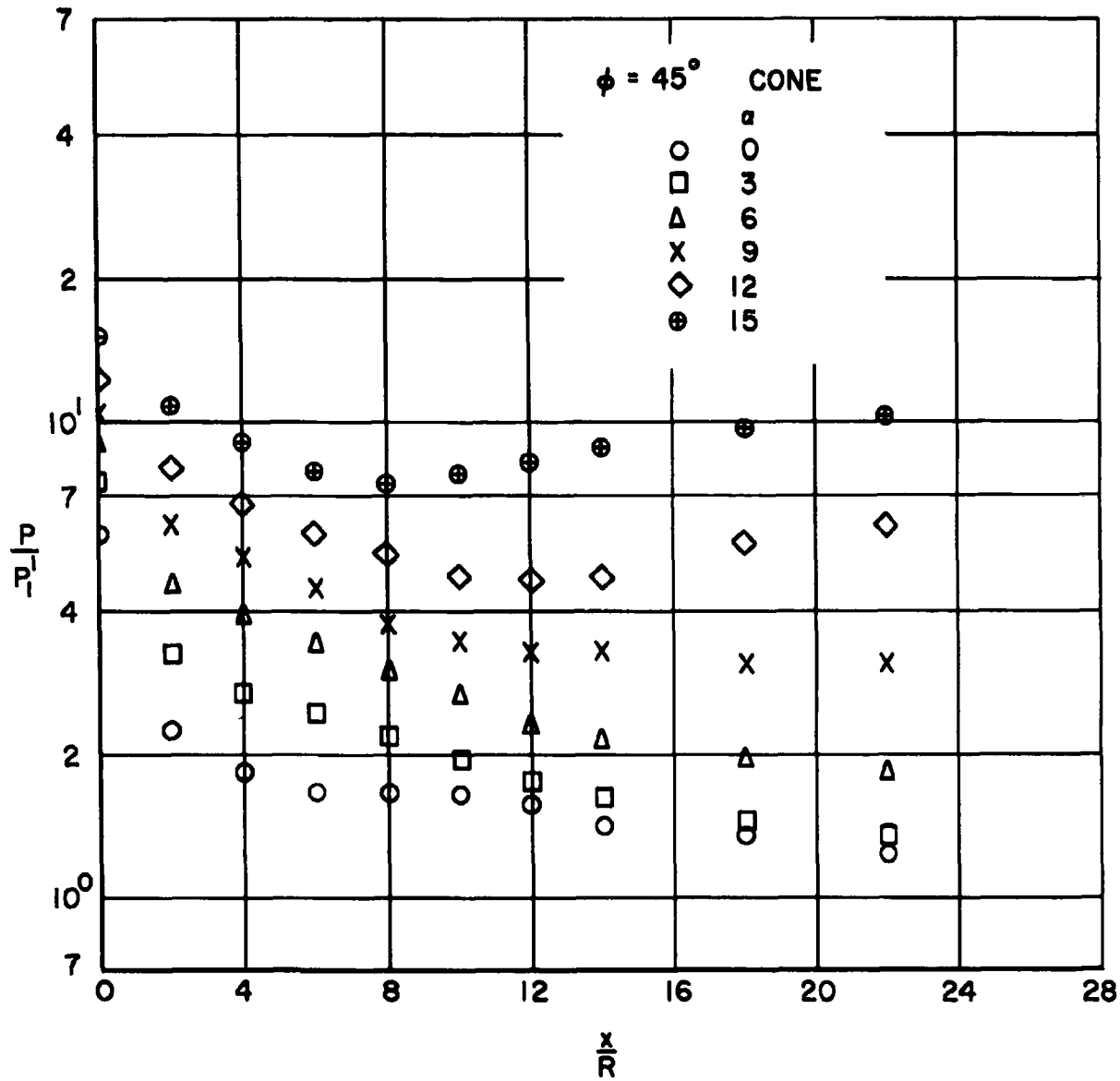

Figure 4d. Pressure distributions for conical nose at $\phi = 45^{\circ}$.

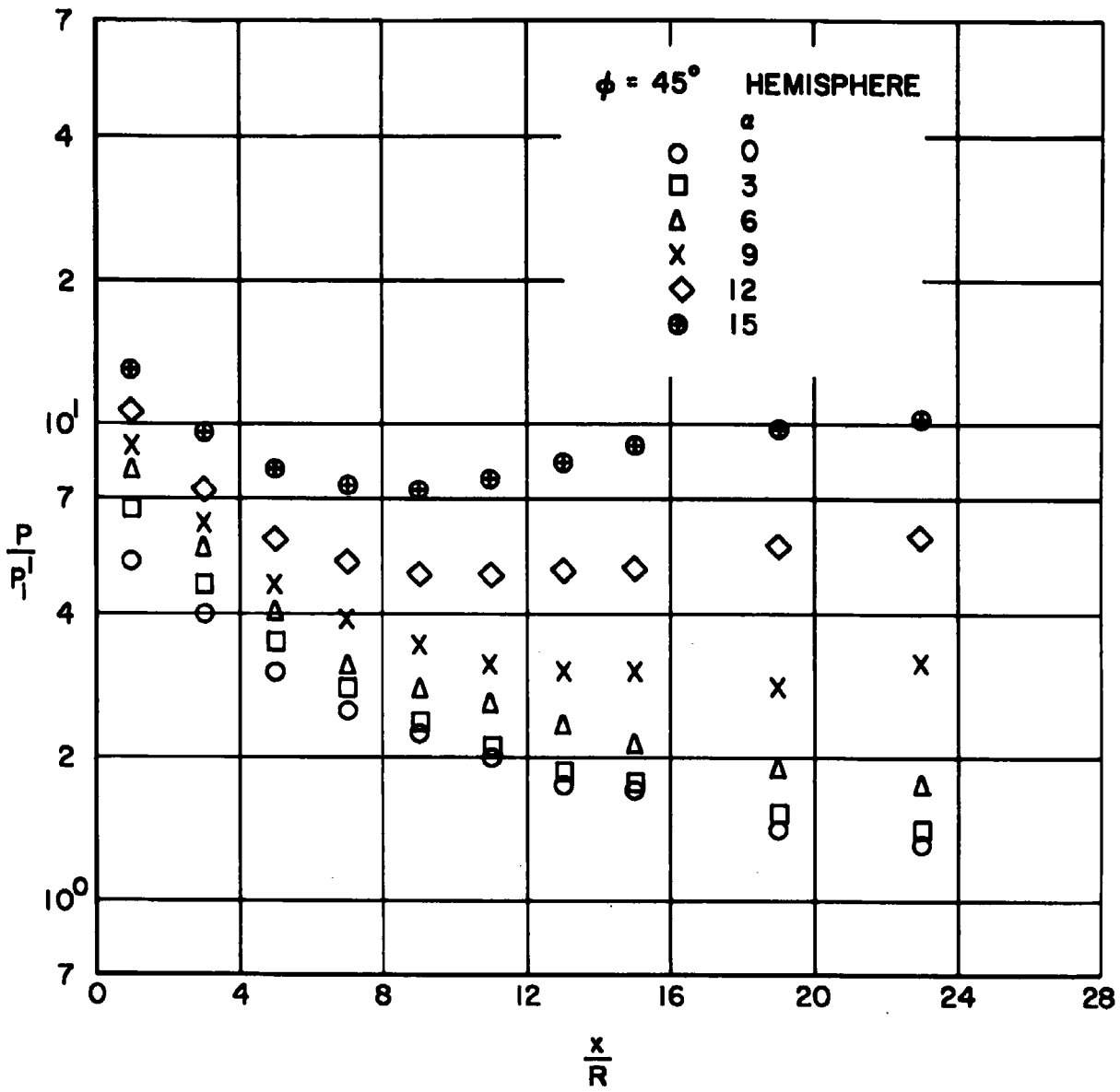

Figure 4e. Pressure distributions for hemispherical nose at $\phi = 45^{\circ}$.

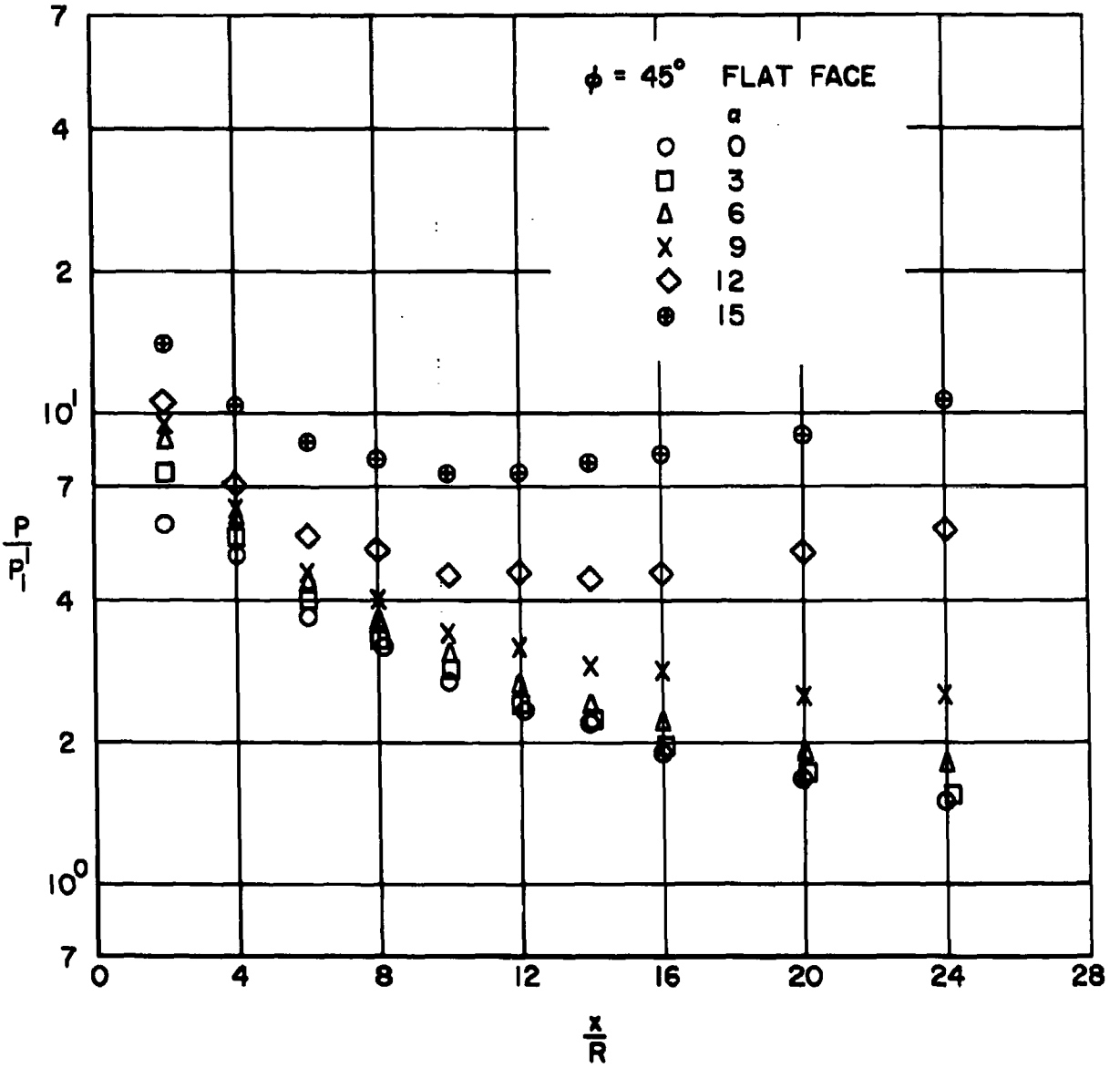

Figure 4f. Pressure distributions for flat faced nose at $\phi = 45^{\circ}$.

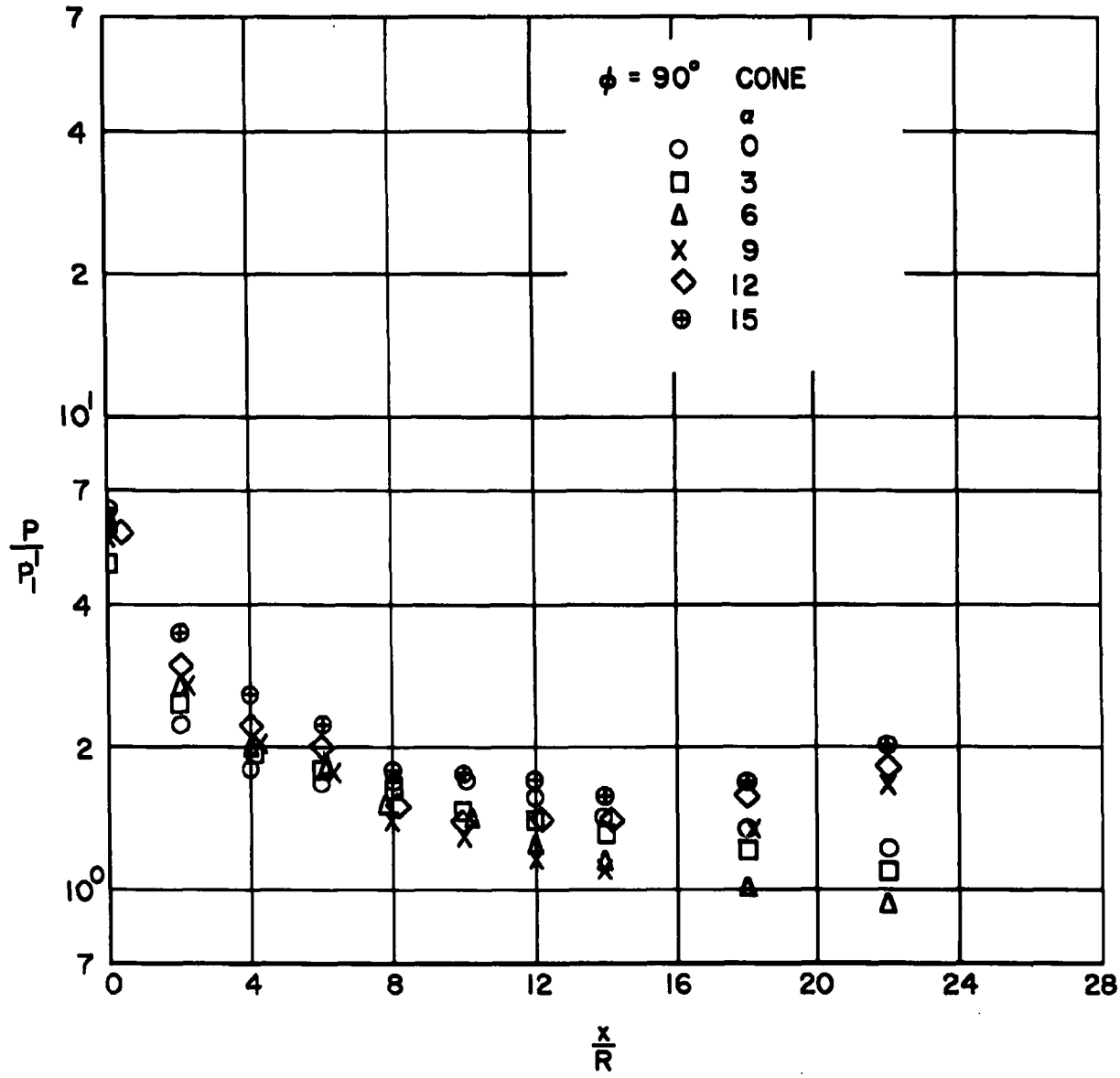

Figure 4g. Pressure distributions for conical nose at $\phi = 90^{\circ}$.

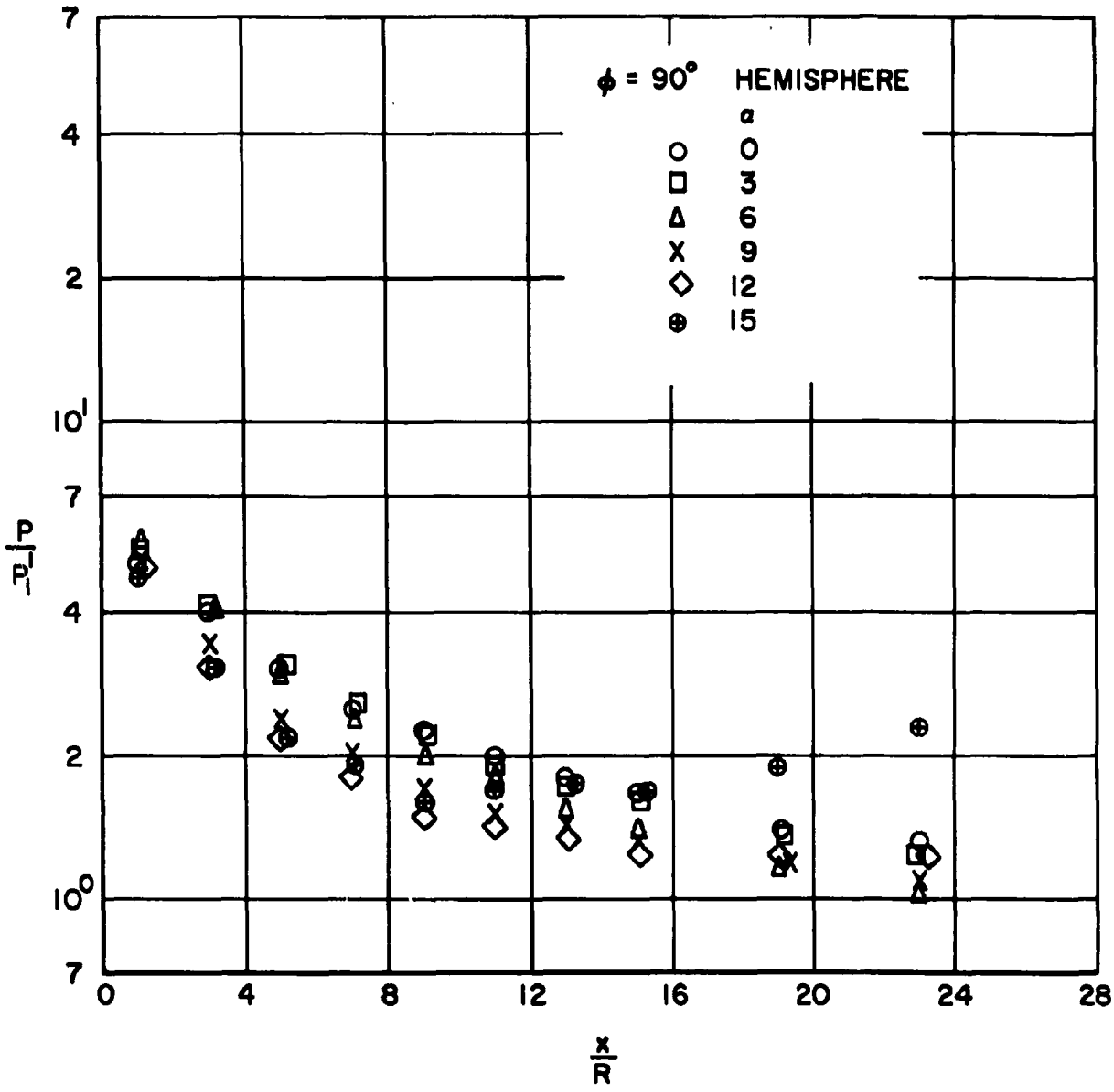

Figure 4h. Pressure distributions for hemispherical nose at $\phi = 90^{\circ}$.

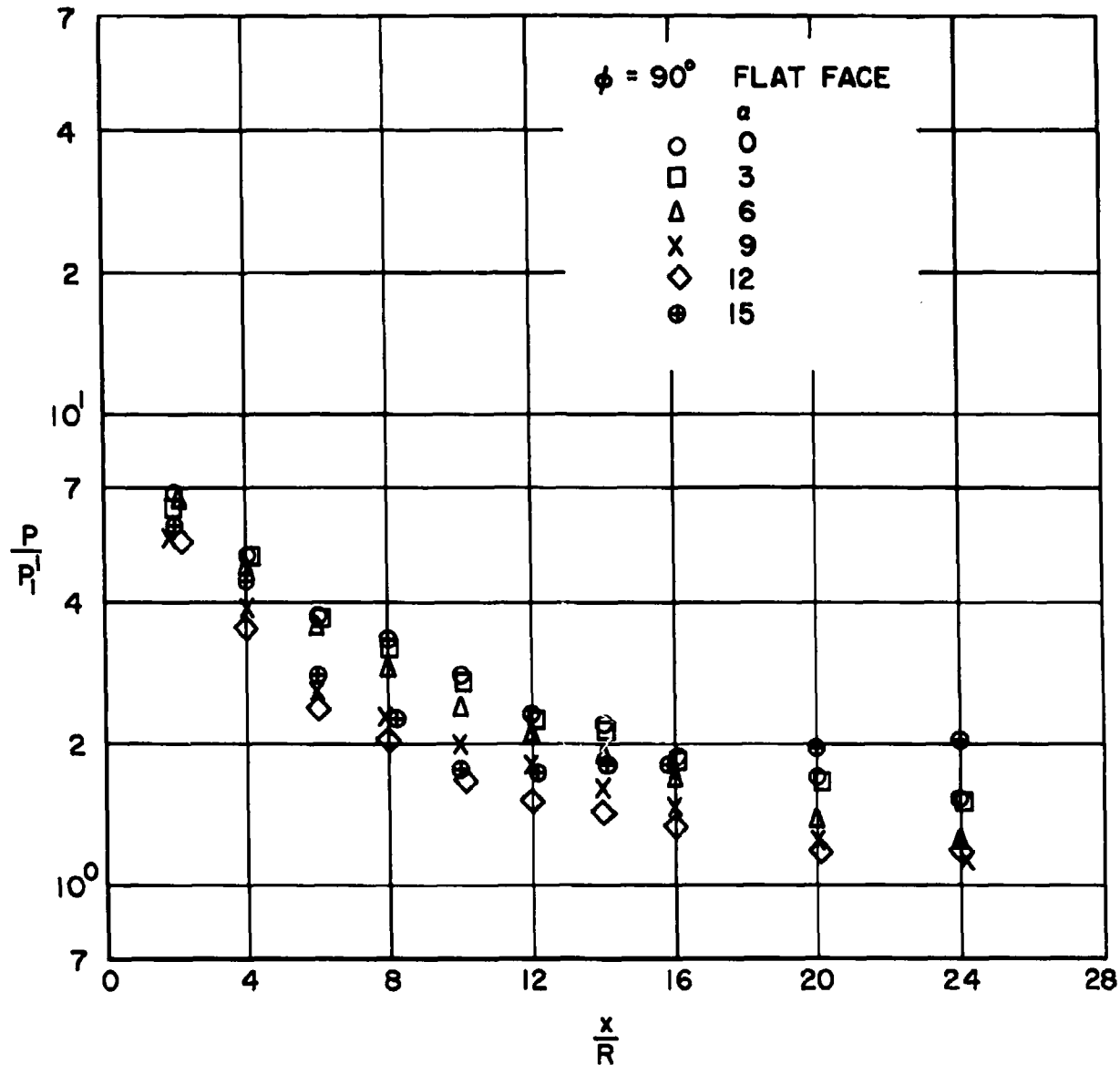

Figure 4i. Pressure distributions for flat faced nose at $\phi = 90^{\circ}$.

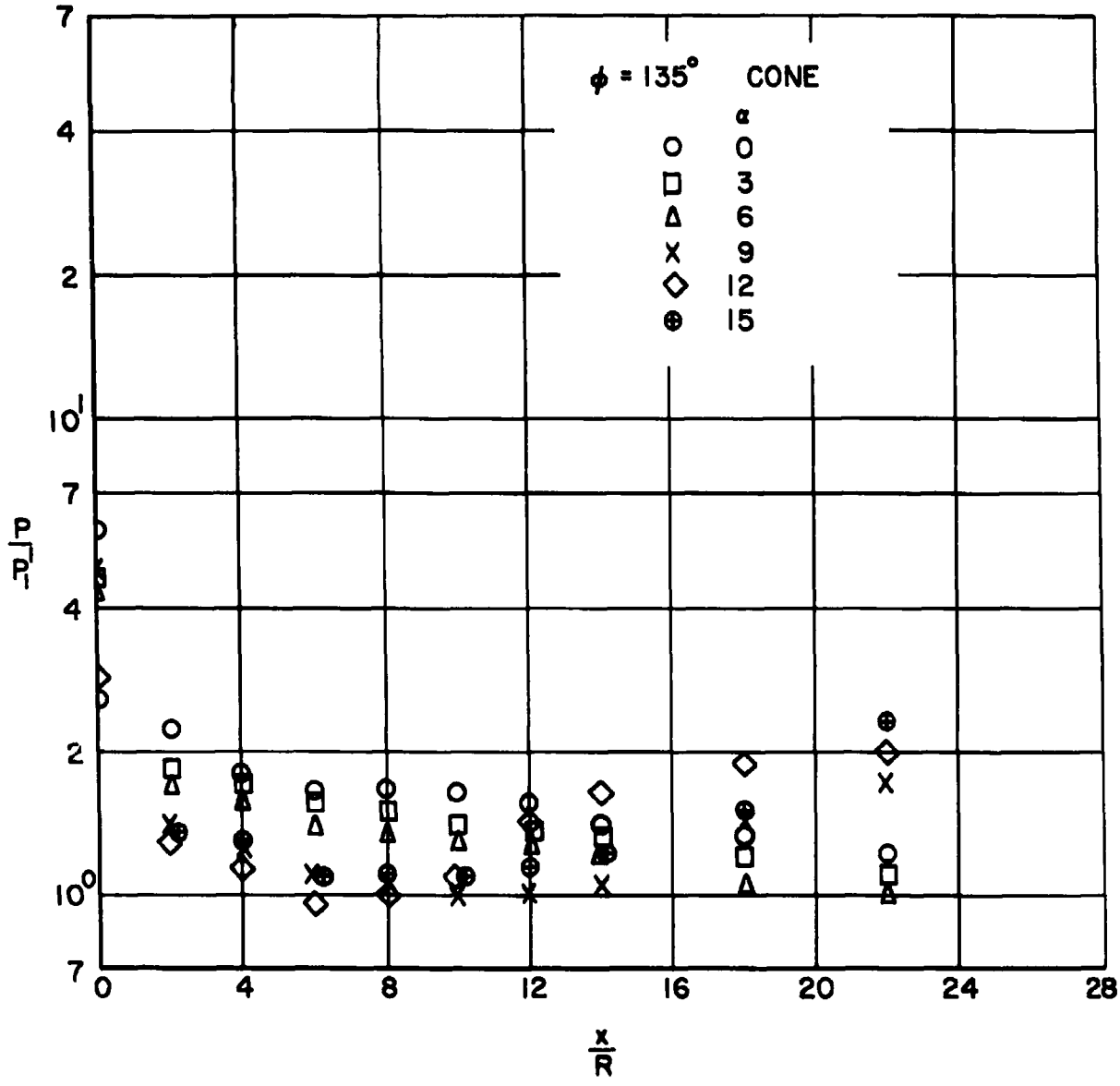

Figure 4j. Pressure distributions for conical nose at $\phi = 135^\circ$.

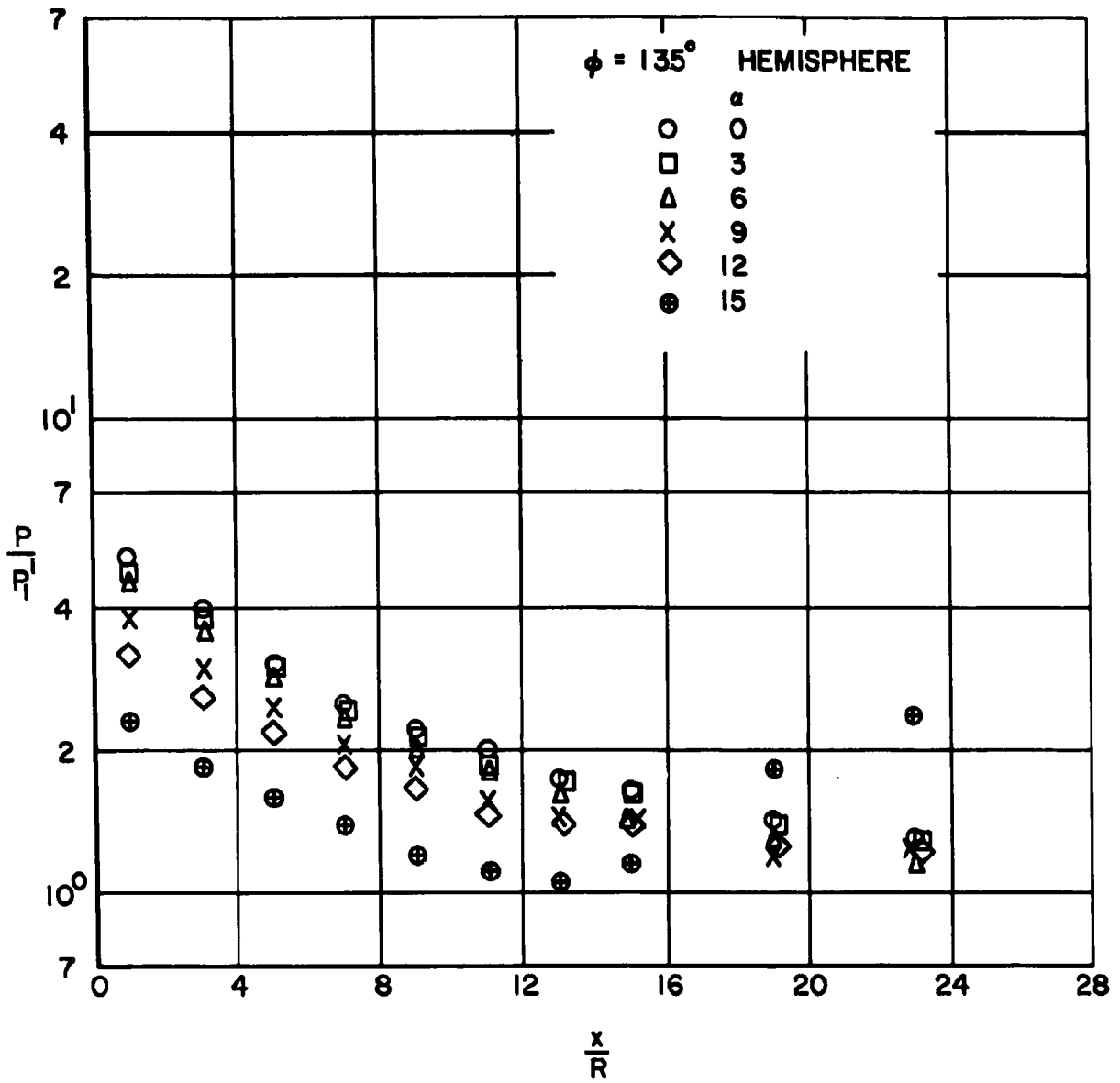

Figure 4k. Pressure distributions for hemispherical nose at $\phi = 135^{\circ}$.

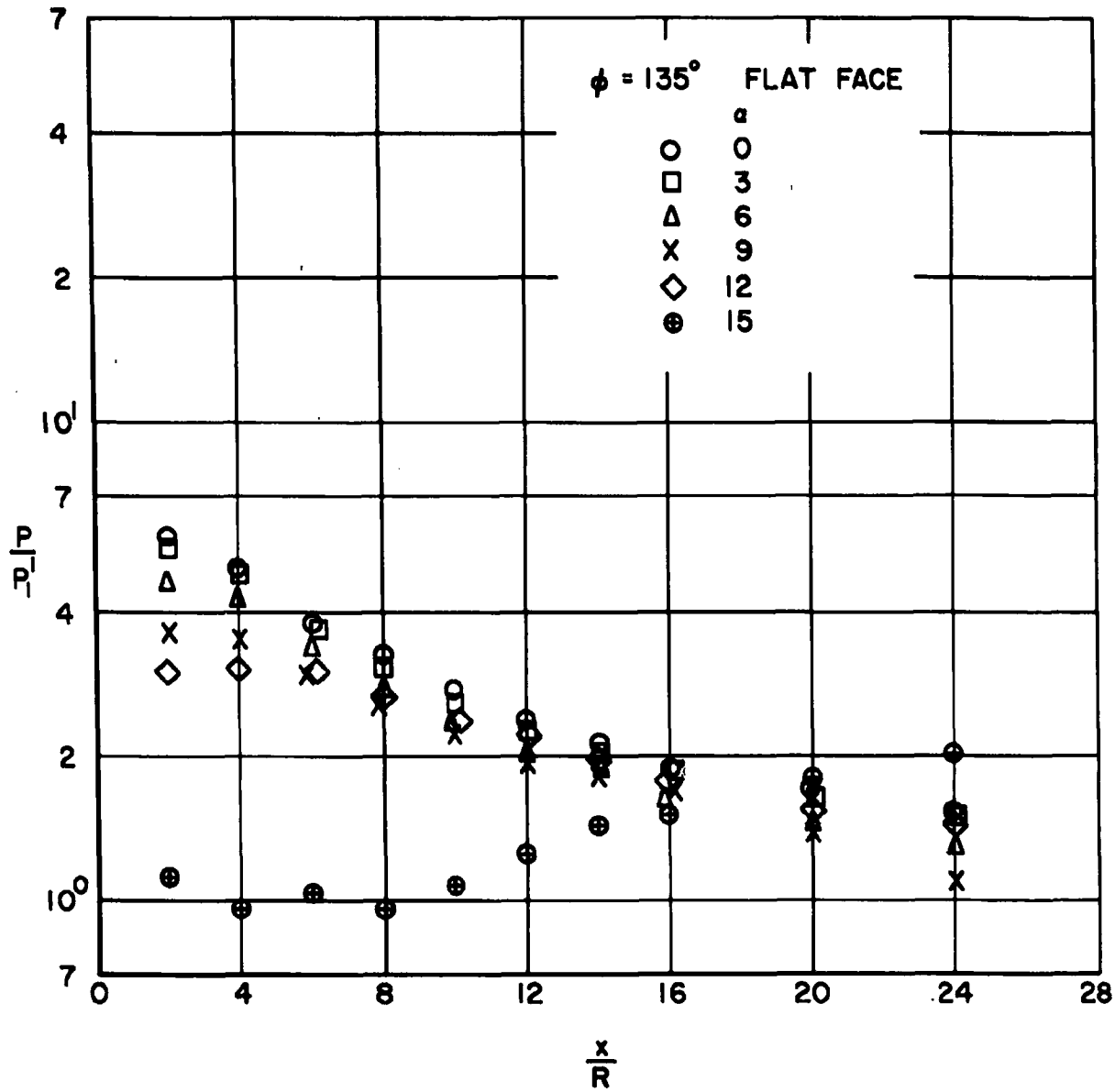

Figure 4ℓ. Pressure distributions for flat faced nose at $\phi = 135^{\circ}$.

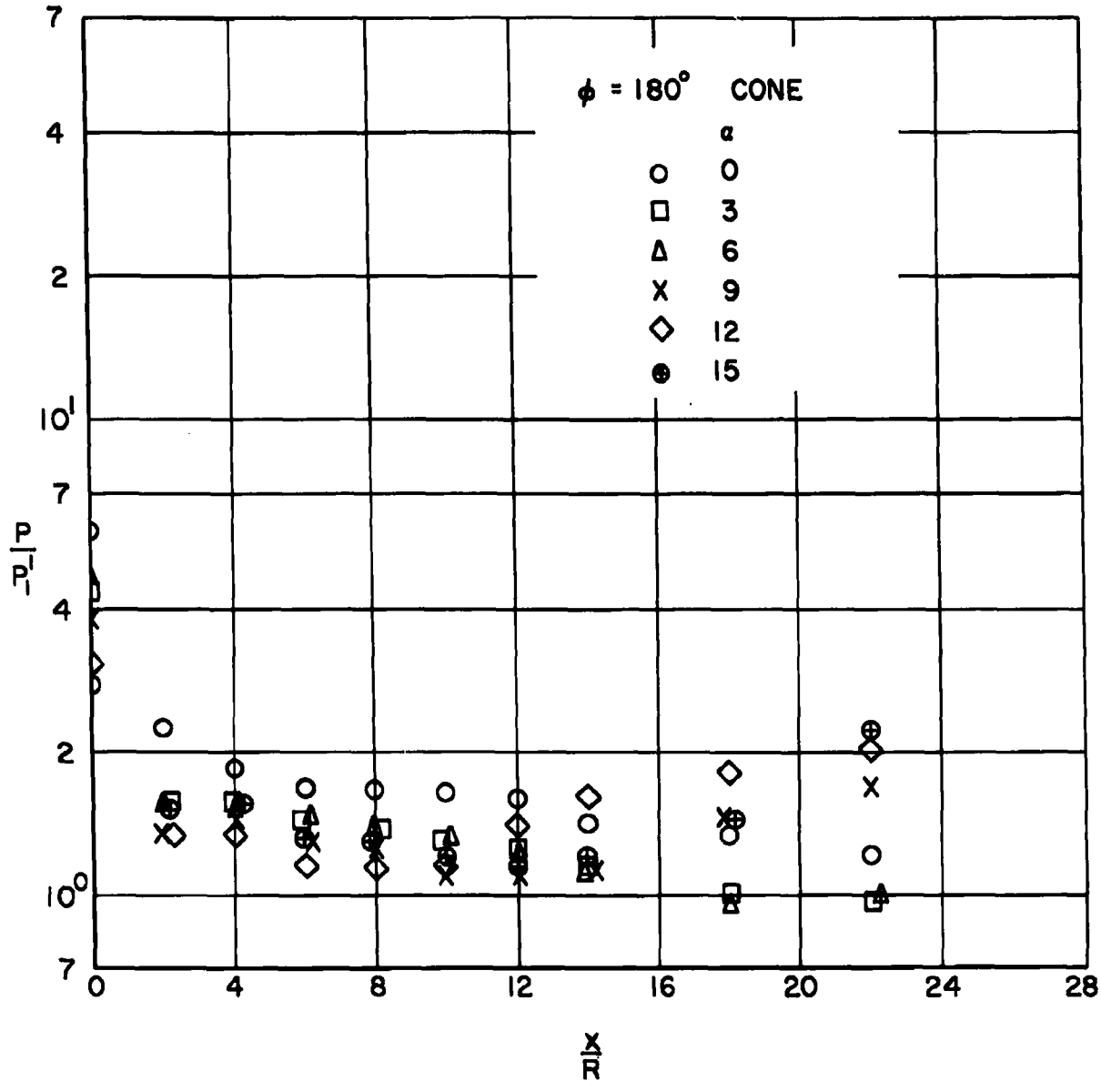

Figure 4m. Pressure distributions for conical nose at $\phi = 180^{\circ}$.

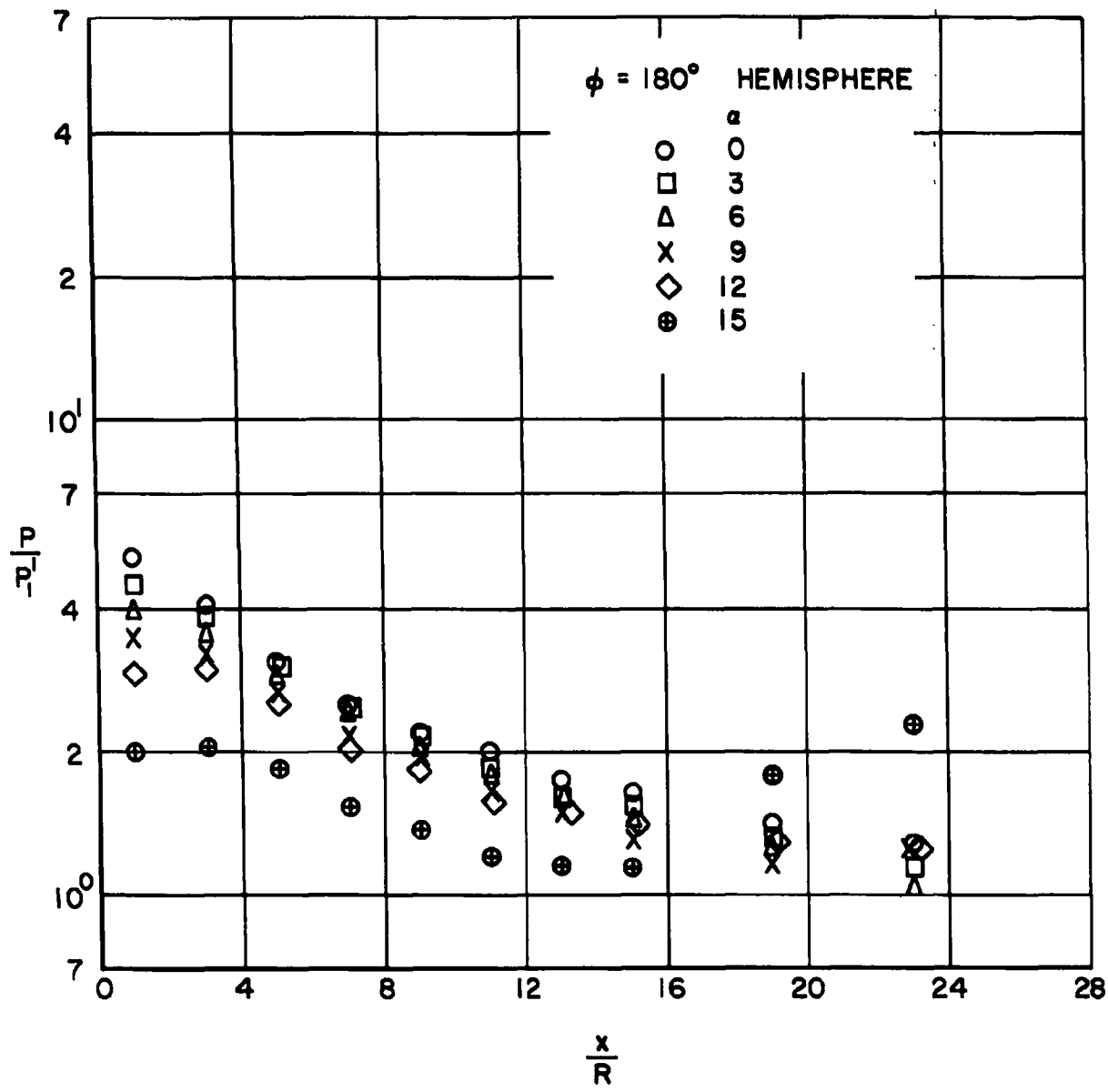

Figure 4n. Pressure distributions for hemispherical nose at $\phi = 180^{\circ}$.

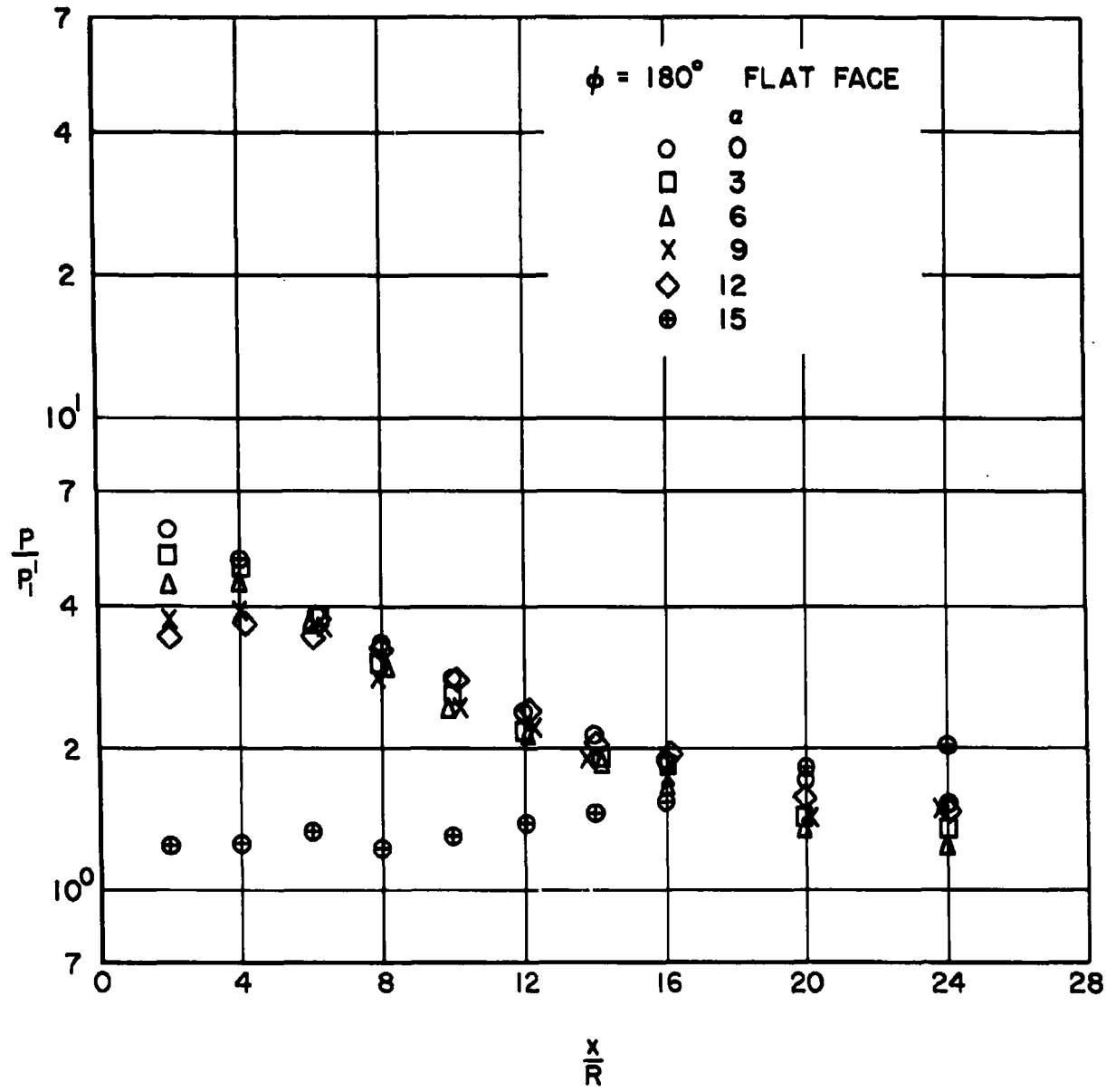

Figure 40. Pressure distributions for flat faced nose at at $\phi = 180^{\circ}$.

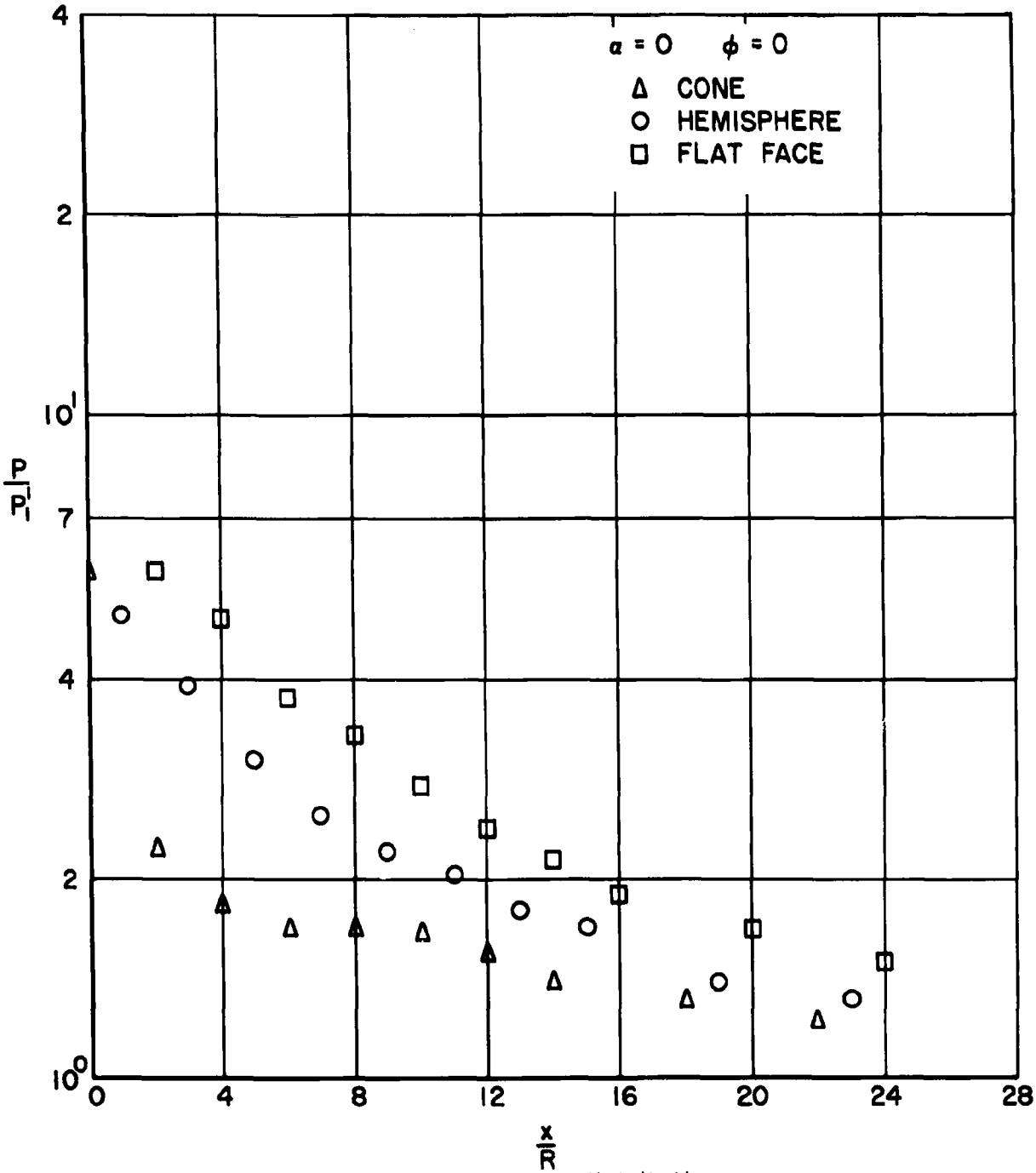

Figure 5a. Summary of pressure distributions at $\alpha = 0^{\circ}$, $\phi = 0^{\circ}$.

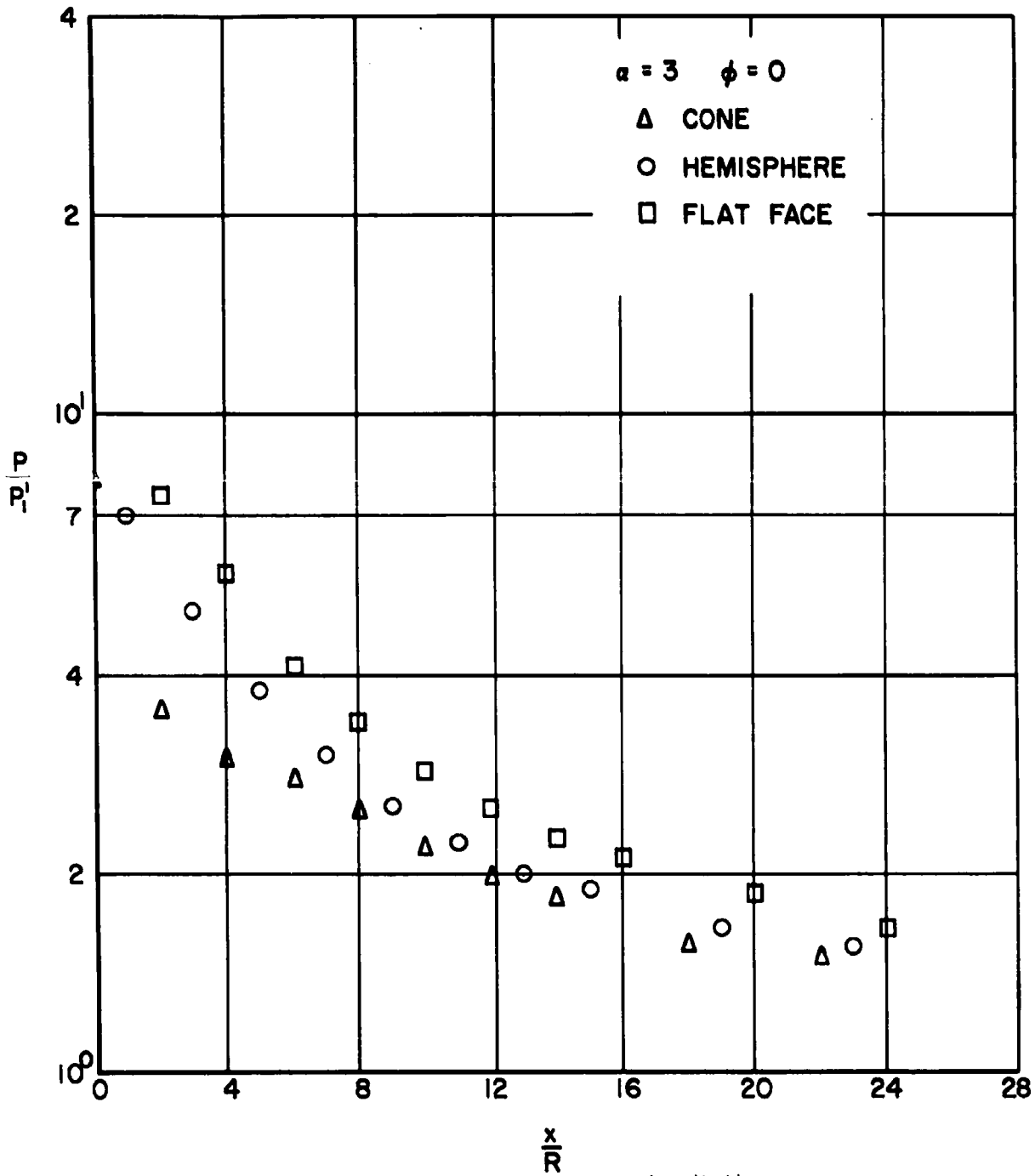

Figure 5b. Summary of pressure distributions at $\alpha = 3^{o}$, $\phi = 0^{o}$.

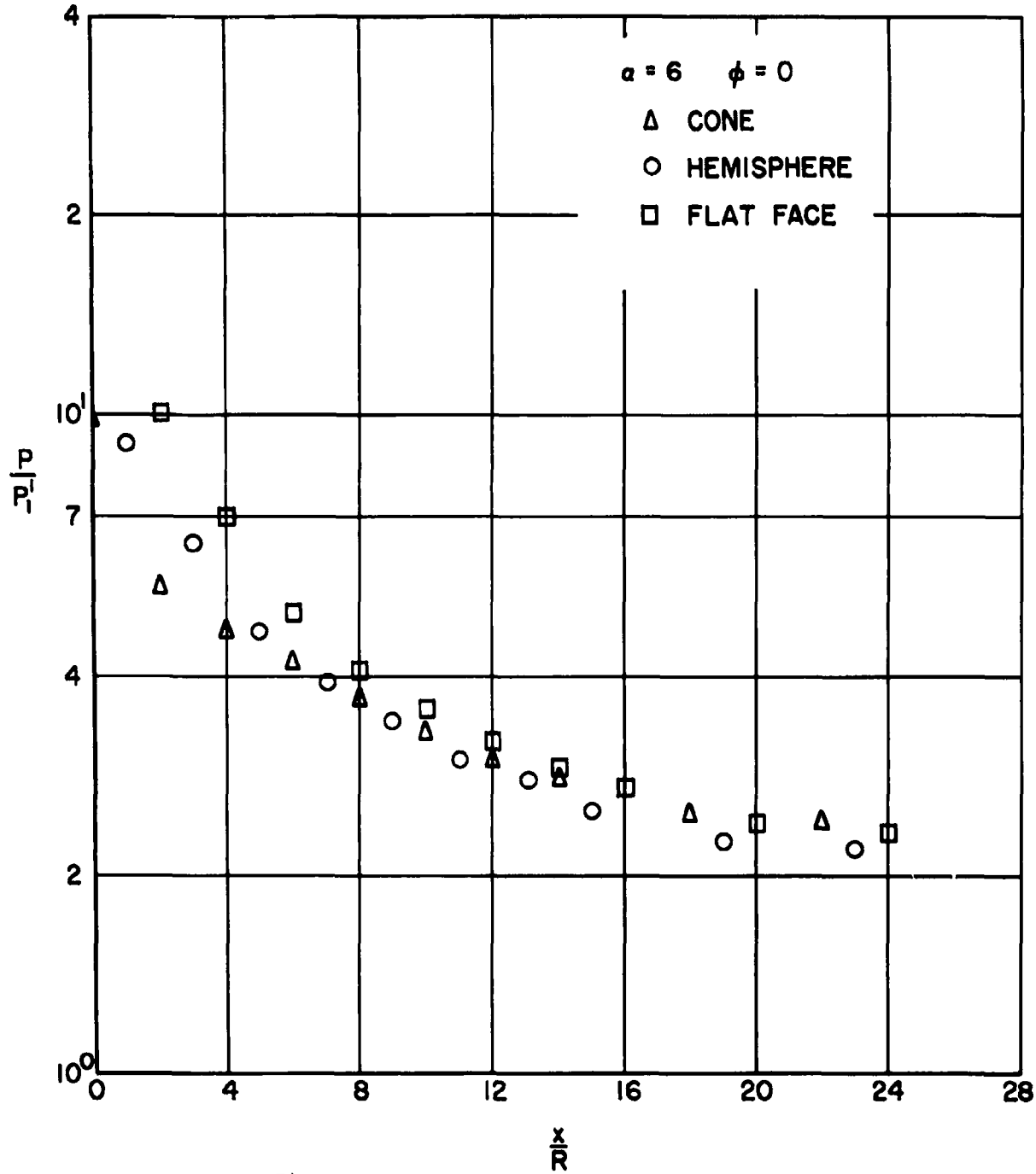

Figure 5c. Summary of pressure distributions at $\alpha = 6^{o}$, $\phi = 0^{o}$.

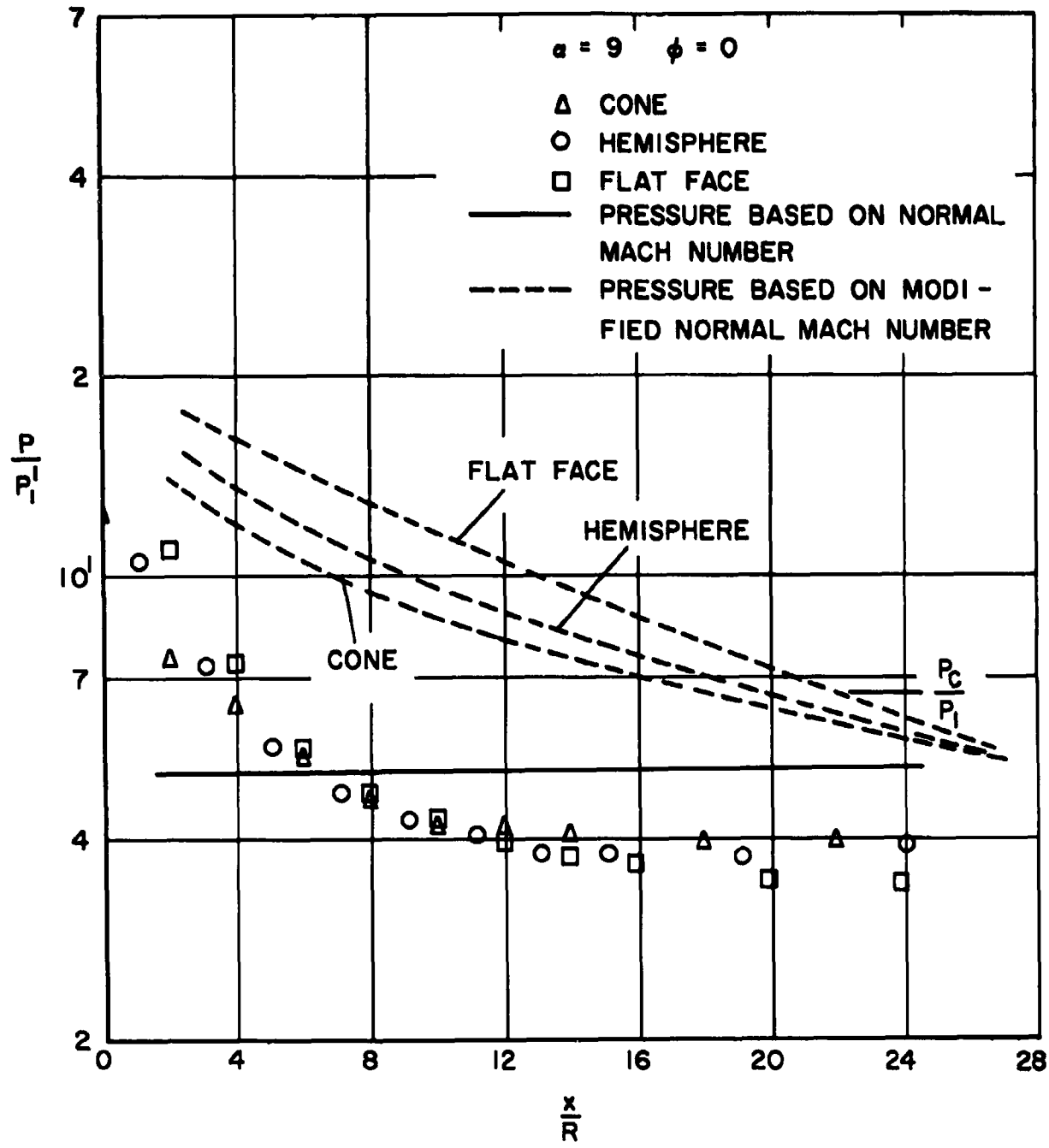

Figure 5d. Summary of pressure distributions at $\alpha = 9^{o}$, $\phi = 0^{o}$.

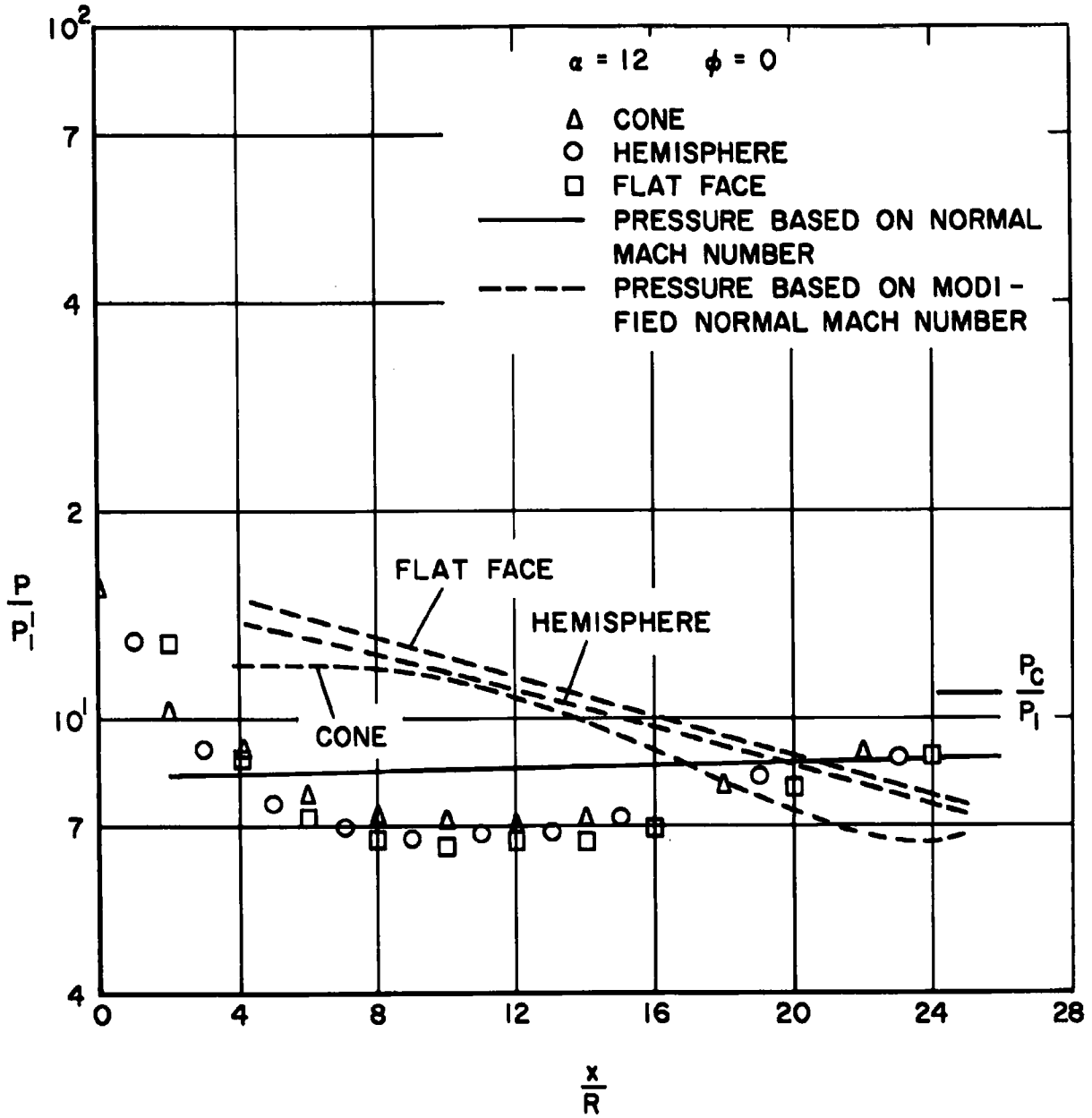

Figure 5e. Summary of pressure distributions at $\alpha = 12^{o}$, $\phi = 0^{o}$.

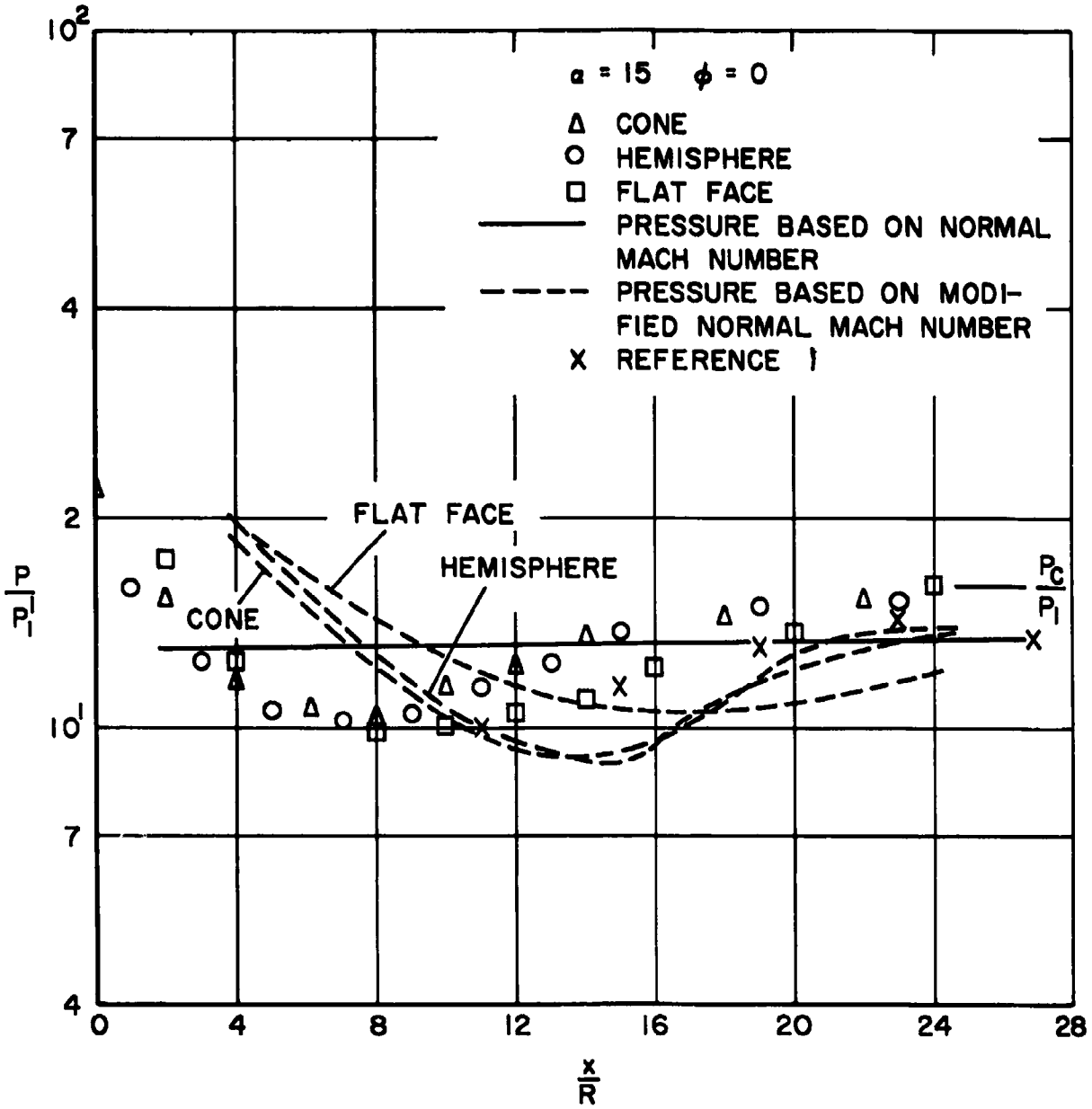

Figure 5f. Summary of pressure distributions at $\alpha = 15^{o}$, $\phi = 0^{o}$.

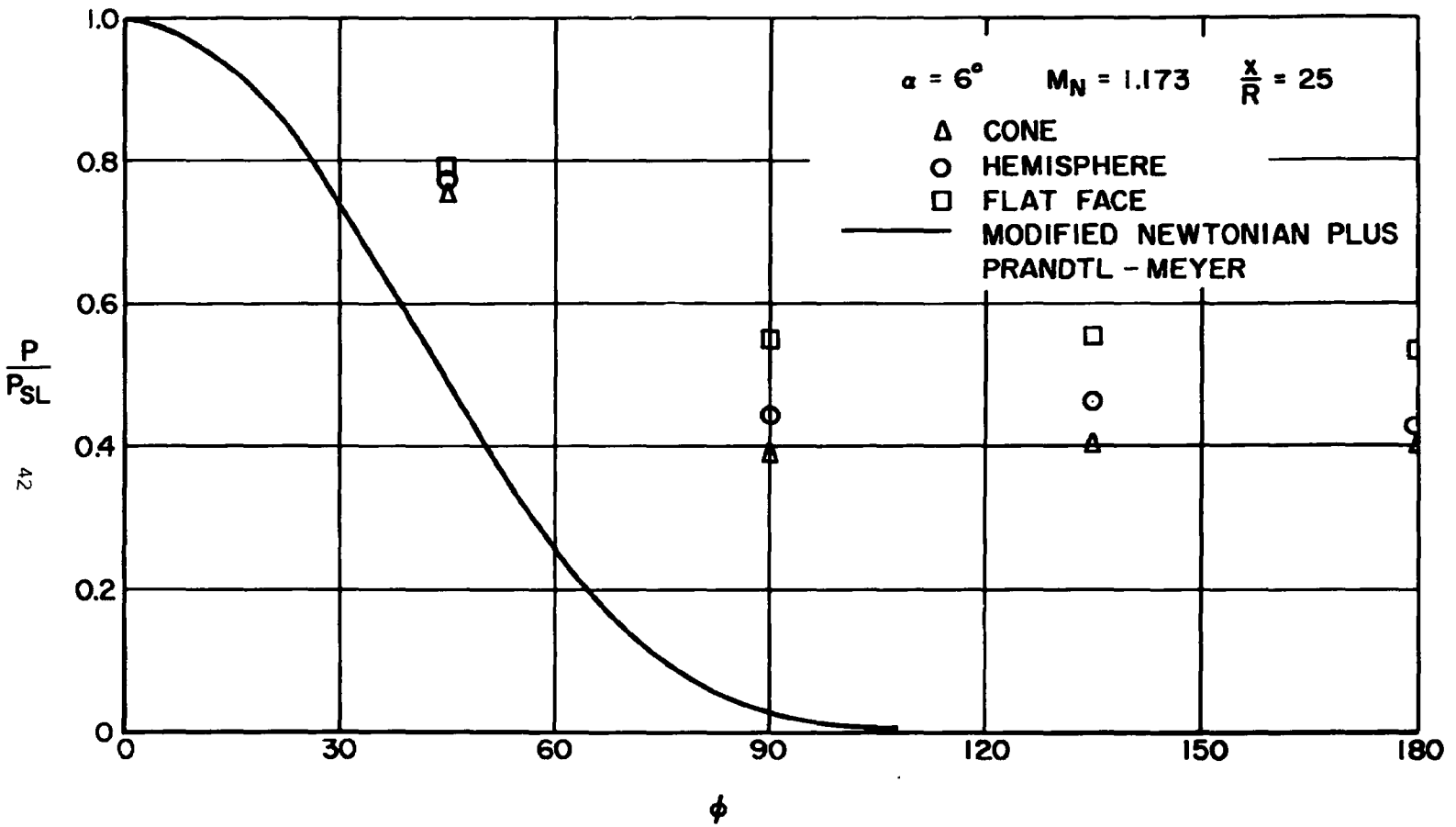

Figure 6a. Crossflow pressure distributions at $\alpha = 6^{\circ}$, $x/R = 25$.

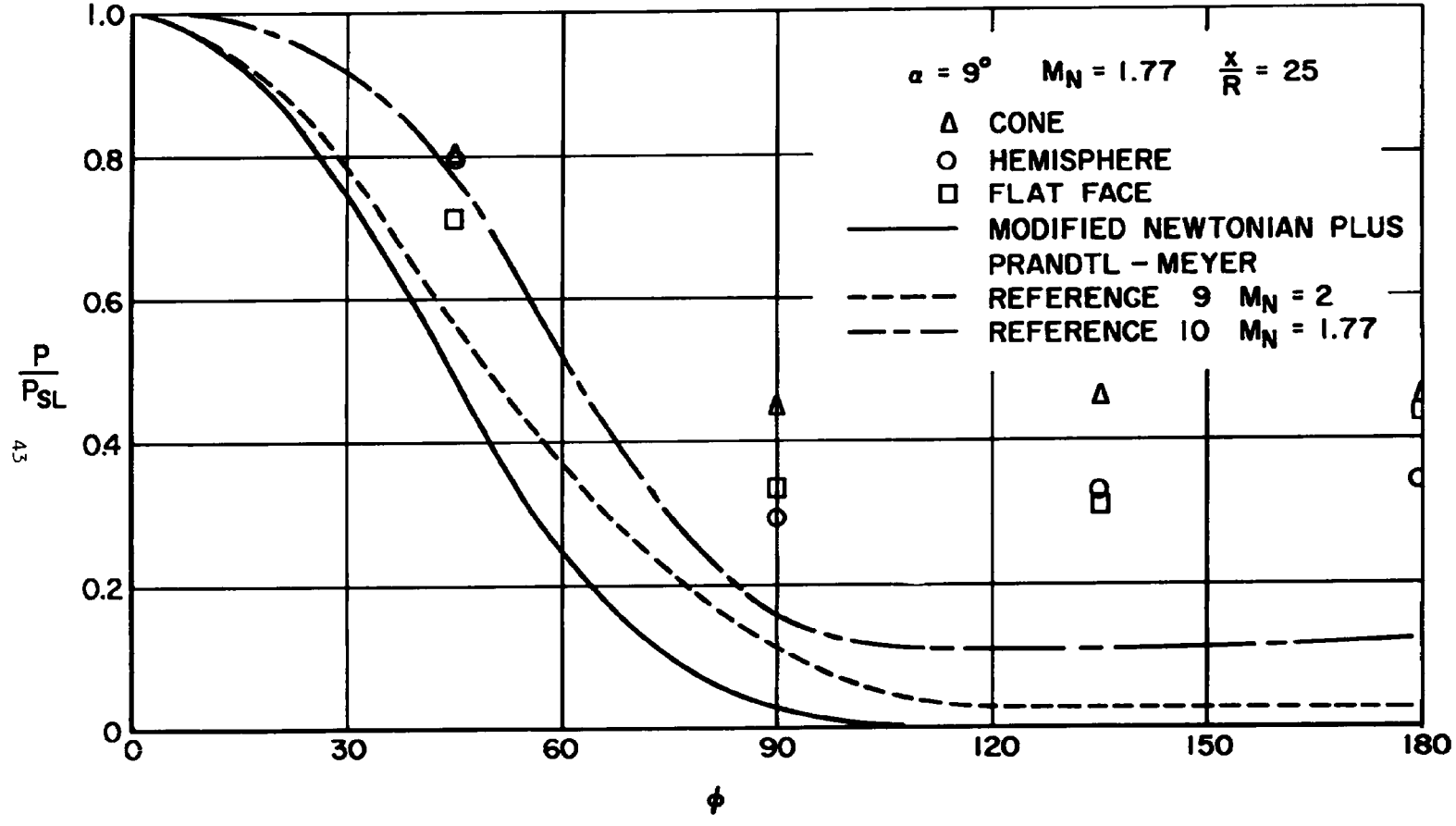

Figure 6b. Crossflow pressure distributions at $\alpha = 9^\circ$, $x/R = 25$.

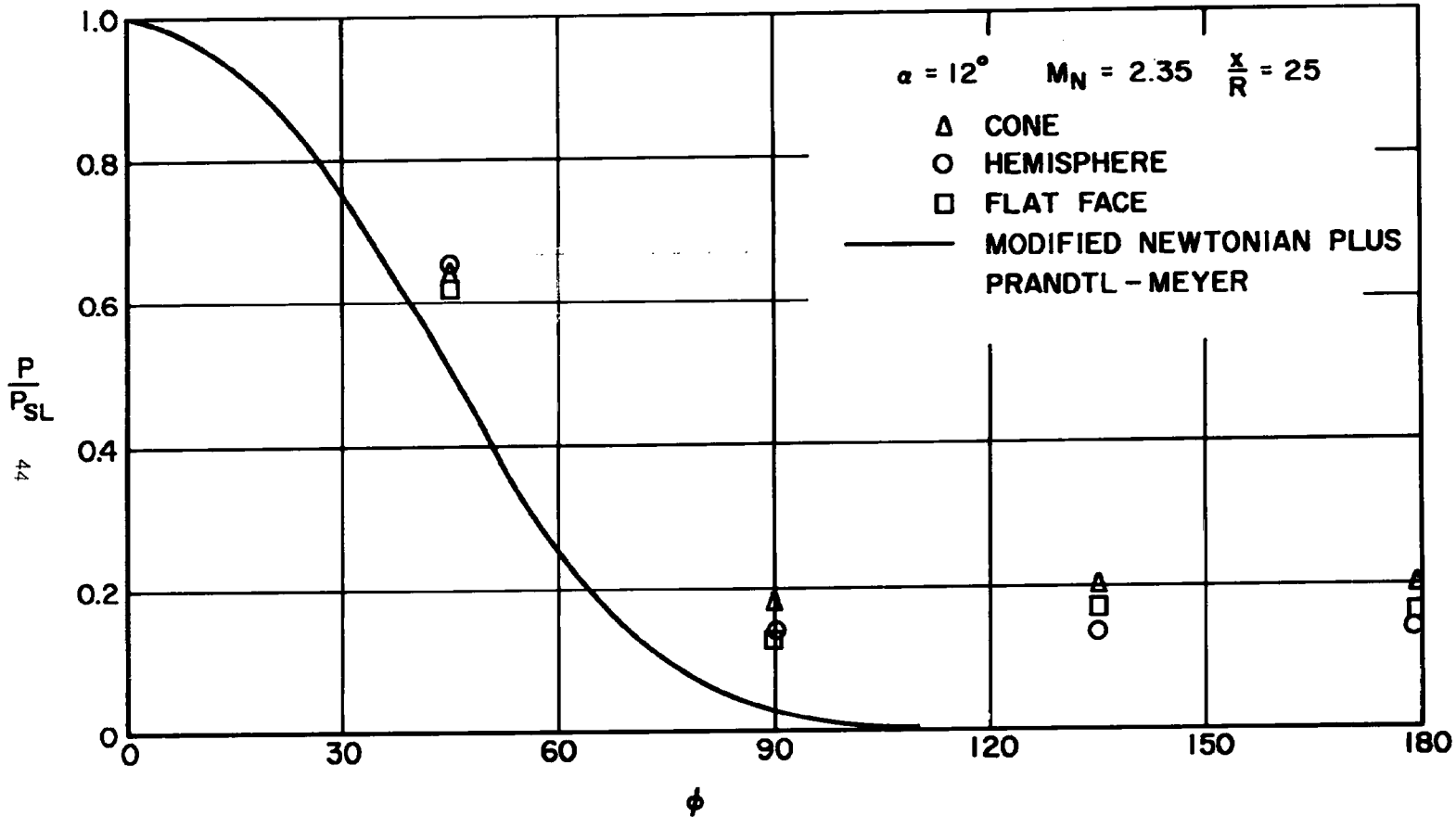

Figure 6c. Crossflow pressure distributions at $\alpha = 12^{\circ}$, $x/R = 25$.

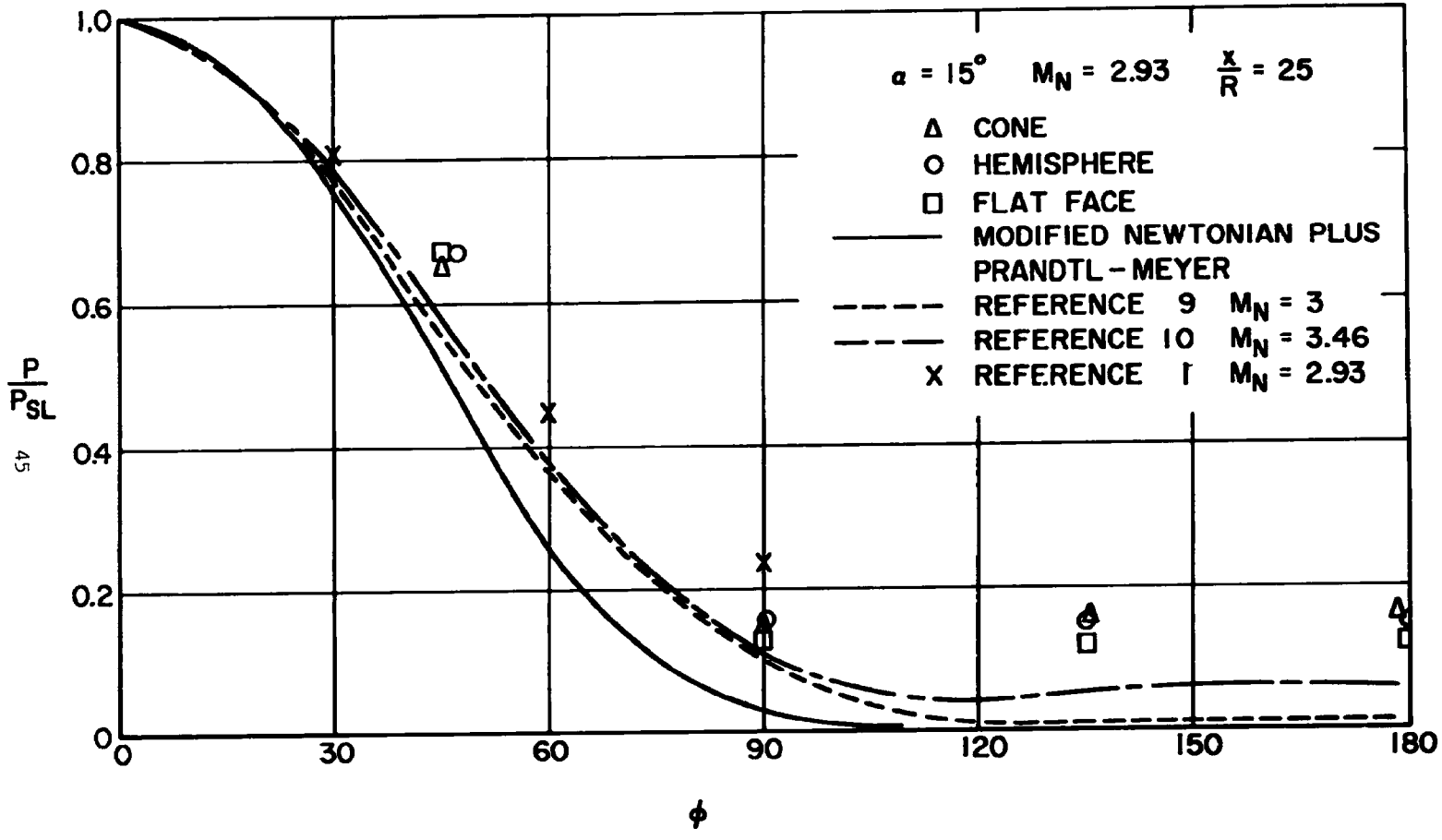

Figure 6d. Crossflow pressure distributions at $\alpha = 15^{\circ}$, $x/R = 25$.

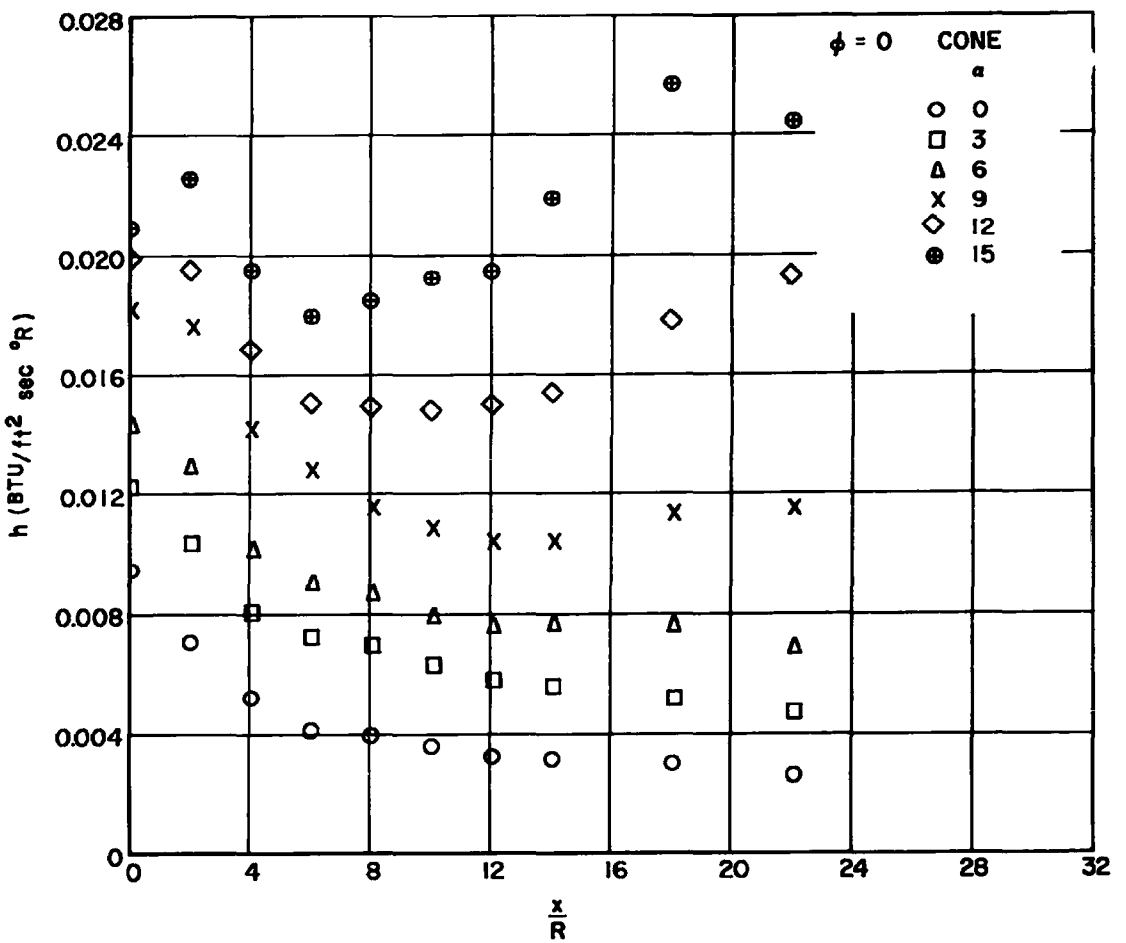

Figure 7a. Heat transfer distributions for conical nose at $\phi = 0^{\circ}$.

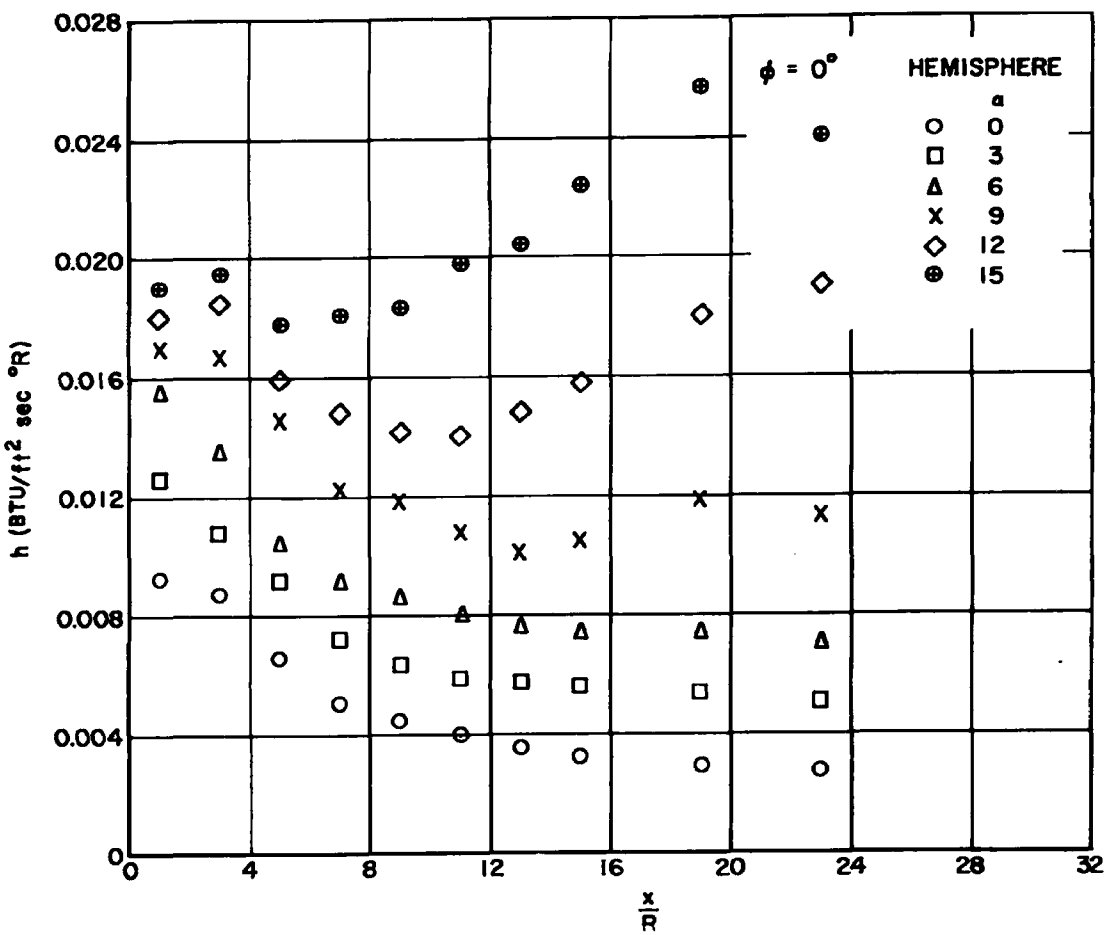

Figure 7b. Heat transfer distributions for hemispherical nose at $\phi = 0^{\circ}$

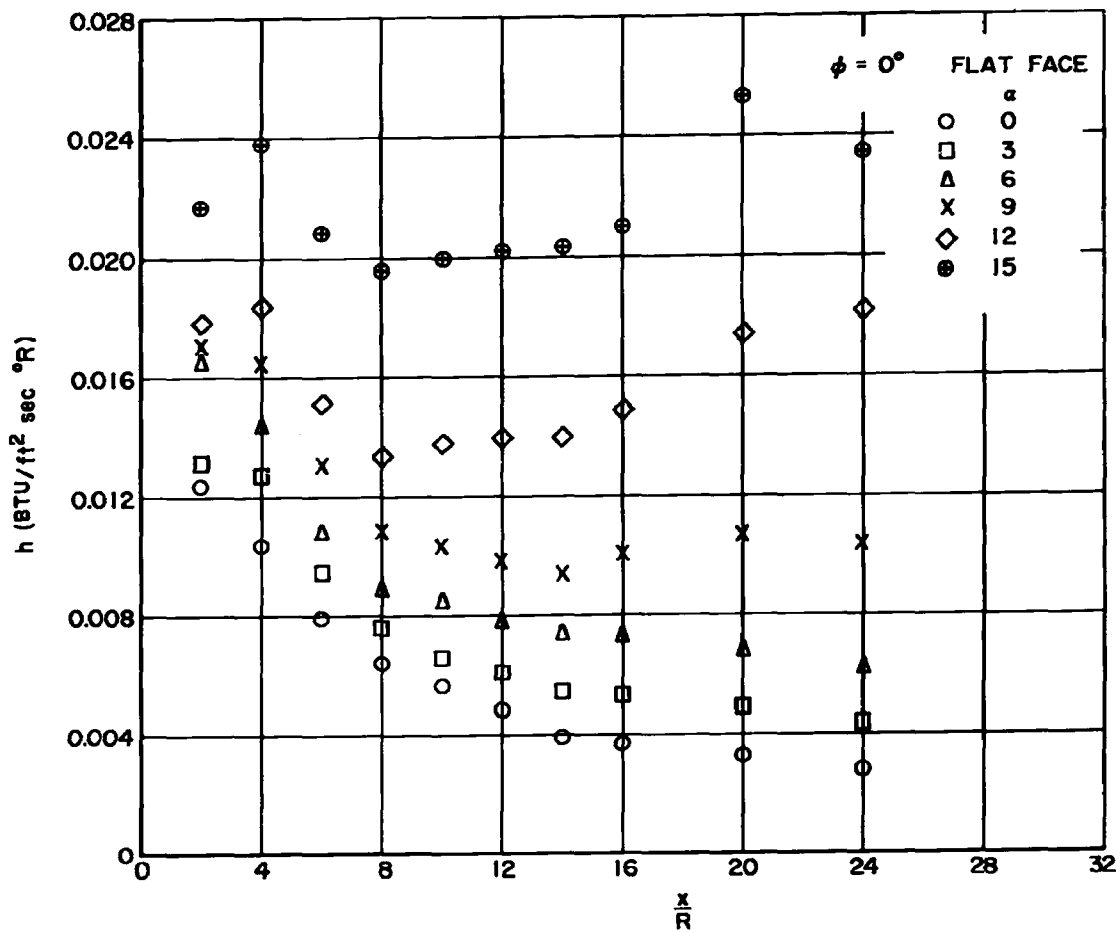

Figure 7c. Heat transfer distributions for flat faced nose at $\phi = 0^{\circ}$.

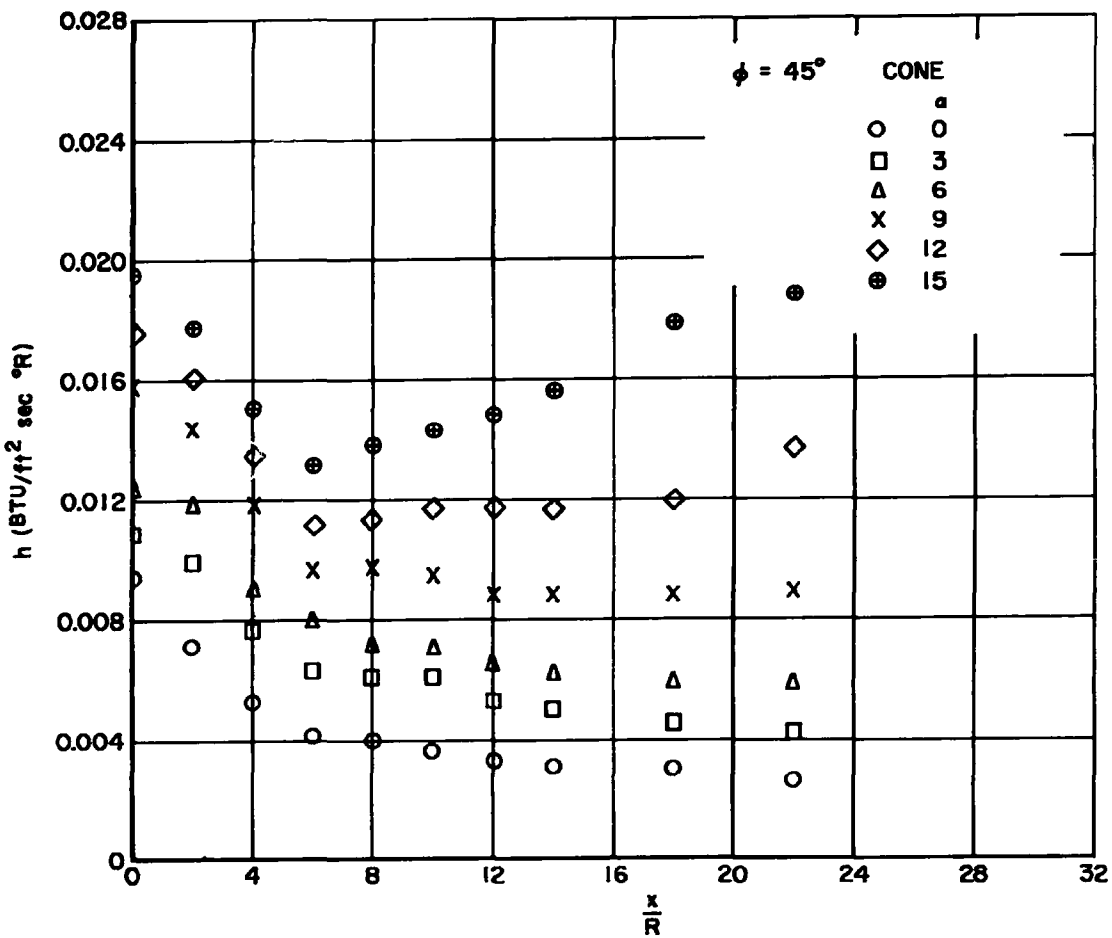

Figure 7d. Heat transfer distributions for conical nose at $\phi = 45^{\circ}$.

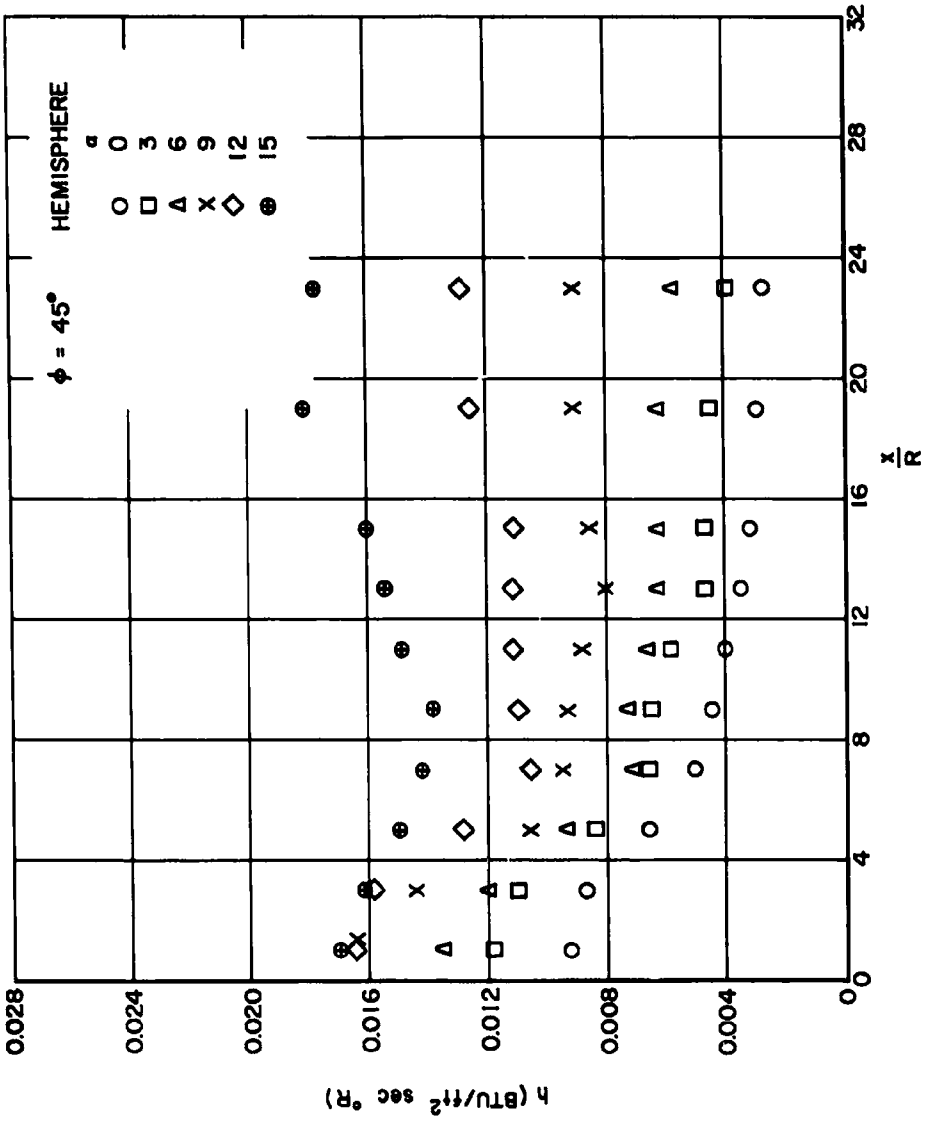

Figure 7e. Heat transfer distributions for hemispherical nose at $\phi = 45^{\circ}$.

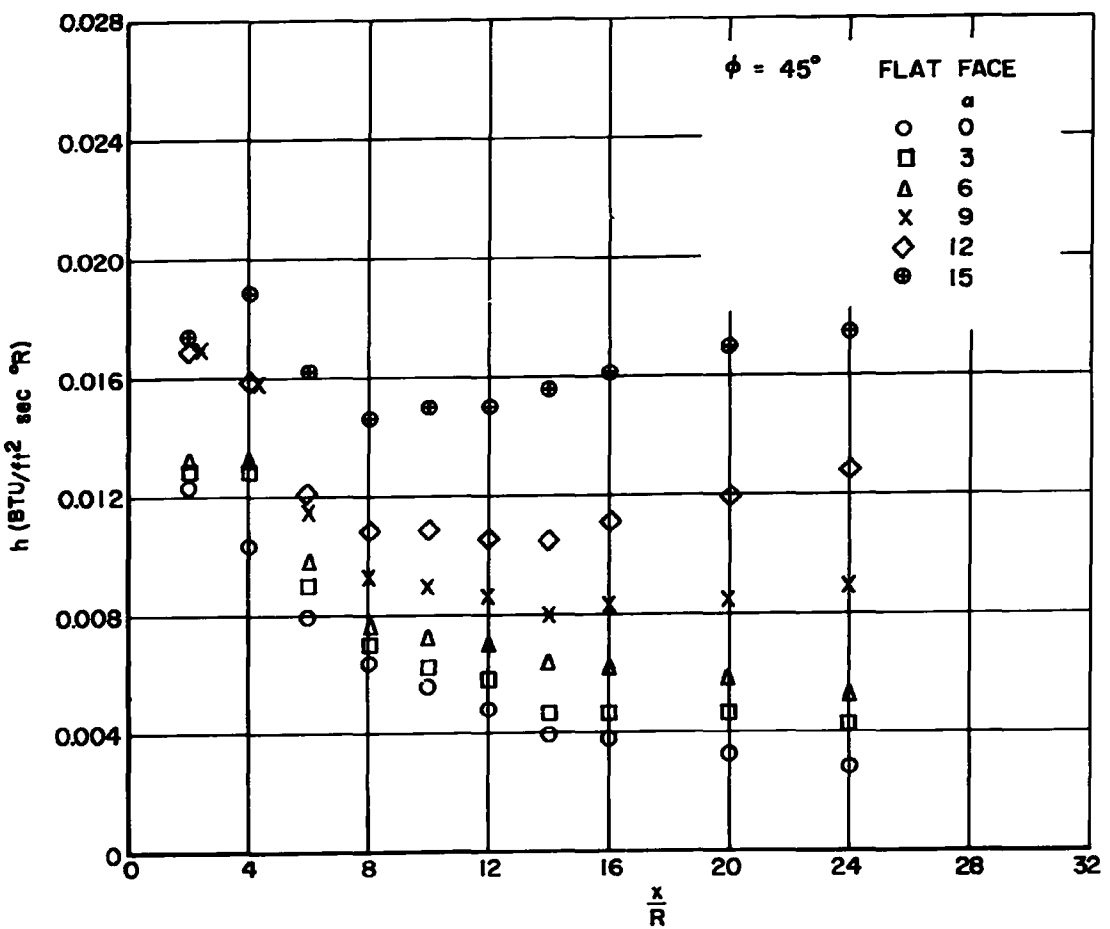

Figure 7f. Heat transfer distributions for flat-faced nose at $\phi = 45^{\circ}$.

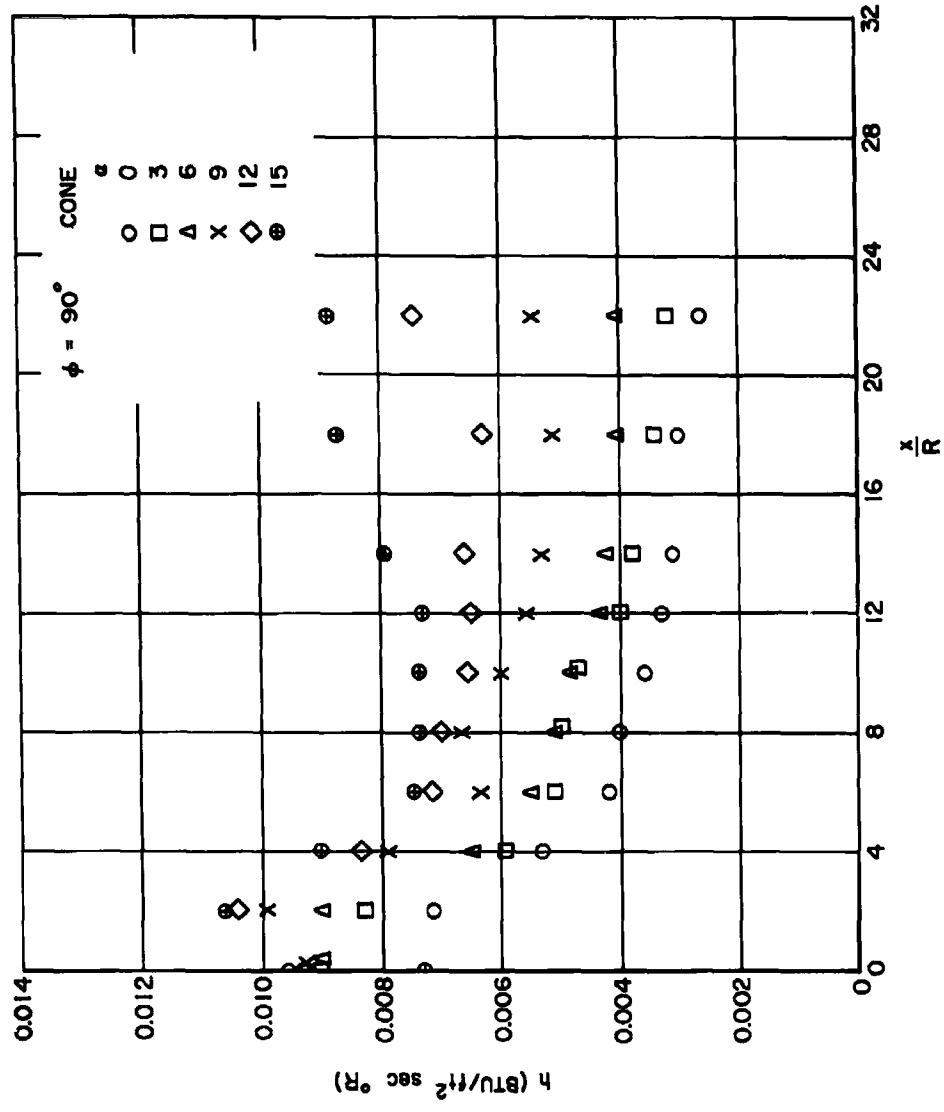

Figure 7g. Heat transfer distributions for conical nose at $\phi = 90^{\circ}$.

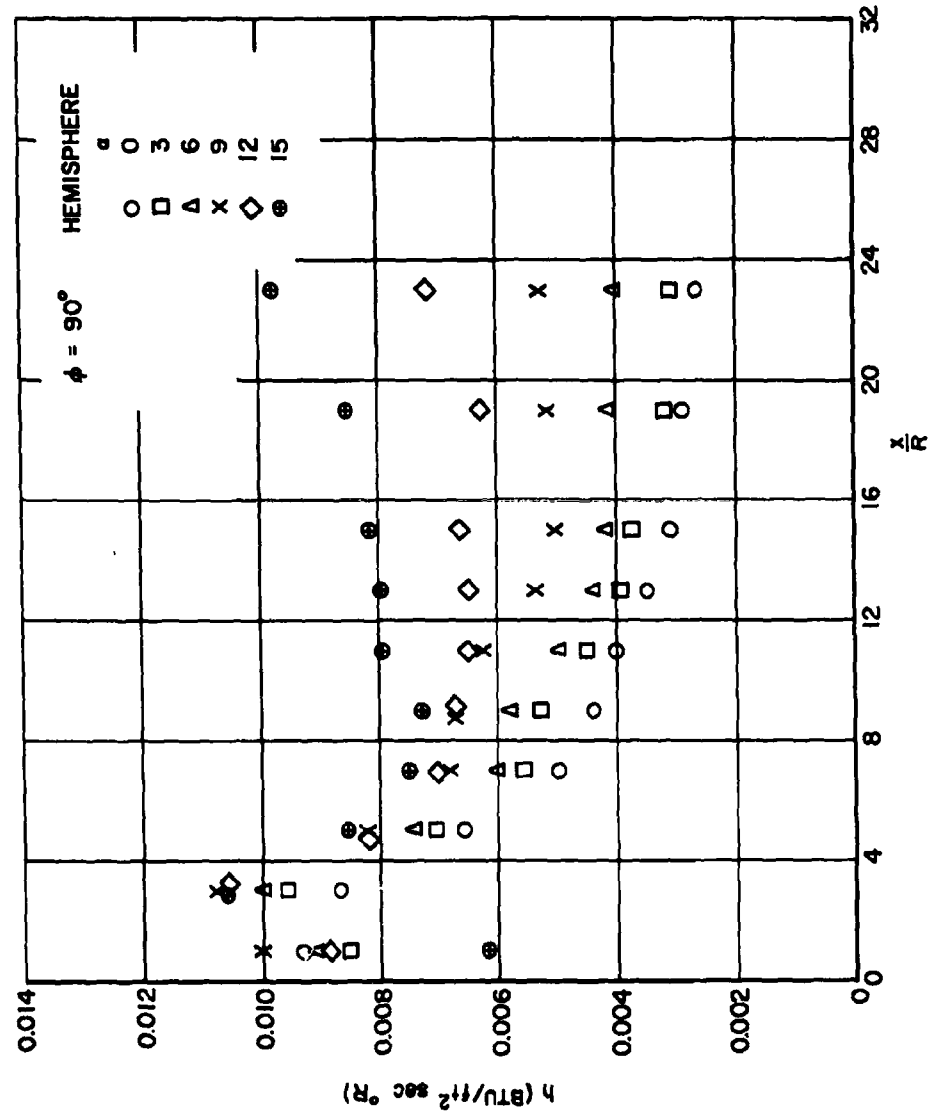

Figure 7h. Heat transfer distributions for hemispherical nose at $\phi = 90^{\circ}$.

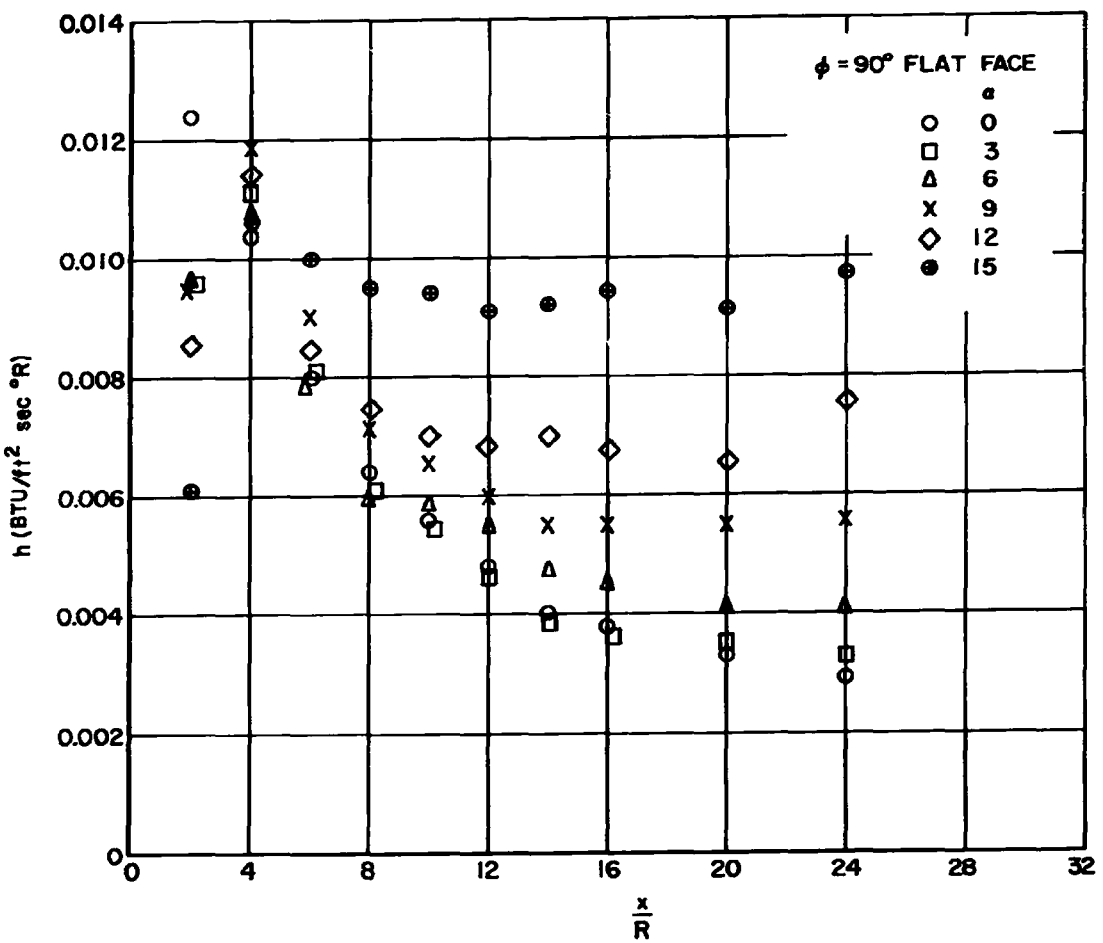

Figure 7i. Heat transfer distributions for flat faced nose at $\phi = 90^{\circ}$.

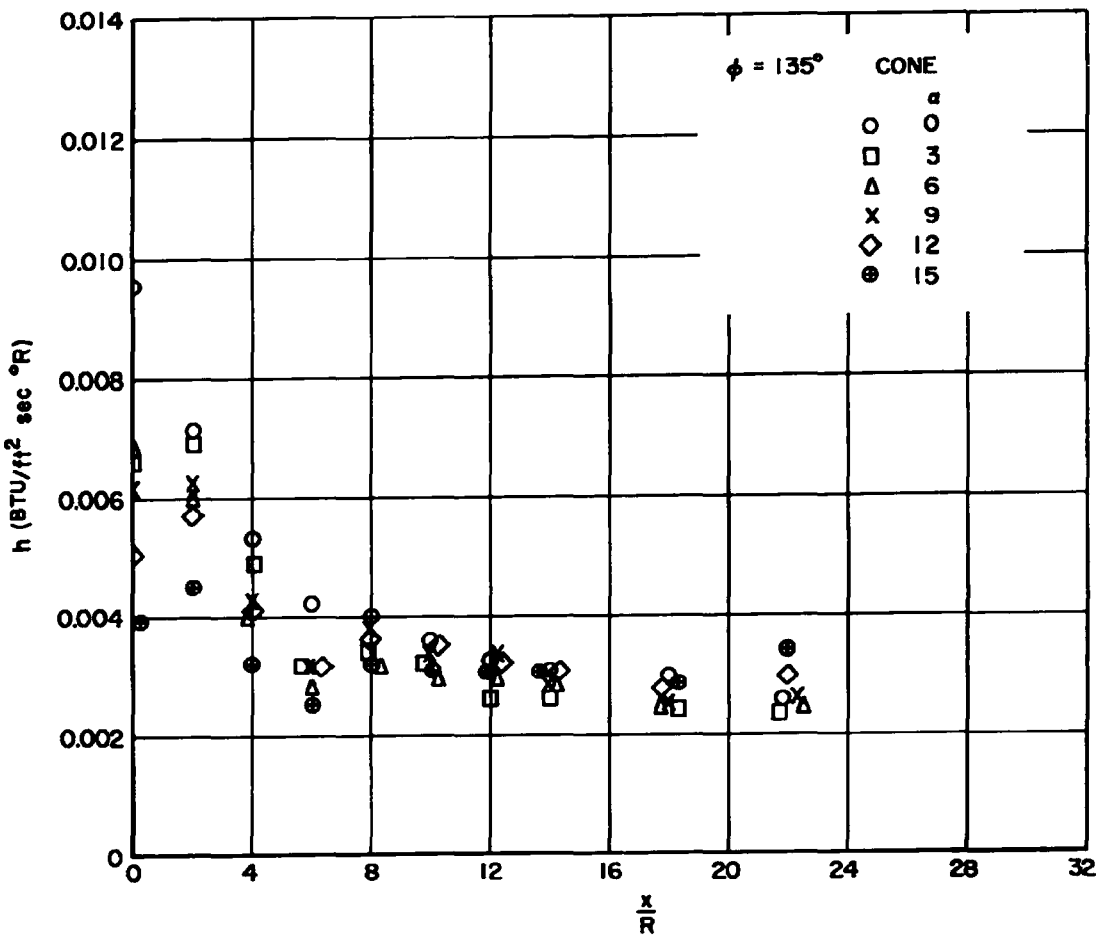

Figure 7j. Heat transfer distributions for conical nose at $\phi = 135°$.

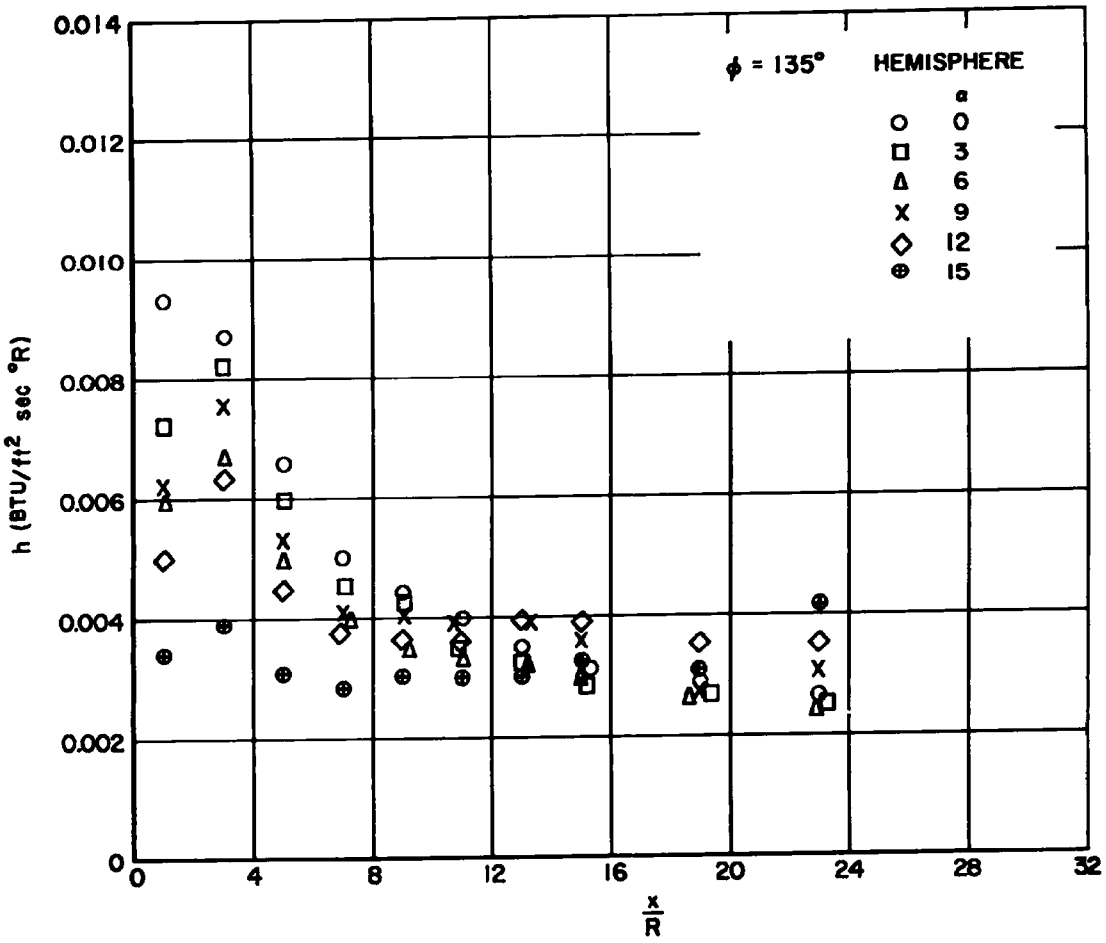

Figure 7k. Heat transfer distributions for hemispherical nose at $\phi = 135^{\circ}$.

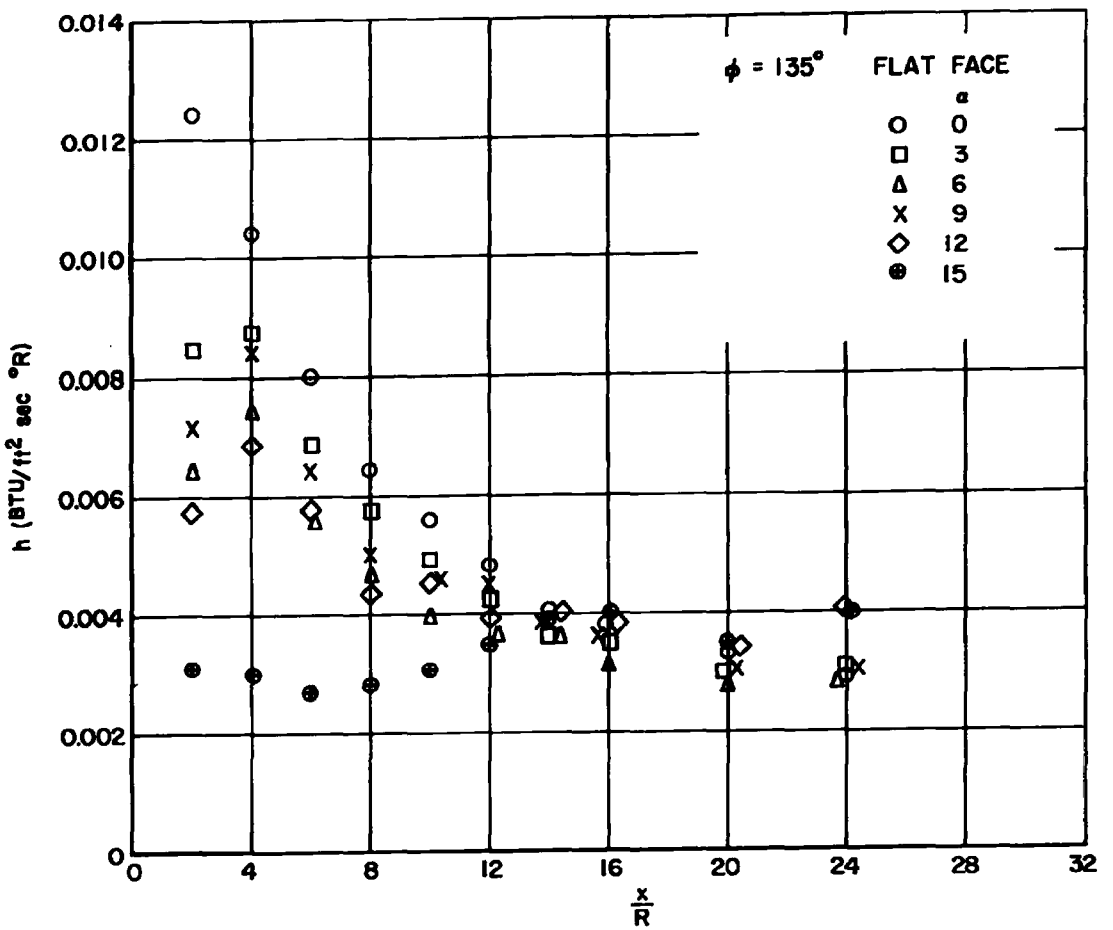

Figure 7ℓ. Heat transfer distributions for flat faced nose at $\phi = 135°$.

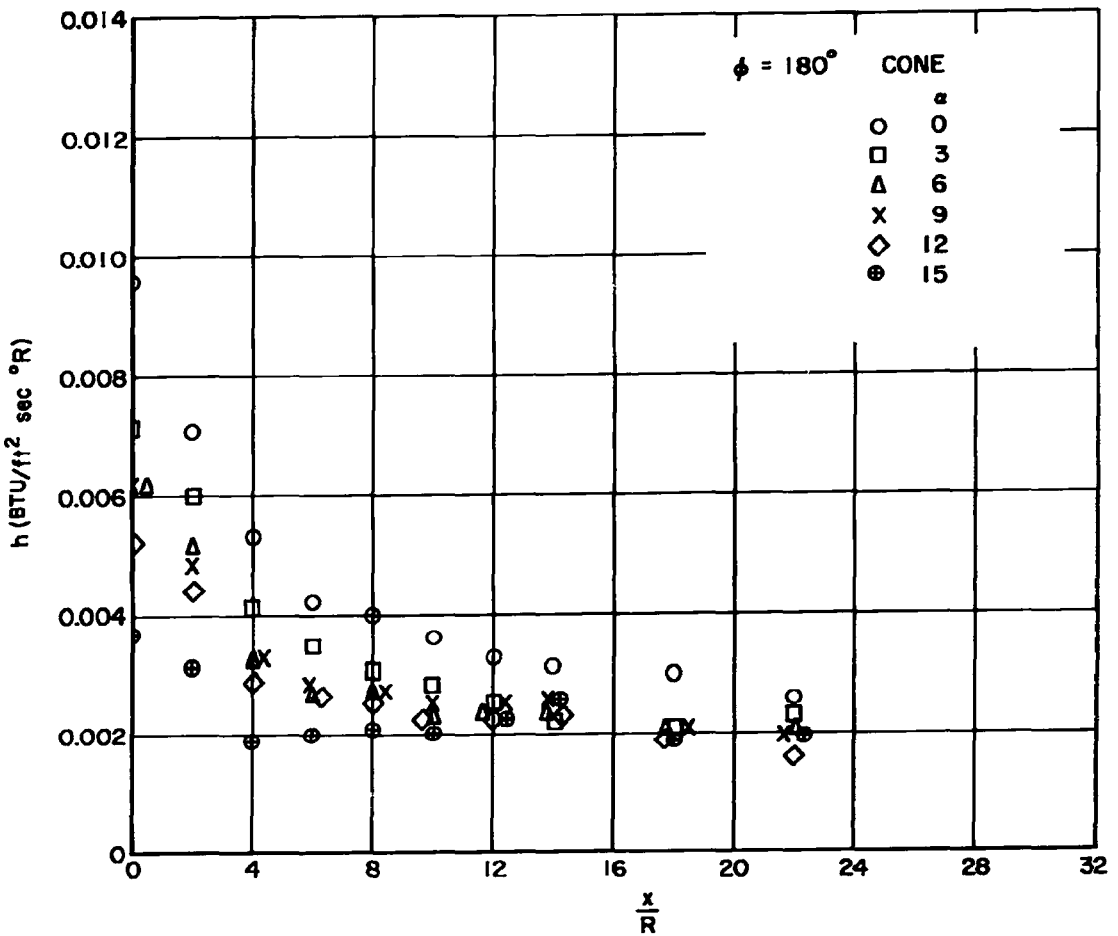

Figure 7m. Heat transfer distributions for conical nose at $\phi = 180^{\circ}$.

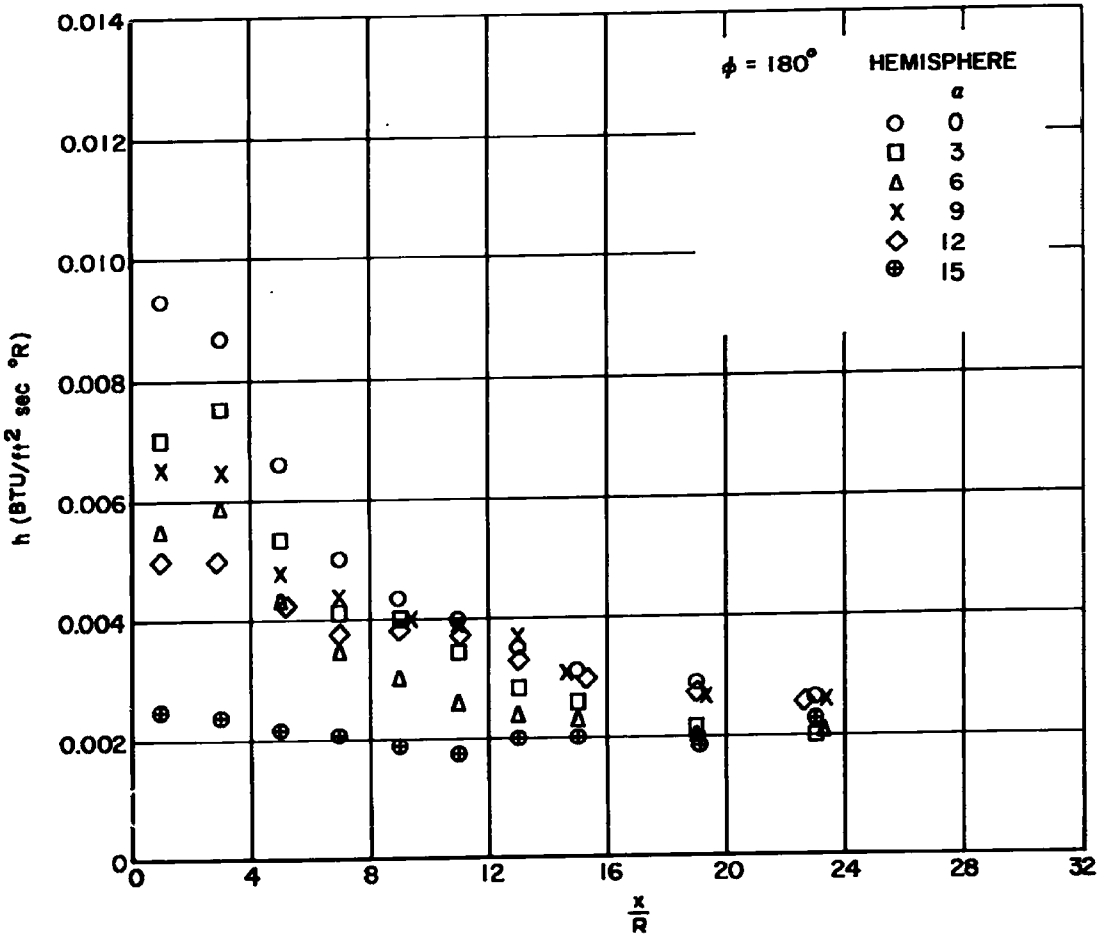

Figure 7n. Heat transfer distributions for hemispherical nose at $\phi = 180^{\circ}$.

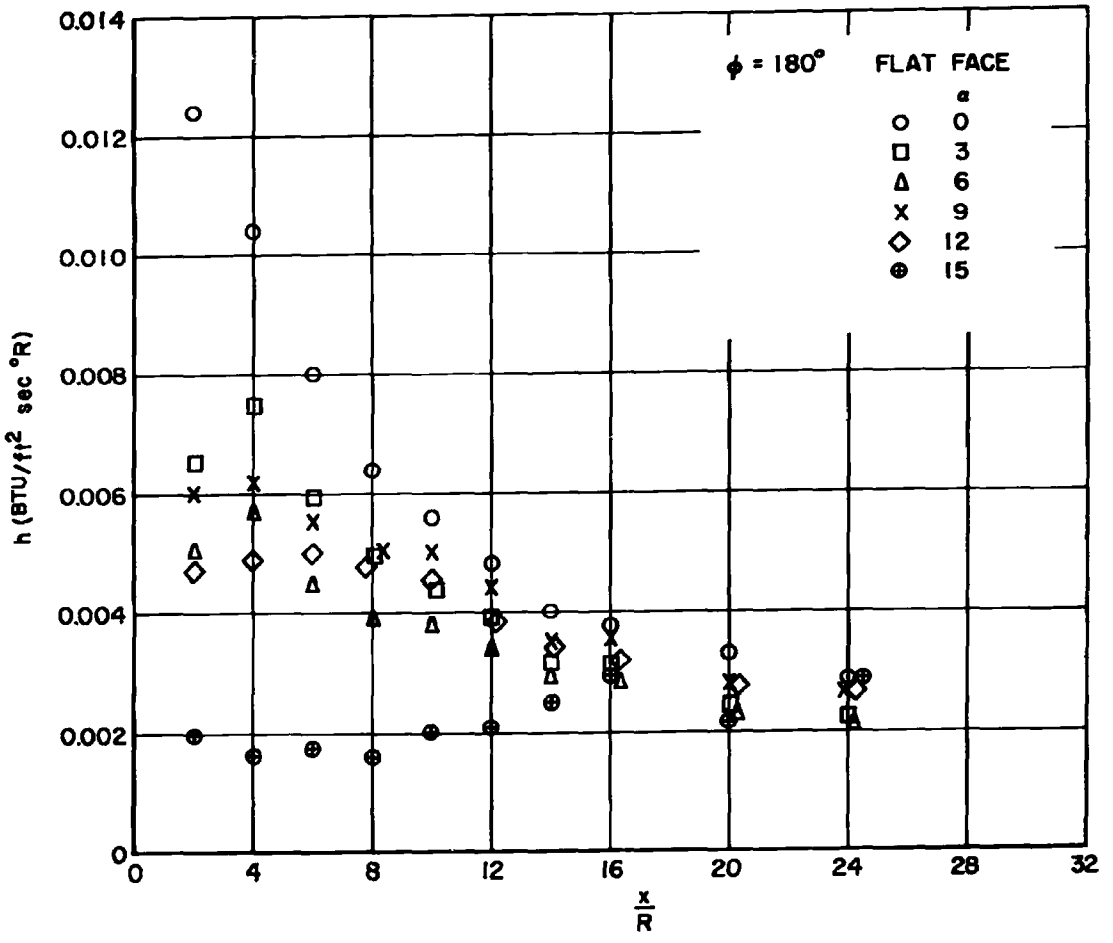

Figure 7o. Heat transfer distributions for flat faced nose at $\phi = 180^{\circ}$.

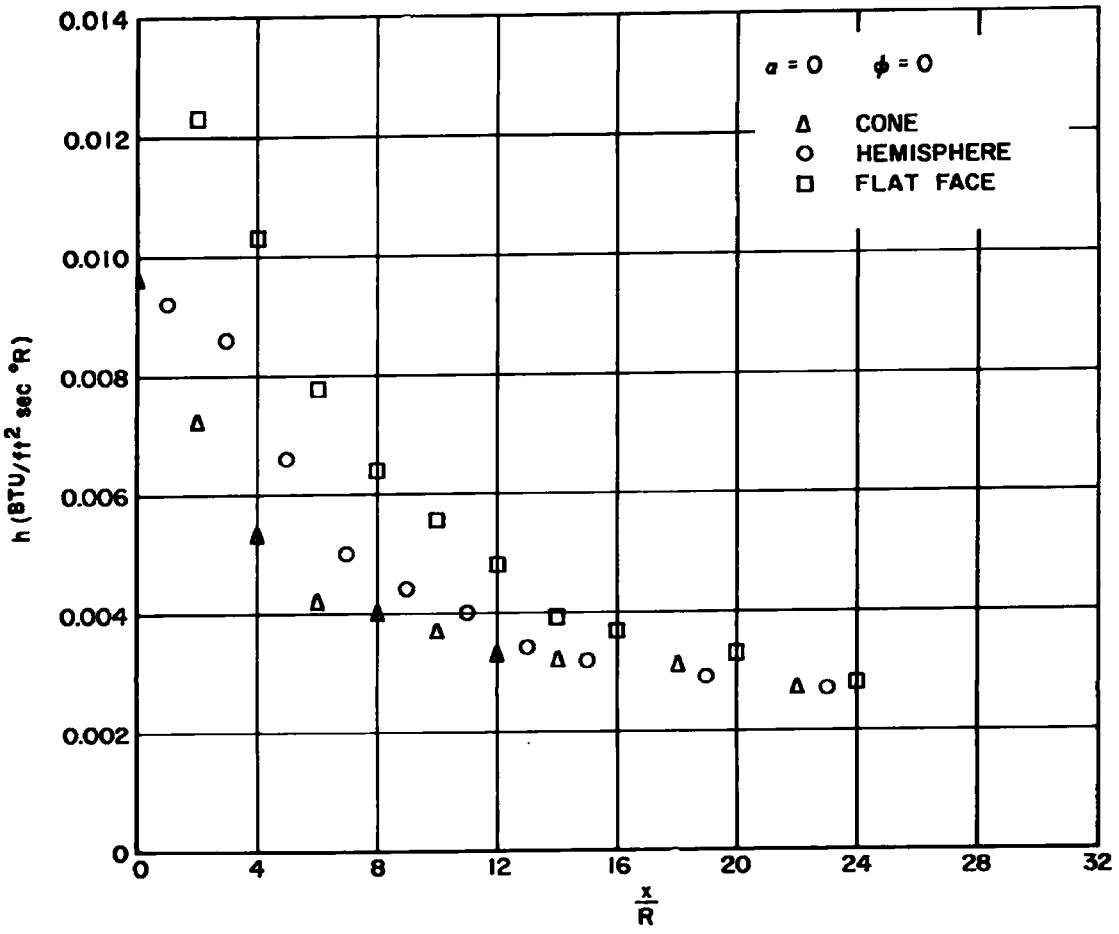

Figure 8a. Summary of heat transfer distributions at at $\alpha = 0^{o}$, $\phi = 0^{o}$.

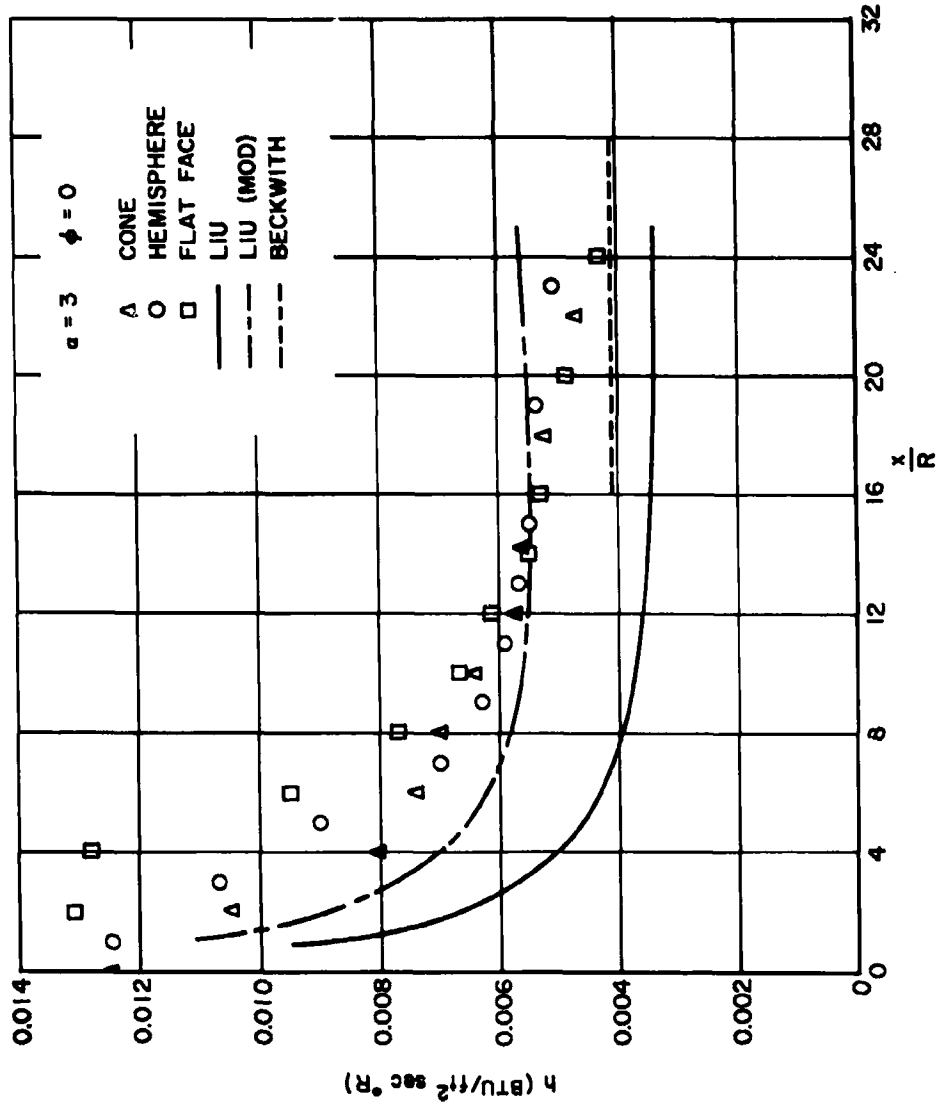

Figure 8b. Summary of heat transfer distributions at $\alpha = 30$, $\phi = 0^{o}$.

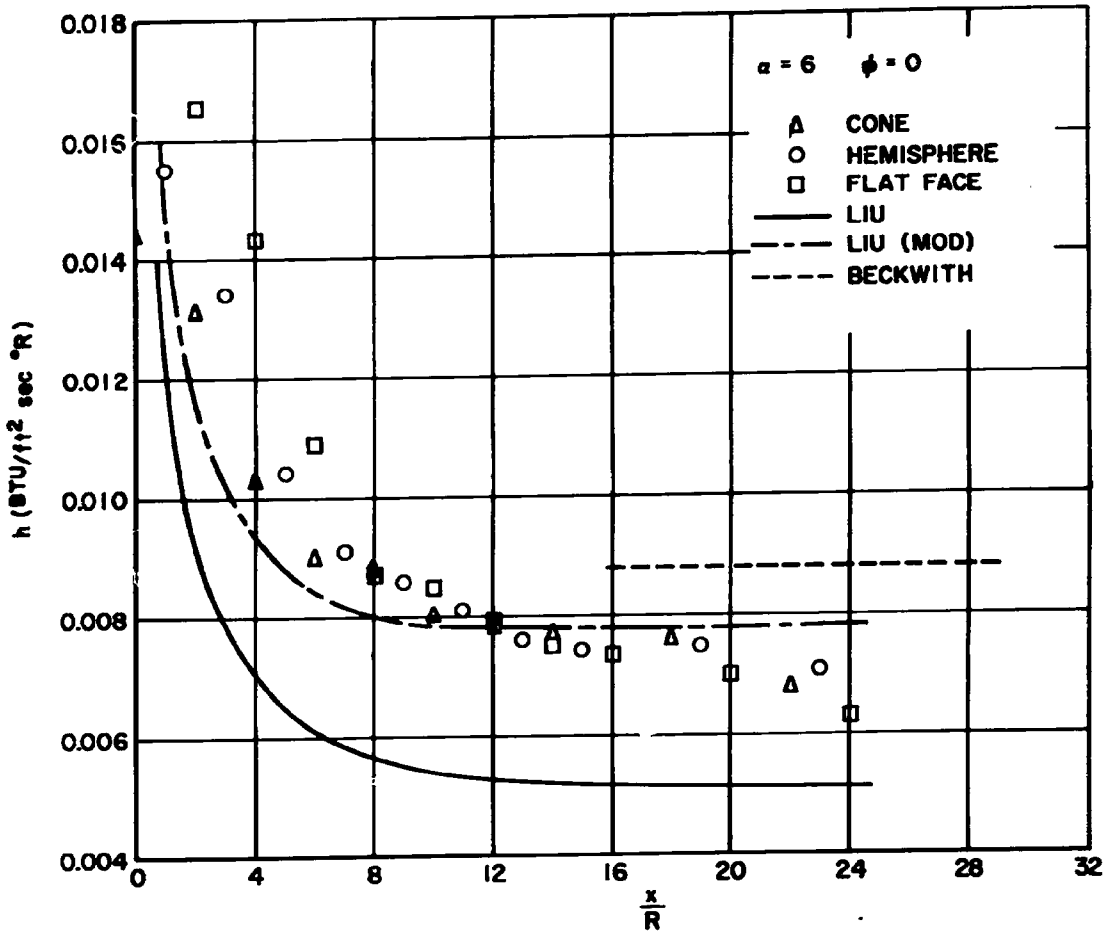

Figure 8c. Summary of heat transfer distributions at $\alpha = 6^{o}$, $\phi = 0^{o}$.

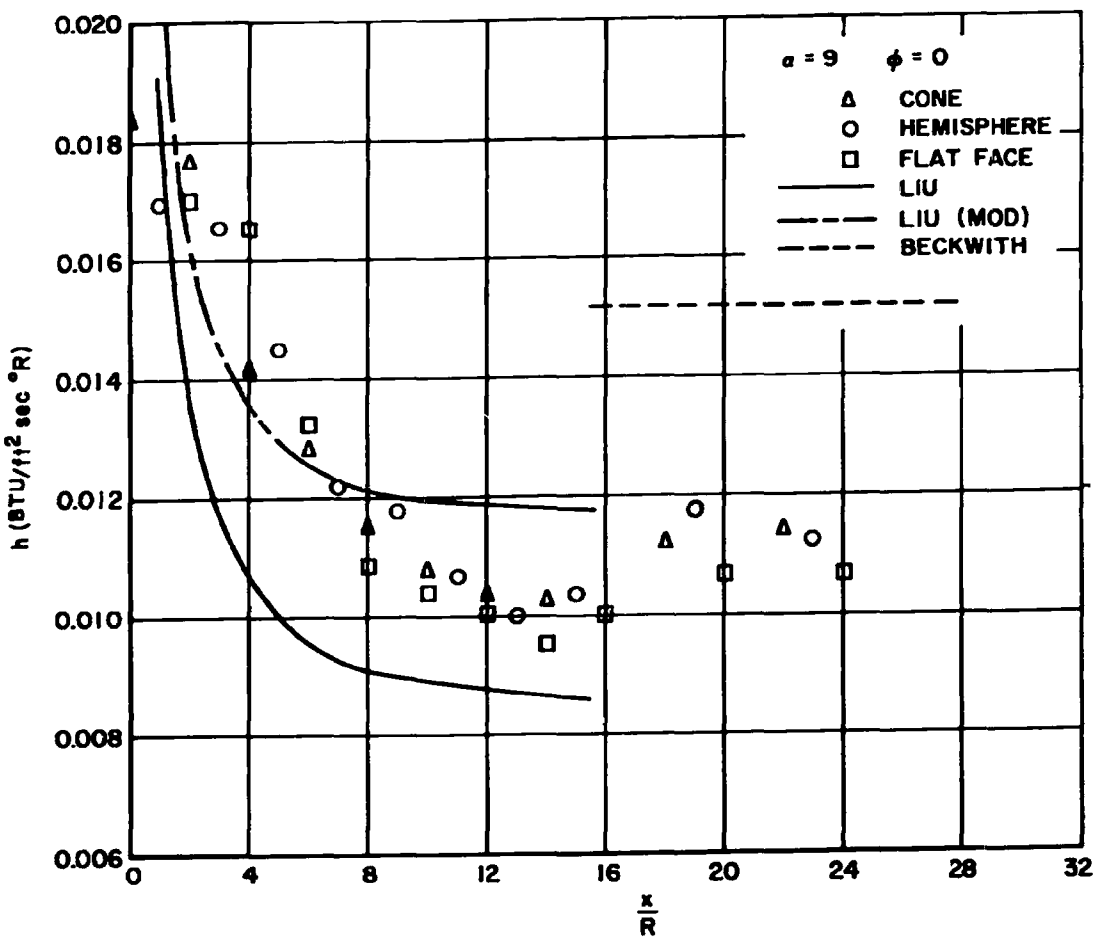

Figure 8d. Summary of heat transfer distributions at $\alpha = 9^{\circ}$, $\phi = 0^{\circ}$.

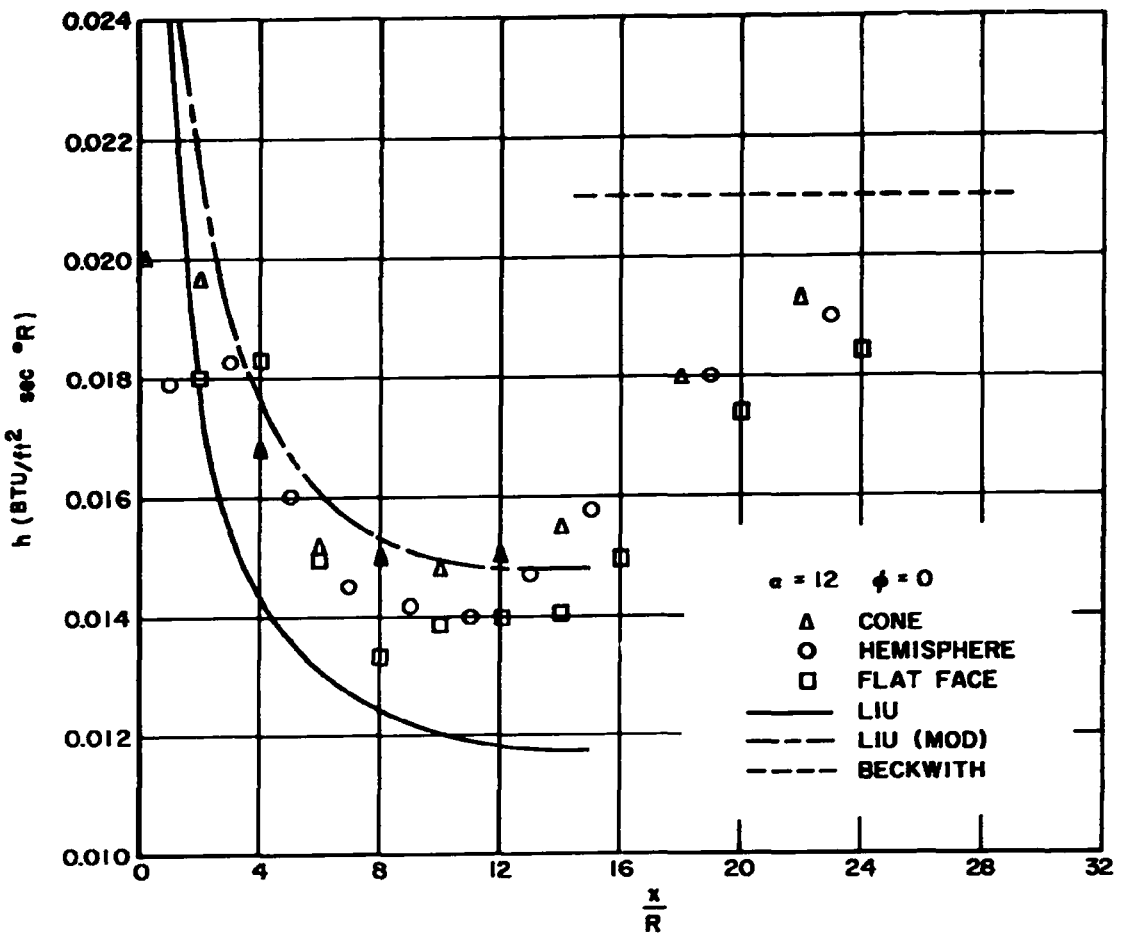

Figure 8e. Summary of heat transfer distributions at $\alpha = 12^{\circ}$, $\phi = 0^{\circ}$.

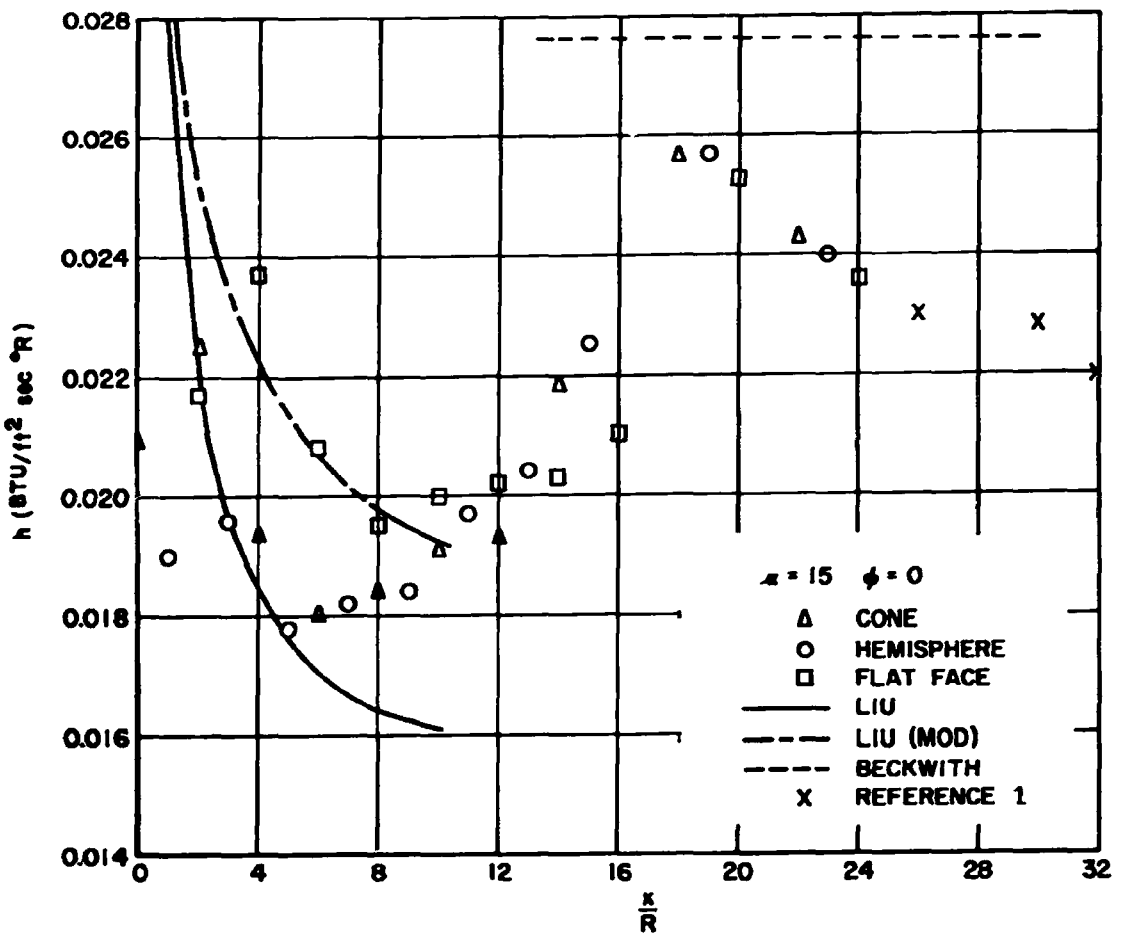

Figure 8f. Summary of heat transfer distributions at $\alpha = 15^{\circ}$, $\phi = 0^{\circ}$.

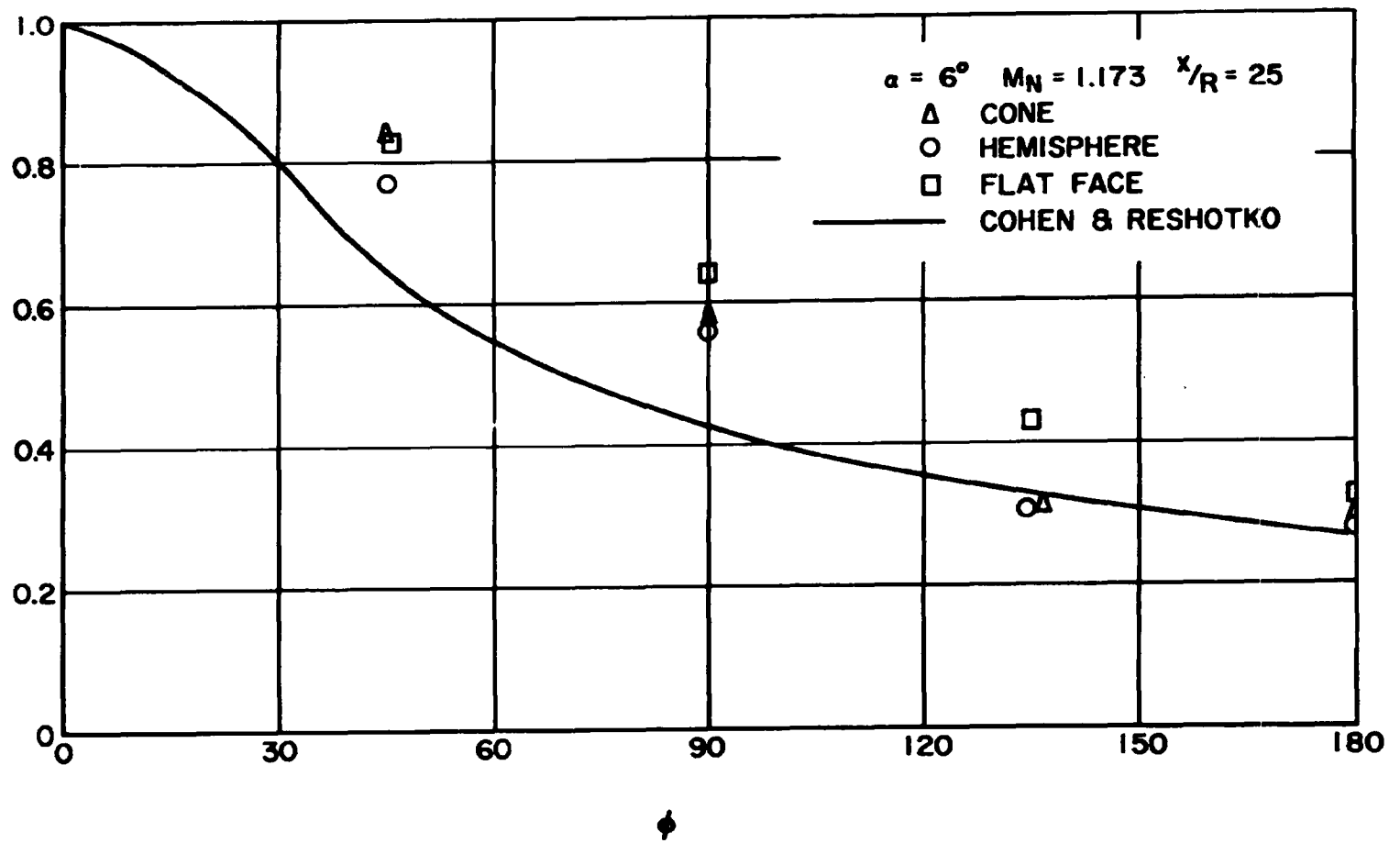

Figure 9a. Crossflow heat transfer distributions at $\alpha = 6^{o}$, $x/R = 25$.

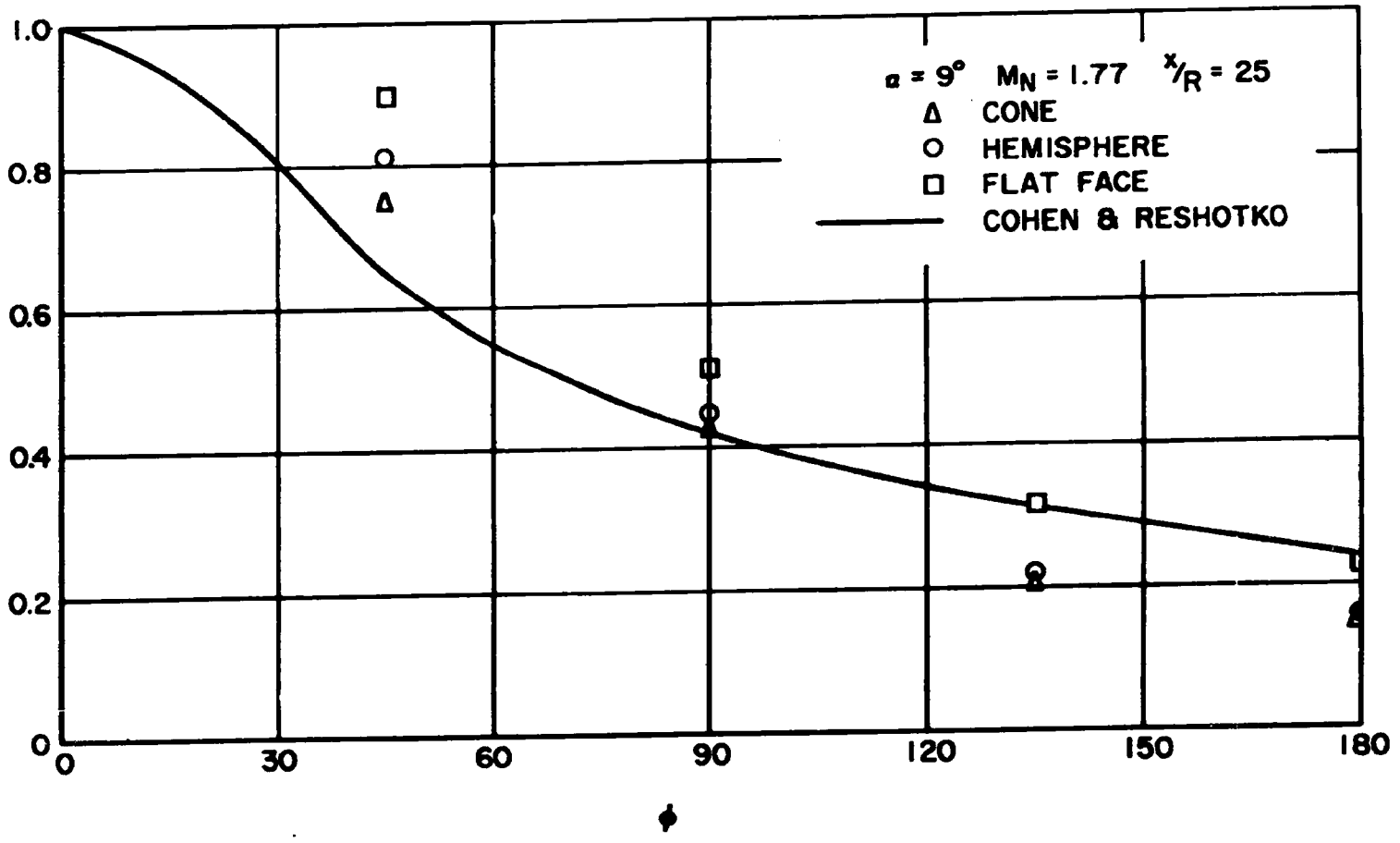

Figure 9b. Crossflow heat transfer distributions at at $\alpha = 9^{o}$, $x/R = 25$.

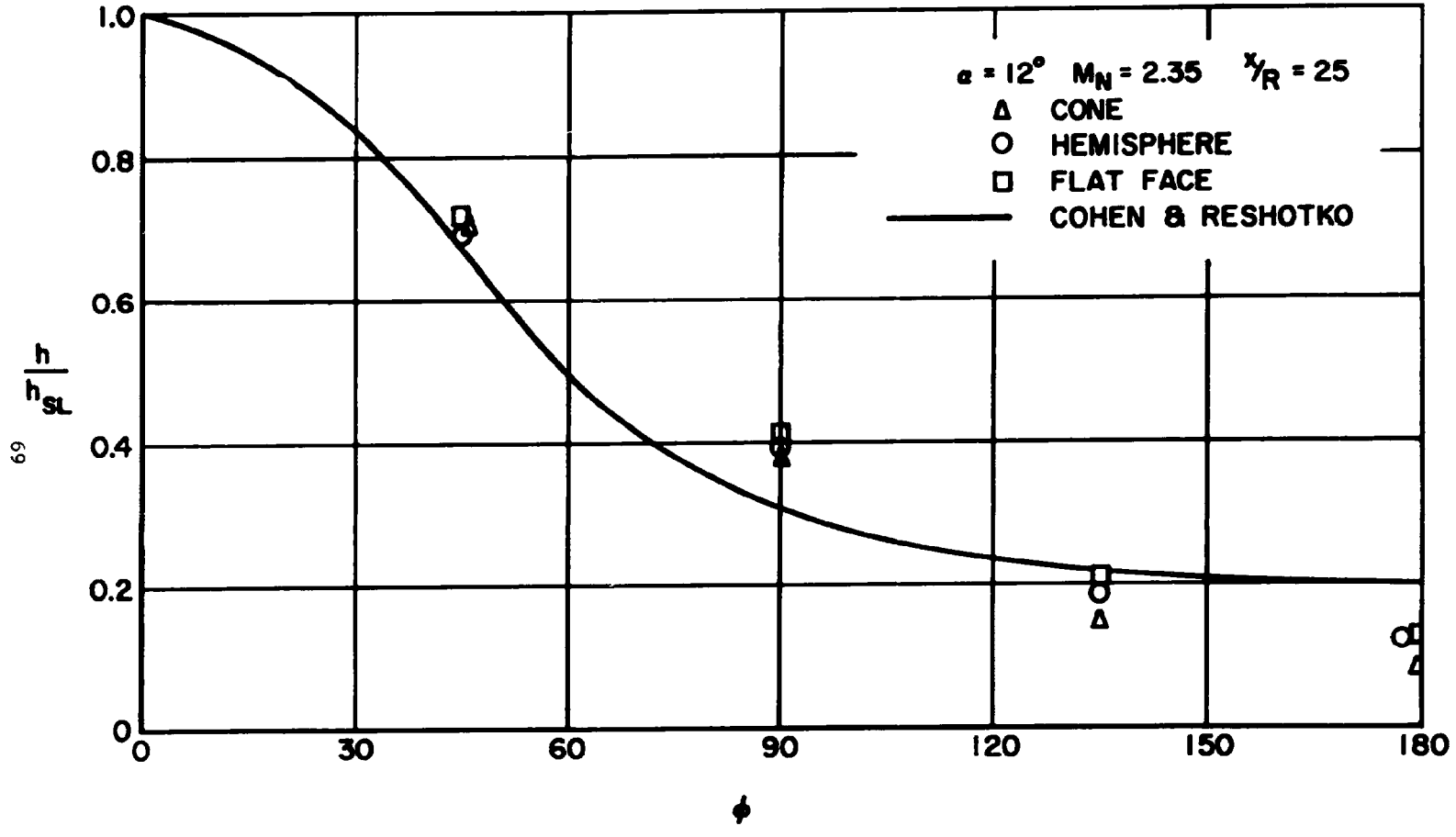

Figure 9c. Crossflow heat transfer distributions at $\alpha = 12^{o}$, $x/R = 25$.

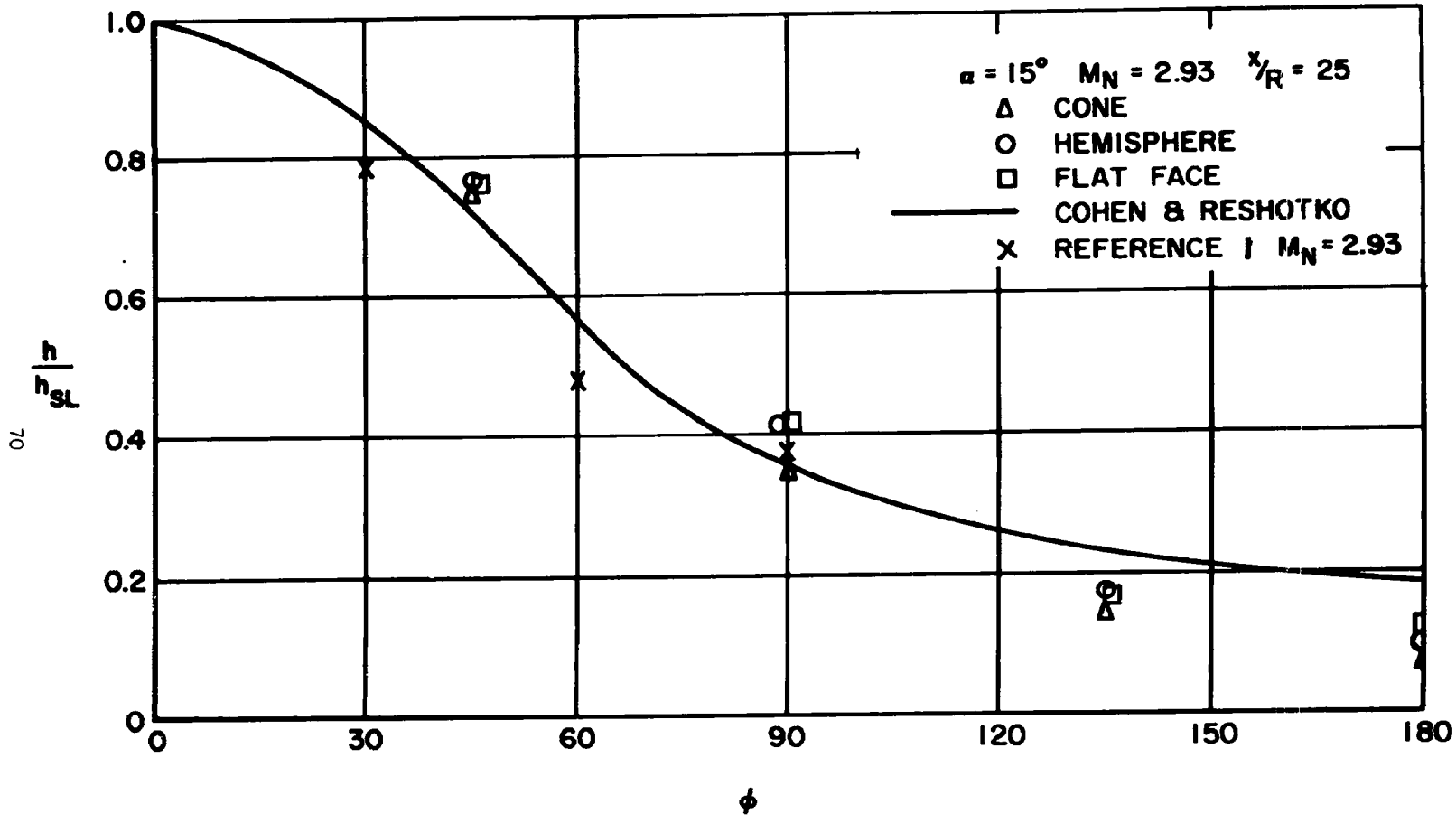

Figure 9d. Crossflow heat transfer distributions at $\alpha = 15^{\circ}$, $x/R = 25$.

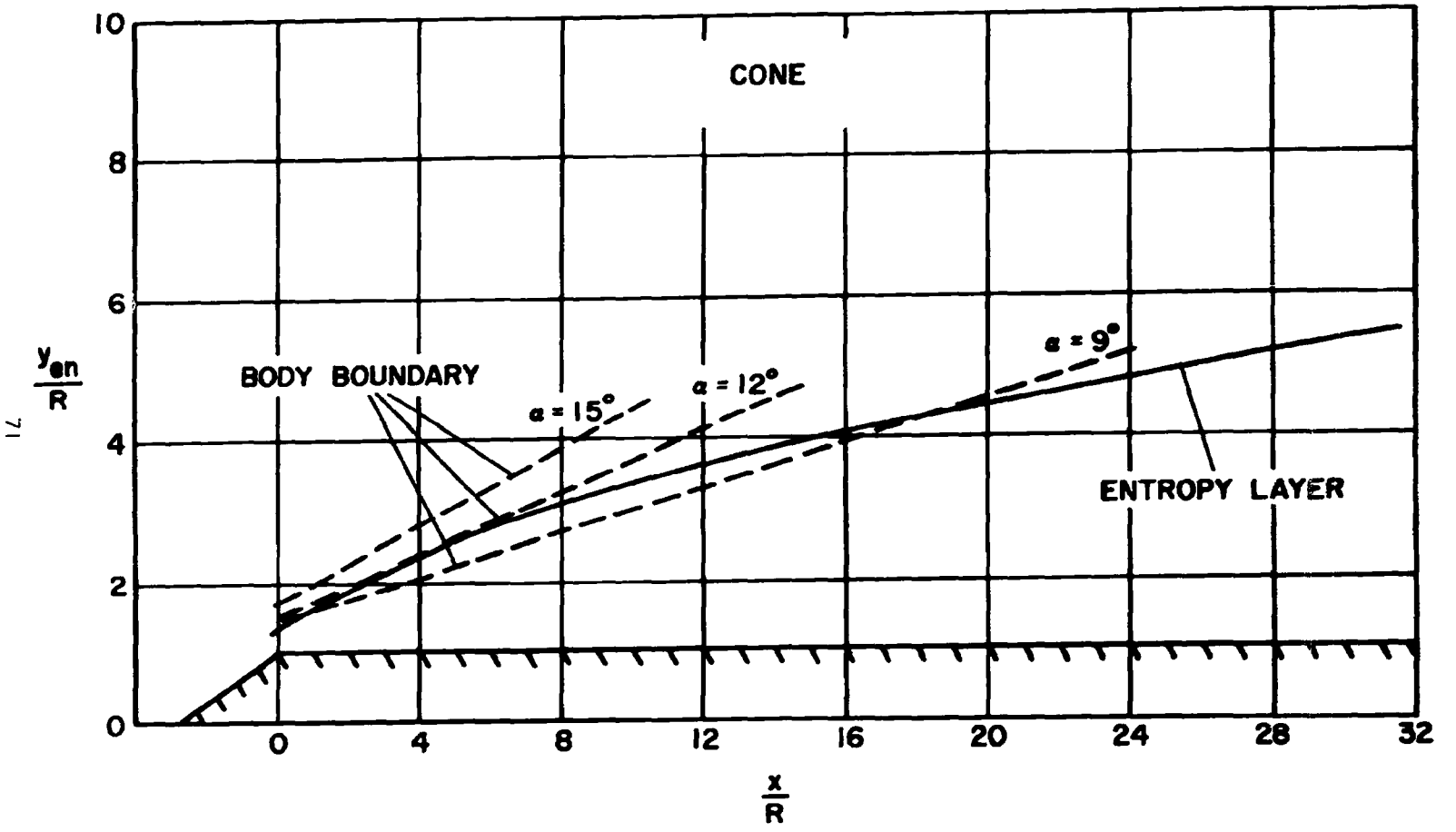

Figure 10a. Entropy layer for conical nose.

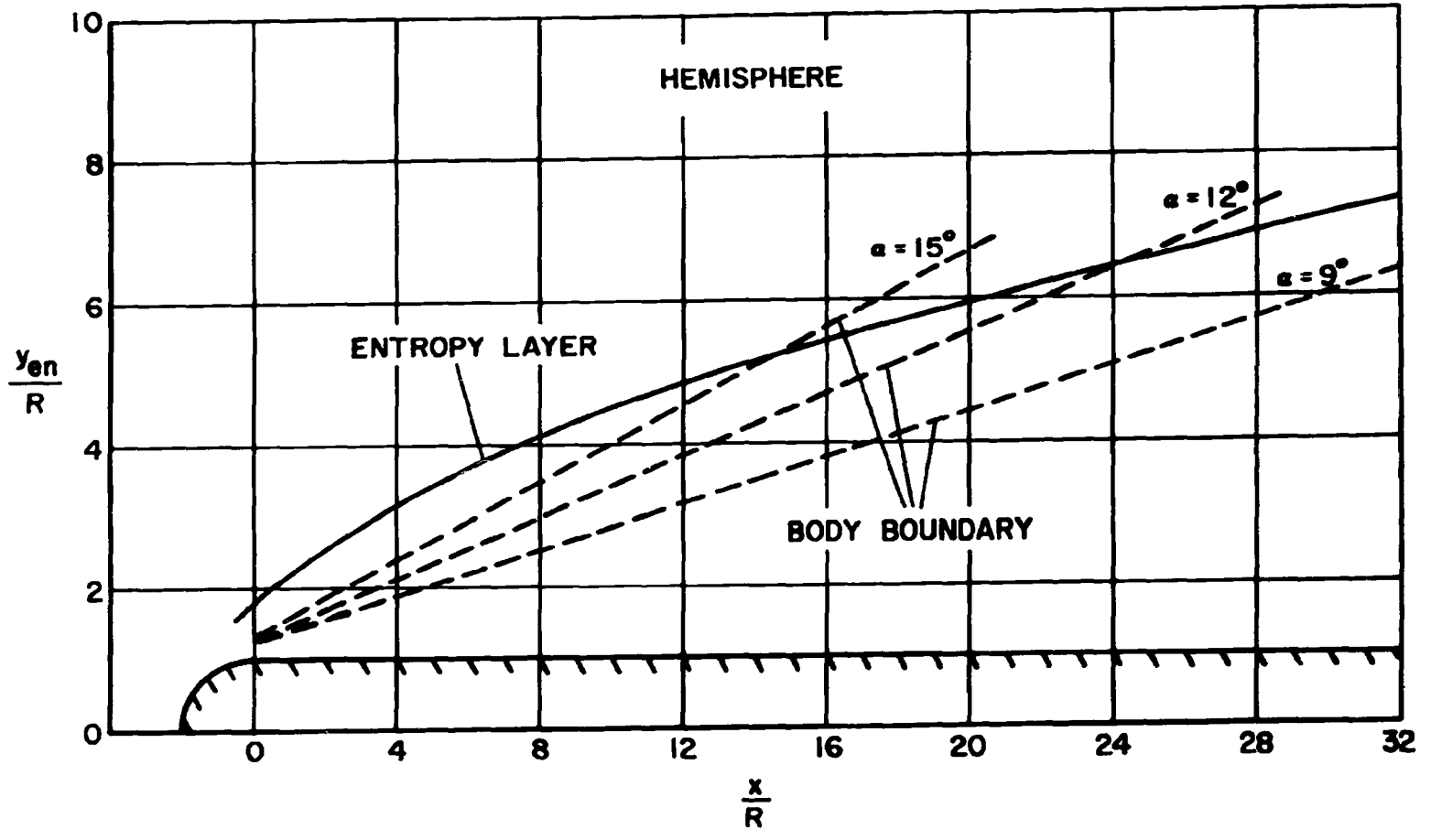

Figure 10b. Entropy layer for hemispherical nose

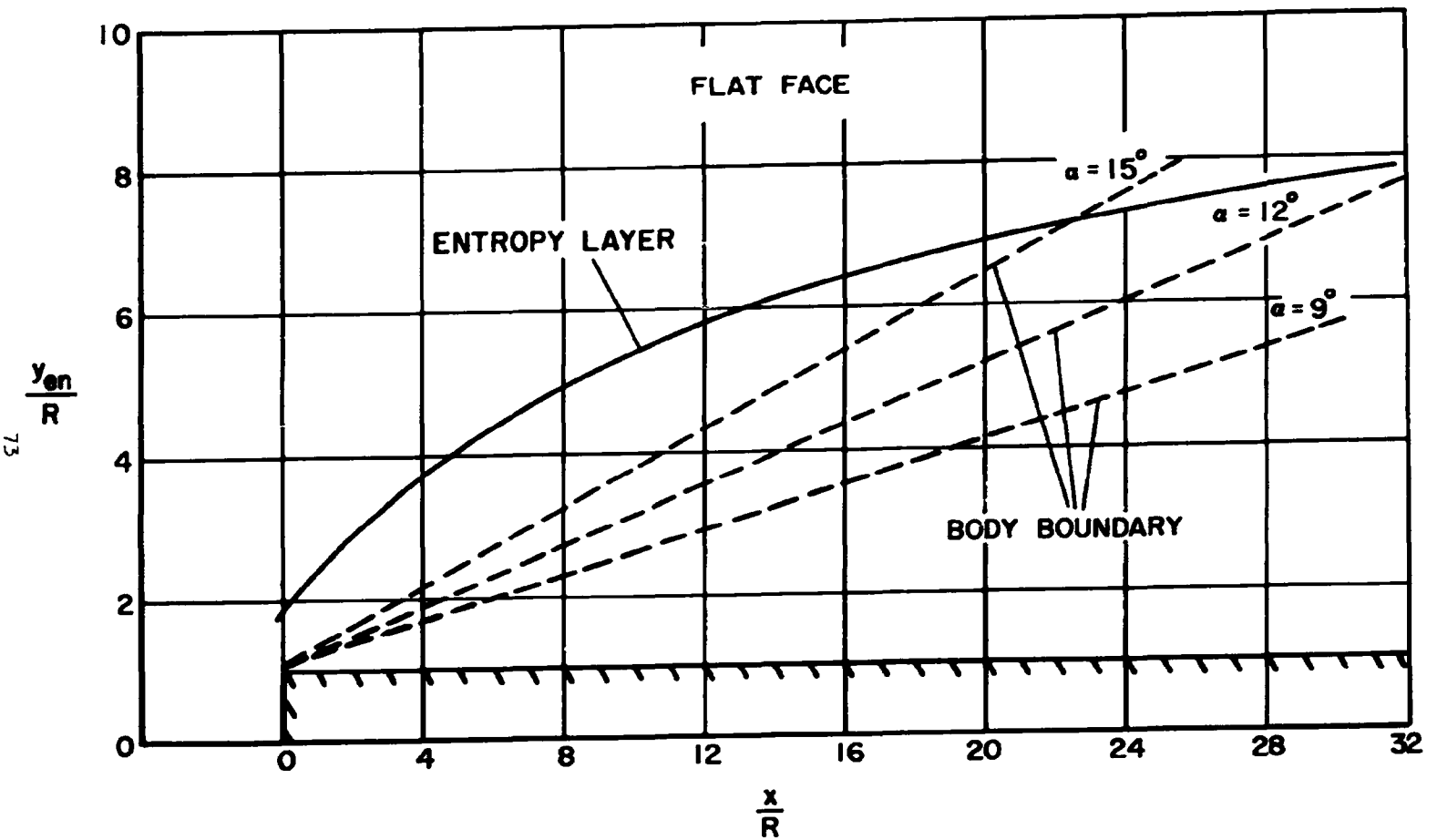

Figure 10c. Entropy layer for flat faced nose.

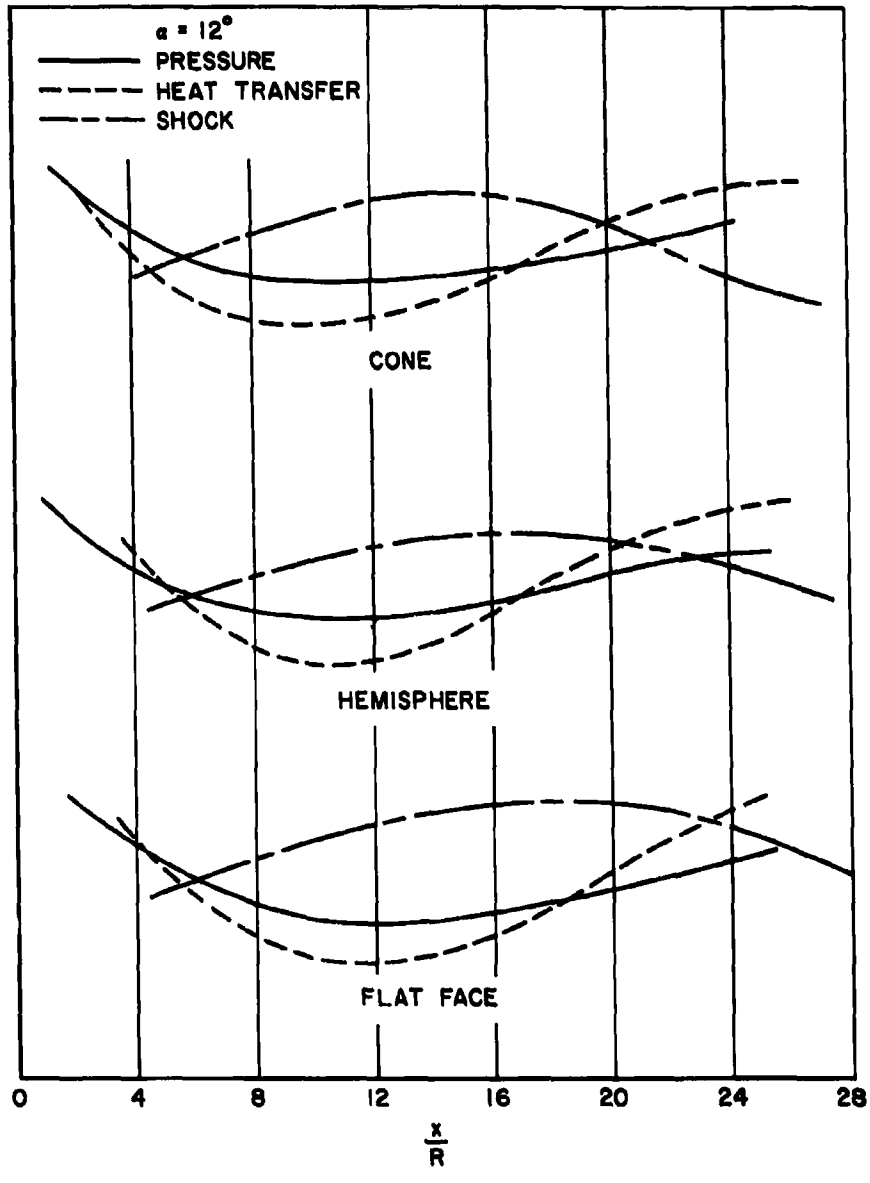

Figure 11a. Complete summary of data at $\alpha = 12^{\circ}$, $\phi = 0^{\circ}$.

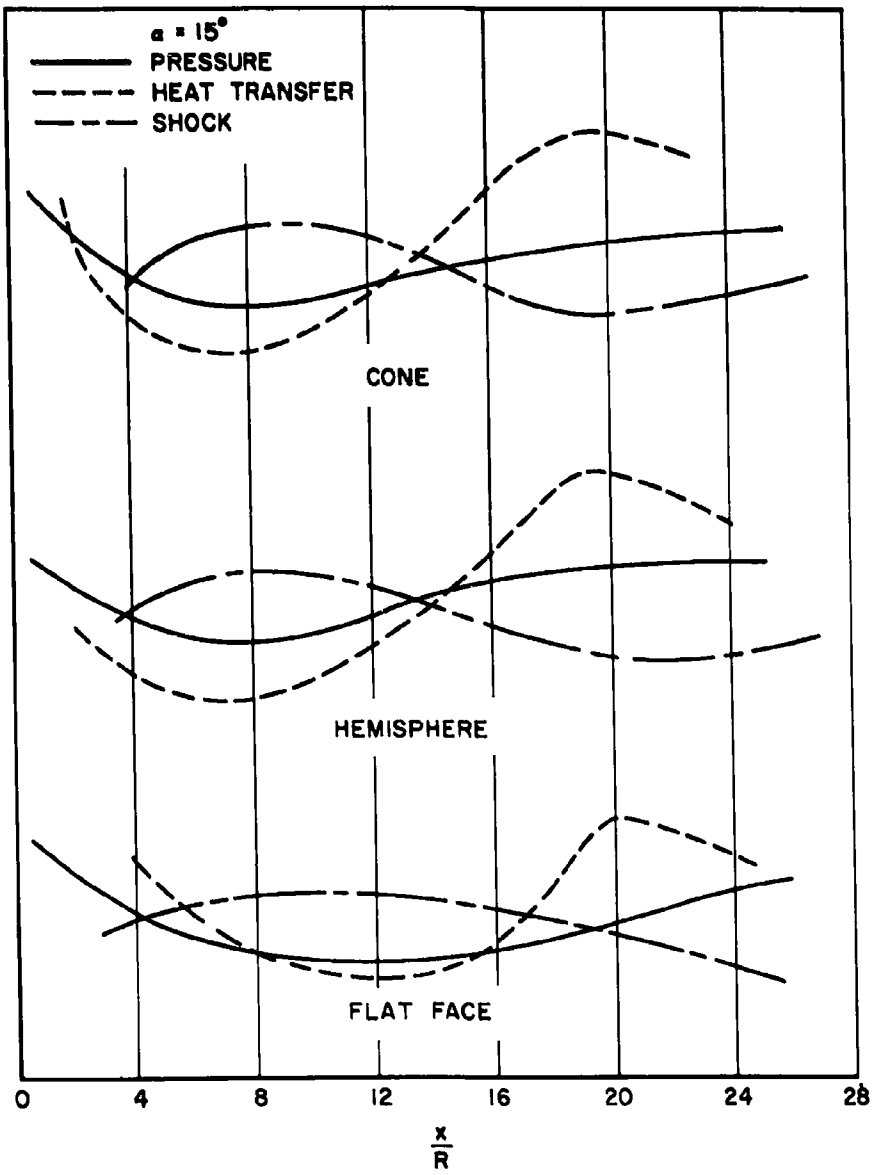

Figure 11b. Complete summary of data at $\alpha = 15^{\circ}$, $\phi = 0^{\circ}$.

Aeronautical Research Laboratories, Wright-Patterson AFB, O. PRESSURE AND HEAT TRANSFER MEASUREMENTS OVER A CIRCULAR CYLINDER AT ANGLES OF ATTACK UP TO 15° at M = 11 by C. C. Horstman, Princeton U., Princeton, N.J. May 1963. 75 p. incl. illus. (Project 7064;Task 7064-01)(Contract AF 33(616)-7629) (ARL 63-81) Unclassified Report

A continuation of a fundamental study of hypersonic wings and control surfaces, some detailed pressure distribution and heat transfer results have been obtained about a circular cylinder with various nose shapes at angles of

(over)

UNCLASSIFIED

UNCLASSIFIED

Aeronautical Research Laboratories, Wright-Patterson AFB, O. PRESSURE AND HEAT TRANSFER MEASUREMENTS OVER A CIRCULAR CYLINDER AT ANGLES OF ATTACK UP TO 15° at M = 11 by C. C. Horstman, Princeton U., Princeton, N.J. May 1963. 75 p. incl. illus. (Project 7064;Task 7064-01)(Contract AF 33(616)-7629) (ARL 63-81) Unclassified Report

A continuation of a fundamental study of hypersonic wings and control surfaces, some detailed pressure distribution and heat transfer results have been obtained about a circular cylinder with various nose shapes at angles of

(over)

UNCLASSIFIED

attack up to 15° and at azimuth angles from zero to 180°. The tests were carried out in the Princeton University 3 inch helium hypersonic wind tunnel at a Mach number of 11. The experimental results were compared with theory along the windward side and in the crossflow plane for both the pressure and heat transfer distributions. Some effects of the nose shapes on the flow over the circular cylinder under study were determined up to 13 cylinder diameters back from the nose.

UNCLASSIFIED

UNCLASSIFIED

attack up to 15° and at azimuth angles from zero to 180°. The tests were carried out in the Princeton University 3 inch helium hypersonic wind tunnel at a Mach number of 11. The experimental results were compared with theory along the windward side and in the crossflow plane for both the pressure and heat transfer distributions. Some effects of the nose shapes on the flow over the circular cylinder under study were determined up to 13 cylinder diameters back from the nose.

UNCLASSIFIED